Transportation Research Part B 138 (2020) 144–178

Contents lists available at ScienceDirect

Transportation Research Part B

journal homepage: www.elsevier.com/locate/trb

A distributionally robust stochastic optimization-based model predictive control with distributionally robust chance constraints for cooperative adaptive cruise control under uncertain traffic conditions

Shuaidong Zhao, Kuilin Zhang*

Department of Civil and Environmental Engineering, Michigan Technological University, Houghton, MI 49931, USA

ARTICLE INFO

Article history:
Received 10 October 2018
Revised 26 April 2020
Accepted 2 May 2020

Keywords:
Cooperative adaptive cruise control
Model predictive control
Distributionally robust stochastic optimization with distributionally robust chance constraints
Uncertain traffic conditions
Semidefinite Program

ABSTRACT

Motivated by connected and automated vehicle (CAV) technologies, this paper proposes a data-driven optimization-based Model Predictive Control (MPC) modeling framework for the Cooperative Adaptive Cruise Control (CACC) of a string of CAVs under uncertain traffic conditions. The proposed data-driven optimization-based MPC modeling framework aims to improve the stability, robustness, and safety of longitudinal cooperative automated driving involving a string of CAVs under uncertain traffic conditions using Vehicle-to-Vehicle (V2V) data. Based on an online learning-based driving dynamics prediction model, we predict the uncertain driving states of the vehicles preceding the controlled CAVs. With the predicted driving states of the preceding vehicles, we solve a constrained Finite-Horizon Optimal Control problem to predict the uncertain driving states of the controlled CAVs. To obtain the optimal acceleration or deceleration commands for the CAVs under uncertainties, we formulate a Distributionally Robust Stochastic Optimization (DRSO) model (i.e. a special case of data-driven optimization models under moment bounds) with a Distributionally Robust Chance Constraint (DRCC). The predicted uncertain driving states of the immediately preceding vehicles and the controlled CAVs will be utilized in the safety constraint and the reference driving states of the DRSO-DRCC model. To solve the minimax program of the DRSO-DRCC model, we reformulate the relaxed dual problem as a Semidefinite Program (SDP) of the original DRSO-DRCC model based on the strong duality theory and the Semidefinite Relaxation technique. In addition, we propose two methods for solving the relaxed SDP problem. We use Next Generation Simulation (NGSIM) data to demonstrate the proposed model in numerical experiments. The experimental results and analyses demonstrate that the proposed model can obtain string-stable, robust, and safe longitudinal cooperative automated driving control of CAVs by proper settings, including the driving-dynamics prediction model, prediction horizon lengths, and time headways. Computational analyses are conducted to validate the efficiency of the proposed methods for solving the DRSO-DRCC model for real-time automated driving applications within proper settings.

* Corresponding author.
E-mail address: klzhang@mtu.edu (K. Zhang).

https://doi.org/10.1016/j.trb.2020.05.001
0191-2615/

1. Introduction

Connected and automated vehicle (CAV) technologies provide a foundation for developing cooperative automated driving control systems for multiple vehicles in a string using real-time Vehicle-to-Vehicle (V2V) communication data (e.g. position, velocity, spacing, and acceleration). Real-time V2V data can be utilized to develop a more robust, smoother, and safer Cooperative Adaptive Cruise Control (CACC) system. A CACC system has the potential to improve driving safety, string stability, driving comfort, road capacity, and energy efficiency. However, existing CACC models ignore the uncertainty of traffic oscillations or assume that predicted traffic conditions are given by traffic management centers.

Uncertainty may exist in real driving scenarios involving CACC because accurate traffic prediction information is rarely available in practice. Traffic information about vehicles in front of the string of CAVs is generally not given, especially when oscillations (i.e. "stop-and-go" traffic) exist. The traffic oscillations lead to uncomfortable driving, safety issues, travel delays, and extra fuel consumption and emissions. Dealing with uncertain traffic conditions in a CACC system utilizing real-time V2V connected vehicle data is a challenge. The objective of this paper is to develop a data-driven optimization-based MPC modeling framework that uses real-time V2V data to improve the string stability, robustness, and driving safety of the longitudinal CACC of a string of CAVs under uncertain traffic conditions. As the paper focuses on longitudinal vehicle dynamic control, sensing errors (e.g. position-reading errors and gap-detecting errors) and communication issues (e.g. communication delays and packet loss) will not be considered.

1.1. Literature review

A rich body of literature has studied CACC problems using closed-loop optimal control models and Model Predictive Control (MPC) models in a connected environment. Closed-loop optimal controllers generate the optimal acceleration or deceleration control for CAV driving by closed-form piece-wise feedback gains. Sheikholeslam and Desoer (1990) develop a longitudinal platoon optimal control to reduce inter-vehicle spacing based on a nonlinear vehicle model. Varaiya (1993) presents a comprehensive overview of vehicle control policies and proposes a follower's spacing and leading vehicle speed-tracking control in highway systems. Naus et al. (2010) propose an optimal feedback control to maintain inter-vehicle spacing and conduct string stability analyses. Ploeg et al. (2014) present a feedback and feedforward optimal control to maintain the spacing between a controlled vehicle and the preceding vehicle. Milanés et al. (2014) model an optimal feedback control and feedforward control to regulate the gap between a controlled vehicle and the preceding vehicle. Chen et al. (2017) develop a truck-platooning control to maintain a constant time headway. Closed-loop optimal control methods perform properly in the absence of input and state constraints. The CACC problem under uncertain traffic conditions is, however, subject to multiple constraints in terms of longitudinal positions, velocities, accelerations, and driving safety. A closed-loop controller could send control signals that cannot satisfy some physical constraints of vehicle dynamics (e.g. a control signal for vehicle accelerations exceeds a vehicle's capability). Differing from closed-loop controllers, MPC models are used to solve the online control problem using real-time data with complicated constraints.

The receding horizon (or rolling horizon) principle, the core idea of MPC, was proposed in Propoi (1963). An MPC model generates control commands by solving an open-loop finite-horizon constrained optimal control within a prediction horizon, implementing the first time step only in an iterative way (Bertsekas, 2005; Rawlings and Mayne, 2009). Most existing MPC-based CACC models focus on free-flow or light traffic conditions in a deterministic system. Kreuzen (2012) presents an MPC control model to minimize the difference between the controlled vehicle state and the preceding vehicle state. Wang et al. (2014) develop an MPC model to control inter-vehicle spacing and speed differences as well as accelerations. Lang et al. (2014) propose an MPC model to control the spacing and speed difference between a controlled vehicle and the preceding vehicle to reduce fuel consumption while considering a minimum distance gap. Sancar et al. (2014) propose a tracking MPC model using the acceleration of the preceding vehicle as the reference signal. Wang et al. (2015) develop an MPC model to mitigate longitudinal collision impacts by adding a safety acceleration or deceleration constraint with given bounds to guarantee driving safety. Gong et al. (2016) formulate a one-horizon MPC model to control inter-vehicle spacing, inter-vehicle speed differences, and accelerations under a distance-gap constraint. Hu et al. (2016) propose an MPC model to reduce the difference between vehicle velocities and speed limits. Bu et al. (2010) propose a generalized MPC-based gap regulation controller to optimize CACC driving. Zhou et al. (2012) formulate an MPC model for the platoon-driving decentralized control that considers communication latency settings. Therefore, existing studies of MPC-based CACC models assume that the CACC control system is deterministic (e.g. a constant reference such as speed limit—Gong et al., 2016; Hu et al., 2016) or the predicted traffic conditions are given during prediction horizons (Kreuzen, 2012; Sancar et al., 2014; Zulkefli et al., 2014; Wang et al., 2015). However, these MPC controllers are not able to deal with the uncertain traffic conditions in a CACC system.

To deal with the uncertainty in MPC models, existing stochastic MPC models assume a known distribution of stochastic parameters (Schwarm and Nikolaou, 1999; Herzog et al., 2006; Primbs, 2009; Patrinos et al., 2011; Bichi et al., 2010; Suh et al., 2016; Zhou et al., 2017b). Robust MPC models assume the bounded compactness of stochastic parameters and use minimax optimization to deal with uncertainty (Scokaert and Mayne, 1998; Lu and Arkun, 2000; Van Hessem and Bosgra, 2002; Bemporad et al., 2003; Goulart et al., 2006; Wang et al., 2009). Both the stochastic MPC and robust MPC models assume perfect information (i.e. accurate values for system parameters or given probability distributions of stochastic parameters—Bertsimas and Thiele, 2006). Unfortunately, accurate traffic prediction information or the exact distribution

of stochastic parameters are rarely available in practice, posing a challenge for MPC-based CACC driving control under uncertain traffic conditions.

First introduced by Scarf (1958), DRSO has been studied in applications of risk management such as portfolio optimization and facility location problems (Calafiore, 2007; Zymler, 2010; Hall et al., 2015; Lam and Zhou, 2015; Glasserman and Yang, 2018). The idea underlying DRSO is to define a data-driven uncertainty set (i.e. a data-driven ambiguity set or distributional set) of possible realizations of uncertain parameters and then optimize against worst-case realizations within the set (Calafiore and El Ghaoui, 2006; Delage and Ye, 2010; Wang et al., 2016; Bertsimas et al., 2018). There are several methods available for constructing a data-driven uncertainty set, such as the moment-bound method (Delage and Ye, 2010), the divergence method (e.g. the likelihood bound method by Wang et al., 2016), and the Wasserstein distance method (Blanchet et al., 2019). For DRSO models under moment bounds, a data-driven uncertainty set for the uncertain parameters is constructed using mean and variance information and the expected value of the objective function in the worst case is then optimized based on the distributions in that set (Scarf, 1958; Calafiore and El Ghaoui, 2006; Liu et al., 2015; Delage and Ye, 2010; Zymler et al., 2013). Constructing a data-driven uncertainty set using mean and variance information in the moment-bound method requires historical data in a matrix form (Delage and Ye, 2010). With the CACC problem, all the controlled vehicles have the same number of observations at each time step, so the moment-bound method is used in this paper.

To ensure that a chance of satisfying a constraint reaches a certain threshold, a Distributionally Robust Chance Constraint (DRCC) based model uses mean and variance information about the uncertain parameters in the constraint (Calafiore and El Ghaoui, 2006; Zymler et al., 2013). In real driving scenarios, uncertainties of traffic flow dynamics may cause violations of MPC constraints, such as safety constraints. This may lead to string instability in the string of controlled vehicles. For safer and more stable driving under such traffic uncertainty, DRCC is applied in this paper to provide safety constraints to handle the uncertain driving dynamics of the immediately preceding vehicle (IPV).

To the best of our knowledge, no existing studies have integrated data-driven optimization models with MPC-based control models for longitudinal cooperative automated driving control under uncertain traffic conditions. Existing studies of CACC problems assume given traffic information in a deterministic system or known distributions of uncertain parameters in a stochastic system. These assumptions restrict the improvement of string stability, robustness, and driving safety for the longitudinal cooperative automated driving of a string of CAVs under uncertain traffic conditions. There is a need to develop a data-driven optimization-based MPC control modeling framework for the CACC problem under uncertain traffic conditions that can better utilize real-time V2V connected vehicle data.

1.2. Proposed method and contributions

To bridge the research gap for a CACC problem under uncertain traffic conditions, this paper proposes a data-driven optimization-based MPC model using V2V connected vehicle data. The rest of this section describes the proposed method in six parts: (1) we develop an online learning-based driving dynamics prediction method to obtain the predicted driving states of the IPV in front of the controlled vehicles; (2) we predict the reference driving states for the controlled vehicles following a CACC driving policy by solving a constrained Finite-Horizon Optimal Control (FHOC) model; (3) we formulate a DRSO-DRCC–based MPC model to obtain the optimal acceleration or deceleration commands for the controlled vehicles using data-driven uncertainty sets constructed by the predicted driving states of the IPV and predicted reference driving states of the controlled vehicles; (4) we use a string stability analysis method to evaluate the proposed model in both the time and frequency domains based on deviations between the controlled and the desired spacing; (5) we propose model reformulations and methods that can obtain tractable solutions by applying the strong duality theory and the Semidefinite Relaxation technique to solve the proposed DRSO-DRCC based MPC model; (6) we also conduct four experiments to assess the proposed model in multiple settings (i.e. with multiple driving dynamics prediction models, prediction horizon lengths, and time headways), and use two scenarios to evaluate the computational efficiency of the proposed methods using Next Generation Simulation (U.S. Department of Transportation Federal Highway Administration, 2016) data.

We summarize the four major contributions of this paper as follows:

The first contribution of this paper is to develop an online learning-based driving dynamics prediction method for the uncertain driving states of preceding vehicles and controlled vehicles using V2V connected vehicle data. Inspired by Townsend's (1983) concept of "forecasting the forecasts of others," the proposed online method learns the heterogeneous driving behaviors of each preceding vehicle from real-time V2V data, which is different from methods applied in existing studies that assume that other connected vehicles will provide their own forecasts to the controlled CAVs. In addition, this online method predicts the CACC reference driving states constrained by the preceding vehicle driving states learned online instead of assuming that the reference driving states for the controlled CAVs are given by traffic management centers.

The second contribution is to integrate a DRSO-DRCC model (i.e. a special case of data-driven optimization models under moment bounds) with an MPC model to improve string stability, robustness, and driving safety for the longitudinal cooperative automated driving of a string of CAVs under traffic uncertainties. We apply DRSO to deal with the controlled vehicle driving uncertainty by constructing a data-driven uncertainty set from mean and variance information about the predicted reference driving states of the controlled vehicles. In addition, we use DRCC to address IPV driving uncertainty by constructing a data-driven uncertainty set using the predicted driving states of the IPV in the safety constraint. To the best of our knowledge, this paper is among the first to integrate a DRSO-DRCC model with an MPC-based control model to solve a longitudinal cooperative automated driving control problem.

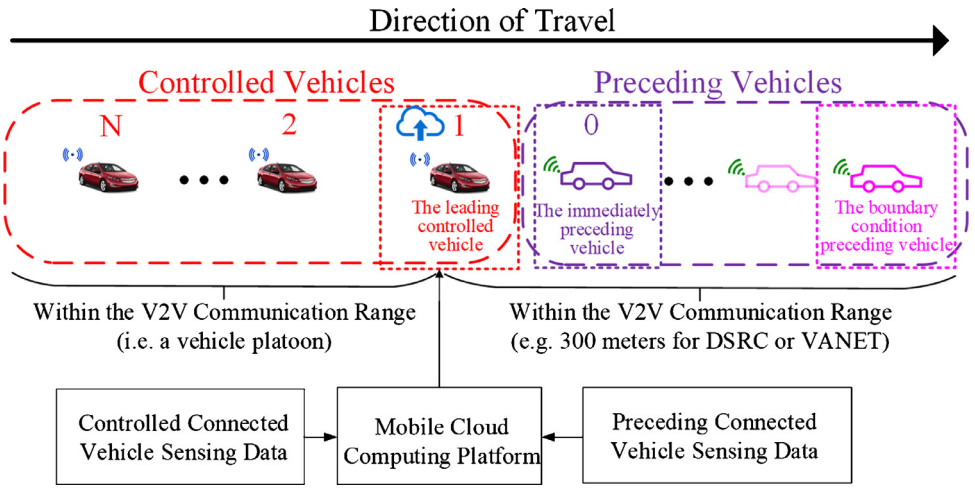

Fig. 1. Illustration of the CACC problem under uncertain traffic conditions.

The paper's third contribution is to propose model reformulations for tractable solutions and solution methods for real-time implementations of the proposed data-driven optimization-based MPC model. To reduce the computational expense caused by the DRCC constraint in the model, we present an equivalent deterministic counterpart to the DRCC constraint. Furthermore, the proposed model reformulations address the computational complexity of the minimax program of the original DRSO model by applying strong duality theory and the Semidefinite Relaxation technique. The method based on a hot start and parallel computing methods in this paper can be implemented for real-time applications of the proposed model, under proper settings for the number of controlled vehicles, prediction horizon lengths, and time headways.

The paper's fourth contribution is to demonstrate the string stability of the proposed data-driven optimization-based MPC model using empirical data. In the numerical analysis, we evaluate the string stability of the proposed model in the time and frequency domains. The experimental results show that the proposed model can generate smoother, more stable, and safer longitudinal cooperative automated driving control of CAVs than human driving by using the proposed FHOC (i.e. Finite-Horizon Optimal Control) model to predict the driving states of the controlled vehicles with a proper time headway (i.e. 1.6 s) under longer prediction horizon lengths.

This paper is structured as follows. In Section 2, we present the problem statement and assumptions. In Section 3, we illustrate the data-driven optimization-based MPC modeling framework for the CACC control under uncertain traffic conditions. The model reformulations and solution methods are described in Section 4. We implement the proposed framework using empirical vehicle trajectory datasets from the NGSIM program. The experiment design and numerical analysis using the NGSIM data are presented in Section 5. Concluding remarks are given in Section 6.

2. Problem statement and assumptions

The goal of this paper is to improve string stability, robustness, and driving safety for the longitudinal cooperative automated driving of a string of CAVs under uncertain traffic conditions by using V2V connected vehicle data (Fig. 1). The uncertainty of traffic conditions poses a challenge to predict the driving states of the IPV in front of the leading controlled vehicle of the string. The problem of interest addressed in this paper is to propose an optimization-based CACC model to achieve smoother, more robust, and safer control than human driving under traffic uncertainties. In this paper, we assume that the controlled vehicles and the preceding vehicles are V2V-enabled. Within a communication range such as a Vehicular Ad-hoc Network (VANET) using Dedicated Short-Range Communications (DSRC), individual vehicle data such as vehicle positions, velocities, spacing, and accelerations can be shared via V2V communications (Fig. 1). The data from all the preceding and the following vehicles will be collected by the leading controlled vehicle and sent to a mobile cloud computing platform, which can be mounted in the leading controlled vehicle. By solving the data-driven optimization-based control problem in real-time, the mobile cloud computing platform will send driving commands to each of the controlled vehicles using V2V communications. The automated driving system in each controlled vehicle will execute the driving commands. To meet the requirements of the CACC (e.g. improving safety, driving stability, and driving comfort), we model a cooperative CAV string subject to constraints with respect to longitudinal positions, velocities, accelerations, and driving safety.

2.1. Definitions

To clearly describe our problem and methodology, the following definitions of the components of the CACC system are used in this study. For illustration purposes, we use contrasting colors and shapes for the defined objects (Fig. 2).

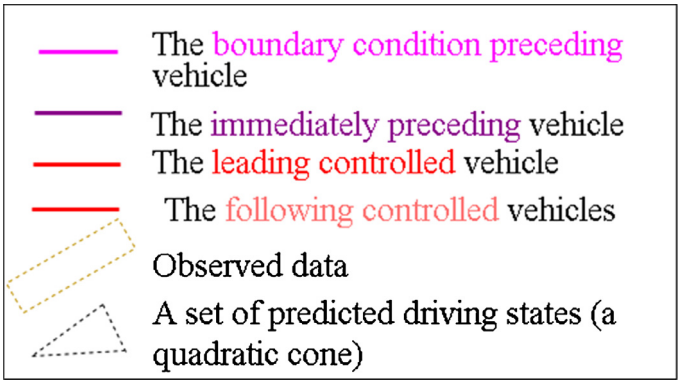

Fig. 2. The legend of the defined objects.

Definition 1. The leading controlled vehicle. The leading controlled vehicle is the first (the leading) vehicle in the controlled string of CAVs.

Definition 2. The following controlled vehicles. The following controlled vehicles are the CAVs following behind the leading controlled vehicle in the string.

Definition 3. The boundary condition preceding vehicle (BCPV). The BCPV is the farthest preceding vehicle within the communication range of the leading controlled vehicle.

Definition 4. The immediately preceding vehicle (IPV). The IPV is the preceding vehicle just in front of the leading controlled vehicle.

Definition 5. The space-time region of observations. The space-time region of observations is the region that contains the observed driving states in space and time dimensions of the preceding vehicles and the controlled vehicles.

Definition 6. The space-time region of predictions. The space-time region of predictions is the region that contains the predicted driving states in space and time dimensions of the preceding vehicles and the controlled vehicles.

2.2. Assumptions and notation

The literature includes various connected and automated driving-control strategies based on a wide variety of control approaches under a range of assumptions. To properly define our problem, we make the following assumptions:

Assumption 1. The controlled and preceding vehicles can share individual information (e.g. positions, gaps, velocities, and accelerations) in real-time (i.e. 0.1-second time interval) via V2V communications within a short-range communication distance (e.g. 300 m). For the sake of simplicity, sensing errors (e.g. position-reading errors and gap-detecting errors) and communication issues (e.g. communication delays and packet loss) are not considered.

Assumption 2. The controlled vehicles are equipped with automated driving systems to execute the received acceleration or deceleration commands.

Assumption 3. The preceding vehicles are human-driven connected vehicles that only share their data with others. The preceding vehicles are not equipped with automated driving systems.

Assumption 4. The problem focuses on the cooperating longitudinal dynamics of the controlled vehicles in a single lane. Lane-changing automation is not considered in this study.

Assumption 5. The predicted driving dynamics of the preceding vehicles are not given by themselves or by traffic-management centers.

Assumption 6. The distributions of stochastic parameters (i.e. the predictive vehicle position and velocity) are not known in advance.

We list the notation for indices, state variables, control variables, sets, parameters, model matrices, and data-driven inputs as follows:

Indices:

n, controlled vehicle index $n = 1, \ldots, N$
k, control time index $k = 1, 2, 3, \ldots$

t, prediction horizon time index $t = k, ..., k + PH$

State variables:

$l_n(t)$, longitudinal position (front bumper)
$v_n(t)$, velocity
$\boldsymbol{x}(t)$, driving state vector: longitudinal position and velocity - $\boldsymbol{x}(t) = [l_1(t), v_1(t), \ldots, l_N(t), v_N(t)]^T_{1\times 2N}$
$\boldsymbol{x}_p^{\xi}(t)$, random state vector for the IPV
$\boldsymbol{x}_r^{\xi}(t)$, random state vector for the controlled vehicles

Control variables:

$u_n(t)$, control variable: acceleration
$\boldsymbol{u}(t)$, control vector: $\boldsymbol{u}(t) = [u_1(t), \ldots, u_N(t)]^T_{1\times N}$
Sets:
$\mathbb{D}_p$, data-driven uncertainty set of the predicted driving states for the random vector $\boldsymbol{x}_p^{\xi}(t)$ of the IPV
$\mathbb{D}_r$, data-driven uncertainty set of the predicted driving states for the random vector $\boldsymbol{x}_r^{\xi}(t)$ of the controlled vehicles
$\mathbb{D}$, data-driven uncertainty set of the predicted driving states for the IPV and the controlled vehicles

Parameters:

ξ, denote one driving state scenario constrained by one of a set of the boundary-condition vehicle driving states
N, number of controlled vehicles
T^{obs}, observation time period
PH, prediction horizon length
T^p, driving-dynamics prediction time period (i.e. the online learned parameters of driving behaviors are stable after T^p)
ΔT^p, driving-dynamics prediction update interval
Δt, MPC control time interval
s_n^{min}, minimum safe spacing between a stopped IPV and a stopped controlled vehicle n depending on vehicle length
τ^{min}, minimum safe time headway
τ^h, time headway
γ_p, confidence level of the DRCC constraint for the IPV
$\gamma_{p,1}$, confidence level of the first-moment constraint in the data-driven uncertainty set $\mathbb{D}_p$
$\gamma_{p,2}$, confidence level of the second-moment constraint in the data-driven uncertainty set $\mathbb{D}_p$
$\gamma_{r,1}$, confidence level of the first-moment constraint in the data-driven uncertainty set $\mathbb{D}_r$
$\gamma_{r,2}$, confidence level of the second-moment constraint in the data-driven uncertainty set $\mathbb{D}_r$
γ_1, confidence level of the first-moment constraint in the data-driven uncertainty set $\mathbb{D}$
γ_2, confidence level of the second-moment constraint in the data-driven uncertainty set $\mathbb{D}$
q_t, discounting factor
τ_n^{Ne}, time displacement (i.e. reaction time) of Newell's car-following model for vehicle n
d_n^{Ne}, space displacement (i.e. safe distance) of Newell's car-following model for vehicle n
$u_n^{Ne}(t)$, acceleration in Newell's car-following model
$v_n^{Ne}(t)$, velocity in Newell's car-following model
$v_n^{M,des}$, given desired velocity in the MICroscopic model for Simulation of Intelligent Cruise control (MIXIC) model
$g_n^{N,des}$, desired distance gap in the MIXIC model
k^M, k_a^M, k_v^M, k_d^M, given constant factors in the MIXIC model
$g_n(t)$, distance gap
$\delta_n(t)$, spacing deviation for string stability analysis in the time domain
$E_n(\omega)$, spacing deviation for string stability analysis in the frequency domain

Model matrices:

$\boldsymbol{Q_p}$, matrix for the driving state $\boldsymbol{x}(t)$ of the leading controlled vehicle in the DRSO objective of the constant-time-headway policy and driving stability
$\boldsymbol{Q_p^{\xi}}$, matrix for the predicted driving state $\hat{\boldsymbol{x}}^{\xi}(t)$ of the leading controlled vehicle in the DRSO objective of the constant-time-headway policy and driving stability
$\boldsymbol{Q_r^{\xi}}$, matrix for the predicted driving state $\hat{\boldsymbol{x}}^{\xi}(t)$ in the reference state tracking of the controlled vehicles in the DRSO objective
$\boldsymbol{Q_r}$, matrix for reference tracking of the controlled vehicles in the DRSO objective
$\boldsymbol{Q}$, matrix for the driving state $\boldsymbol{x}(t)$ of the following controlled vehicles in the DRSO objective
$\boldsymbol{R}$, matrix for the driving comfort of the following controlled vehicles in the DRSO objective
$\boldsymbol{K_l}$, matrix for the leading controlled vehicle driving state in the DRCC

$\boldsymbol{G_l}$, matrix for the predicted driving state of the leading controlled vehicle in the DRCC
$\boldsymbol{K_f}$, matrix for the following vehicle driving state in the safety and speed limit constraints
$\boldsymbol{G_f}$, matrix for the following controlled vehicles in the safety and speed limit constraints
$\boldsymbol{A}$, state dynamic matrix for the driving states of the controlled vehicles
$\boldsymbol{B}$, state dynamic matrix for acceleration of the controlled vehicles

Data-driven inputs:

$l_n^{obs}(k)$, observed longitudinal position
$v_n^{obs}(k)$, observed velocity
$l_b(t)$, longitudinal position of the BCPV
$v_b(t)$, velocity of the BCPV
$\hat{l}_b^{\xi}(t)$, predicted longitudinal position of the BCPV under uncertainties
$\hat{v}_b^{\xi}(t)$, predicted velocity of the BCPV under uncertainties
$\hat{l}_n^{\xi}(t)$, predicted longitudinal position under uncertainties
$\hat{v}_n^{\xi}(t)$, predicted velocity under uncertainties
$\hat{\boldsymbol{x}}_p^{\xi}(t)$, predicted driving states for the IPV - $[\hat{l}_0^{\xi}(t), \hat{v}_0^{\xi}(t)]_{1\times 2}^T$
$\hat{\boldsymbol{x}}_r^{\xi}(t)$, predicted driving states for the controlled vehicles - $[[\hat{l}_1^{\xi}(t), \hat{v}_1^{\xi}(t), \ldots, \hat{l}_N^{\xi}(t), \hat{v}_N^{\xi}(t)]]_{1\times(2N)}^T$
$\hat{\boldsymbol{x}}^{\xi}(t)$, predicted driving states for the IPV and the controlled vehicles: $[[\hat{l}_0^{\xi}(t), \hat{v}_0^{\xi}(t), \ldots, \hat{l}_N^{\xi}(t), \hat{v}_N^{\xi}(t)]]_{1\times(2N+2)}^T$
$\bar{\boldsymbol{x}}_p^{\xi}(t)$, expectation of the driving states of the IPV from historical observations
$\hat{\boldsymbol{\sigma}}_{00}(t)$, covariance matrix of the driving states of the IPV from historical observations
$\hat{\boldsymbol{\mu}}_p$, estimate of the mean of the predicted driving states of the IPV
$\hat{\boldsymbol{\Sigma}}_p$, estimate of the covariance matrix of the predicted driving states of the IPV
$\hat{\boldsymbol{\mu}}_r$, estimate of the mean of the predicted driving states of the controlled vehicles
$\hat{\boldsymbol{\Sigma}}_r$, estimate of the covariance matrix of the predicted driving states of the controlled vehicles
$\hat{\boldsymbol{\mu}}$, estimate of the mean of the predicted driving states of the IPV and the controlled vehicles
$\hat{\boldsymbol{\Sigma}}$, estimate of the covariance matrix of the predicted driving states of the IPV and the controlled vehicles

3. A data-driven optimization-based MPC modeling framework

This section proposes mathematical formulations for a data-driven optimization-based MPC modeling framework for the CACC under uncertain traffic conditions. This framework contains three steps for the dynamic CACC driving control of the controlled vehicles (Fig. 3). First, it requires online prediction of the driving dynamics of the IPV and the controlled vehicles at control time step k. We estimate the uncertain driving states of the BCPV as the boundary conditions for the prediction of the following and preceding vehicles. Constrained by the boundary conditions, we can predict the uncertain driving states of the IPV by learning the driving behaviors of the preceding vehicles. Restricted by predicted driving states of the IPV, we predict the driving state reference of the controlled vehicles via a CACC driving policy. Second, we solve the DRSO-DRCC model at control time step k to obtain the optimal acceleration or deceleration commands for the controlled CAVs. The predicted uncertain driving states of the controlled vehicles will be used as the driving state reference in the tracking term of the objective function of the DRSO-DRCC based MPC model. The predicted uncertain driving states of the IPV will be used in the DRCC safety constraints of the model. The DRSO-DRCC–based MPC model will be solved to obtain the optimal acceleration or deceleration control. Third, the optimal acceleration or deceleration commands are sent to the controlled CAVs at control time step k. The three steps that comprise this procedure will then be repeated in the rolling horizon framework.

3.1. Online learning-based driving dynamics prediction under traffic uncertainties

This section presents an online method for predicting the uncertain driving states of the preceding vehicles (especially the BCPV and the IPV) and the controlled vehicles over a prediction horizon. The existing predictive vehicle driving control models assume that both surrounding vehicle driving records (i.e. positions and velocities) and traffic signal information can be given by the traffic management center via Infrastructure-to-Vehicle (I2V) communications (Gong et al., 2009; Zulkefli et al., 2014). However, the predicted information regarding the vehicle positions and velocities of the preceding vehicles over a prediction horizon are generally not given in practice. The predictive driving-state references for the controlled vehicles are constrained by the predicted driving states of the preceding vehicles, which may not be given in advance.

To predict the driving states of the preceding vehicles for each individual vehicle, we present an online driving-dynamics prediction method based on the concept of “forecasting the forecasts of others” in Townsend (1983). In CACC driving scenarios, reflecting safety concerns, the driving states of each vehicle are directly constrained by its own IPV. At every control time step, after applying the concept of time geography (Hägerstrand, 1970; Miller, 2005) using observed velocity samples during a past time horizon, we estimate a set of uncertain driving states of the farthest preceding vehicle within the V2V

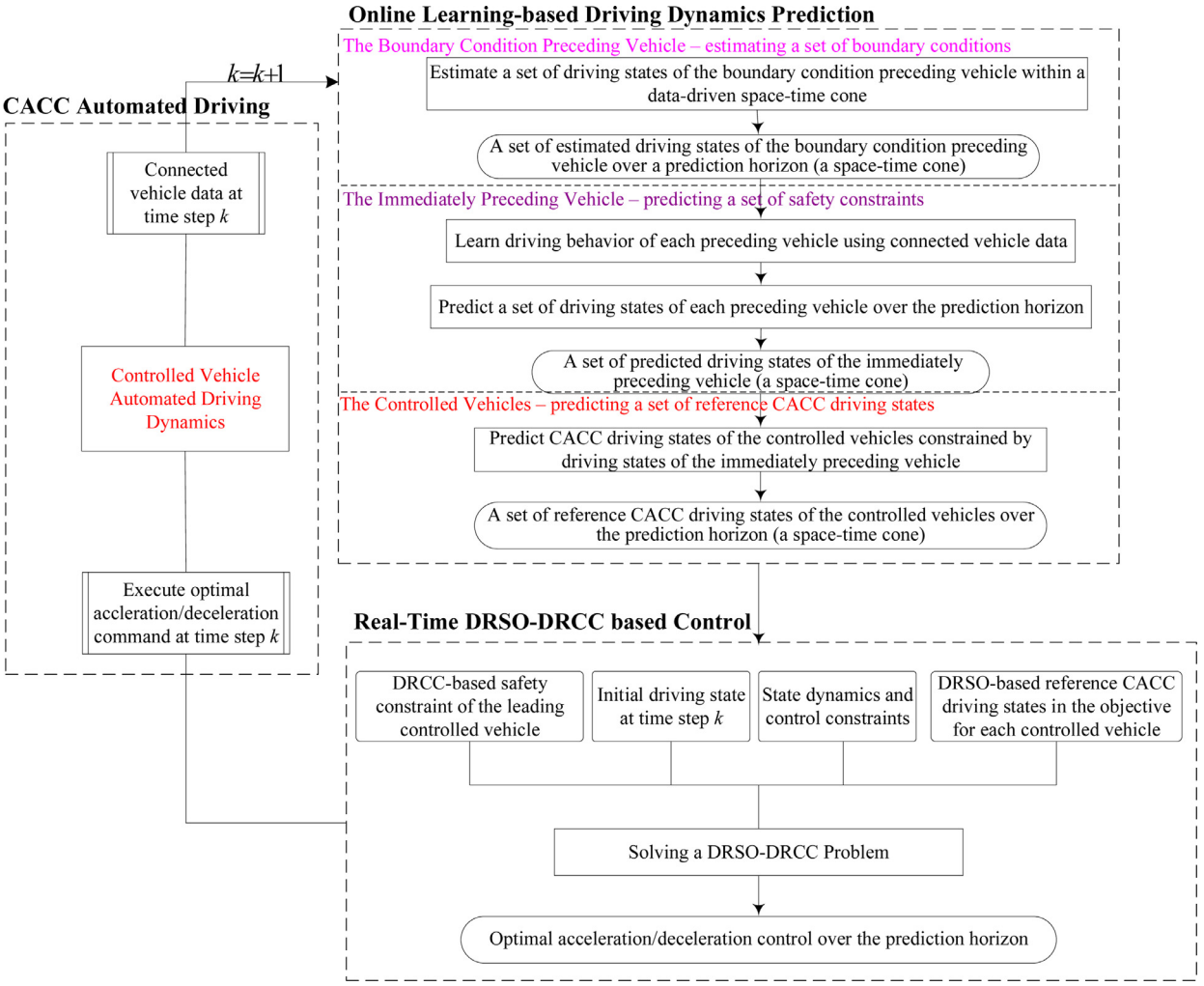

Fig. 3. The proposed data-driven optimization-based MPC modeling framework.

communication range of the leading controlled CAV. The predicted driving states of this preceding vehicle, which essentially is a space-time cone (Ma et al., 2017; Zhao and Zhang, 2017; Zhou et al., 2017a), serve as the boundary conditions for the driving-dynamics prediction regarding its following vehicles. For the other preceding vehicles, we propose an online learning method using real-time connected vehicle data to learn the heterogeneous driving behaviors by dynamically updating the parameter estimates of car-following models such as Newell's model (Newell, 2002) and the Intelligent Driver Model (IDM; see Treiber et al., 2000). Based on the online learned parameters, we predict the uncertain driving states of the IPV constrained by the predicted driving states of the BCPV.

For a set of predicted uncertain driving states of the BCPV, we will obtain a set of predicted uncertain driving states of the IPV using the online driving-dynamics prediction method. The predicted driving states of the IPV will be used to construct the data-driven uncertainty set for the DRCC safety constraint of the proposed data-driven optimization-based MPC model. Solving a constrained FHOC (i.e. Finite-Horizon Optimal Control) model constrained by the IPV, we predict the driving states of the controlled vehicles over a prediction horizon.

3.2. Predictive uncertain driving states of the BCPV

This section presents a method for estimating a set of uncertain driving states for the boundary-condition vehicle. Zhou et al. (2017a) and Ma et al. (2017) analytically construct a feasible vehicle trajectory set as a space-time cone or prism by allowing finite acceleration and deceleration in a trajectory-planning problem. In this paper, we estimate a set of uncertain driving states of the BCPV over a prediction horizon as a set of trajectories, which is also a space-time cone in space and time dimensions, using historical observations rather than analytical methods that consider only vehicle acceleration capability. Note that one feature of MPC models is that they implement only the first-step optimal control over a prediction

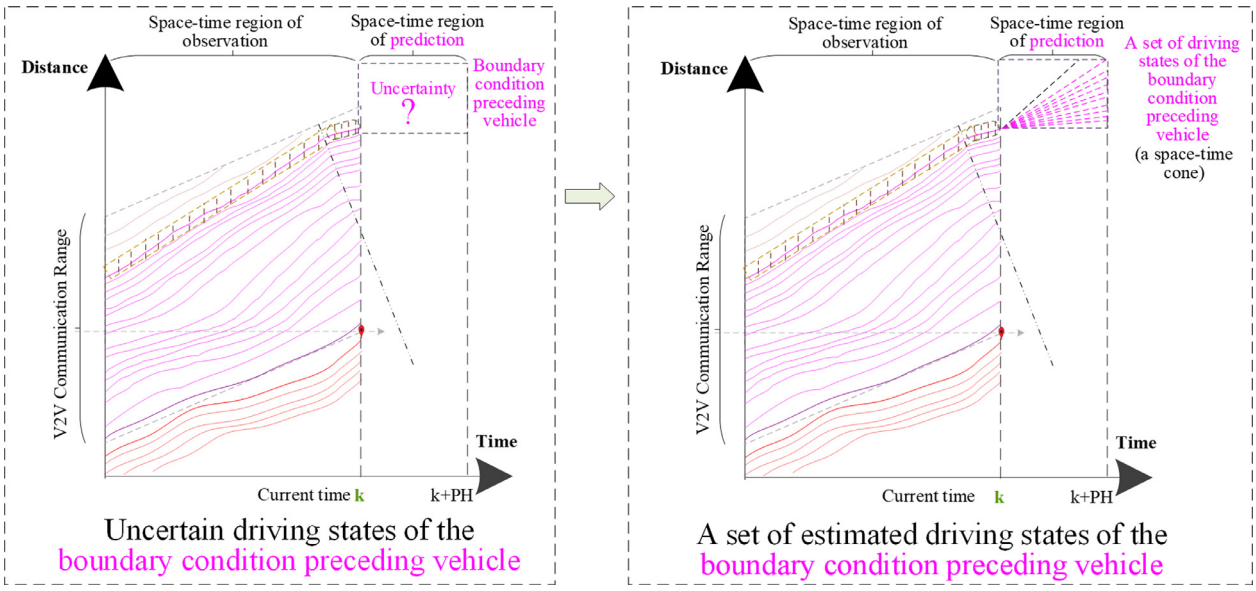

Fig. 4. Estimate a set of driving states of the BCPV.

horizon $[k, \ldots, k + PH]$ at current control time step k. This feature makes it possible to estimate the driving dynamics over a prediction horizon by simply assuming the BCPV is driving at a constant velocity over the prediction horizon. Note that, even by assuming constant velocity driving on the part of the BCPV, the traffic oscillations (the shock in Fig. 4) will still be captured by the preceding vehicle prediction model in Section 3.1.2.

At control time step k, we collect velocity samples from the historical data during $[k - T^{obs}, k]$ (e.g. T^{obs} is equal to 5 s) to derive a set of observed vehicle velocities $\{\hat{v}_b^{\xi_i}(t) | \forall i = 1, \ldots, M\}$, as seen in Fig. 4. Based on the sampled velocity observations, we calculate a set of driving states, $\{[\ \hat{l}_b^{\xi_i}(t) \quad \hat{v}_b^{\xi_i}(t)\ ]^T | \forall t = k, \ldots, k + PH, \forall i = 1, \ldots, M\}$, of the BCPV driving at constant velocities. The set of driving states, which is a space-time cone in space and time dimensions, is considered a set of boundary conditions for the prediction of the driving states of the other preceding vehicles. The upper bound of the set of the BCPV driving states is calculated by speed limits while the lower bound is estimated by a stopped velocity. From the collected velocity samples, $\{\hat{v}_b^{\xi_i}(t) | \forall i = 1, \ldots, M\}$, at time step k, we can calculate the number of observations, $\{N_i | i = 1, \ldots, M\}$, for each of the driving states in the set $\{[\ \hat{l}_b^{\xi_i}(t) \quad \hat{v}_b^{\xi_i}(t)\ ]^T | \forall t = k, \ldots, k + PH, \forall i = 1, \ldots, M\}$. The number of observations and the estimated set of driving states of the BCPV will be used to construct the data-driven uncertainty set based on moment information presented in Section 3.2.

3.3. Learning-based predictive uncertain driving states of the IPV

This section presents a learning-based method for predicting a set of uncertain driving states of the IPV, given the set of boundary driving conditions from Section 3.1.1. As Fig. 5 shows, given a set of boundary driving conditions, we learn online the heterogeneous driving behaviors of each preceding vehicle using V2V connected vehicle data. The online learning method dynamically calibrates car-following models (e.g. the Newell or IDM models, etc.) based on the observed driving states for each preceding vehicle that shares information but without a response to other connected vehicle information (see the middle plot in Fig. 5). Note that we can also use other car-following models, such as the connected IDM model in Talebpour and Mahmassani (2016), for preceding vehicles that use connected vehicle data for driving-assistance applications (e.g. safety warning). Based on the online calibrated car-following model parameters of each individual preceding vehicle and the boundary driving conditions, we predict a set of uncertain driving states for all the preceding vehicles over a prediction horizon. We will then obtain a set of learning-based predictive uncertain driving states of the IPV for a given set of boundary conditions from Section 3.1.1 using the observed connected vehicle data (the right plot in Fig. 5).

To learn the heterogeneous driving behaviors, we calibrate car-following models dynamically. We take Newell's car-following model as an example in Eqs. (1)–(2) to show the process. In this paper, we also implement the IDM model to predict the driving states of the preceding vehicles.

$$\min_{\tau_n^{Ne}, d_n^{Ne}} \sqrt{\frac{\sum_{t=k-T^{obs}}^{k} \left[v_n(t) - v_n^{Ne}(t)\right]^2}{T^{obs}}}, n = 1, \ldots, N \tag{1}$$

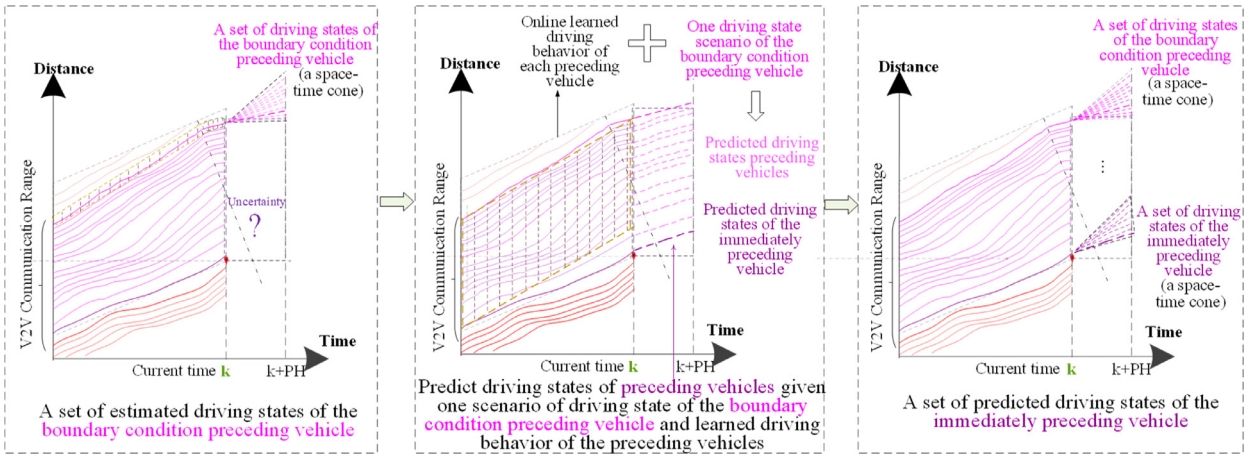

Fig. 5. Predict a set of driving states of the IPV. (For interpretation of the references to colour in this figure legend, the reader is referred to the web version of this article.)

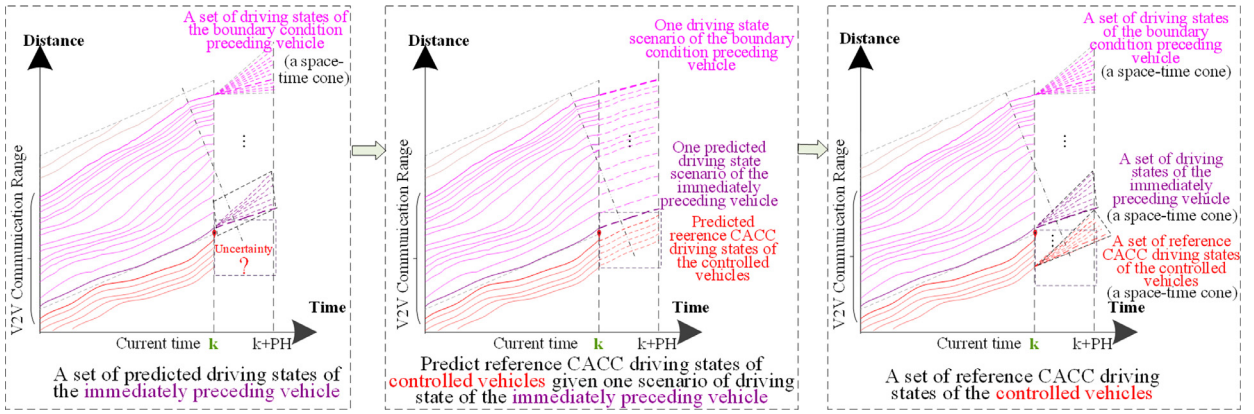

Fig. 6. Predict a set of CACC driving states of the controlled vehicles . (For interpretation of the references to colour in this figure legend, the reader is referred to the web version of this article.)

s.t.

$$v_n^{Ne}(t) = \frac{1}{\tau_n^{Ne}}[l_{n-1}(t) - l_n(t)] - \frac{d_n^{Ne}}{\tau_n^{Ne}} - \frac{\tau_n^{Ne}}{2}u_n(t),\ \ n = 1, \ldots, N,\ \ t = k - T^{obs}, \ldots, k \tag{2}$$

where τ_n^{Ne} and d_n^{Ne} are Newell's car-following time and distance parameters respectively, v_n^{Ne} is the velocity calculated by Newell's car-following model, the observed velocity $v_n(t)$ of the preceding vehicle n, the location $l_{n-1}(t)$ and $l_n(t)$ of preceding vehicles $n-1$ and n, during the observed period $[t|t = k - T^{obs}, \ldots, k]$. The velocity-acceleration relationship in Eq. (2) is based on Eq. (9) in Newell (2002). We calibrate the model parameters independently for each preceding vehicle.

$$v_n\left(t + \frac{\tau_n^{Ne}}{2}\right) = \frac{1}{\tau_n^{Ne}}[l_{n-1}(t) - l_n(t)] - \frac{d_n^{Ne}}{\tau_n^{Ne}},\ \ n = 1, \ldots, N \tag{3}$$

With the individually learned parameters τ_n^{Ne}, d_n^{Ne}, we predict the driving states over a prediction horizon for each preceding vehicle, especially for the IPV, by Eq. (3), which is based on the velocity equation in Newell (2002). The predicted driving states of the IPV, - $\hat{l}_0^{\xi}(t)$ and $\hat{v}_0^{\xi}(t)$, which are determined by solving Eq. (3) for each given boundary condition, will be the input for the CACC driving-states prediction model of Section 3.1.3.

3.4. Predictive uncertain driving state reference for the controlled vehicles by a CACC driving policy

This section presents a CACC policy for obtaining a set of predictive driving references for the controlled vehicle, given the set of IPV driving states from Section 3.1.2. As Fig. 6 shows, we can obtain a set of reference driving states of the controlled vehicles through a CACC driving policy based on a set of predicted driving states of the BCPVs. Given any predicted driving state $\hat{l}_0^{\xi}(t)$ and $\hat{v}_0^{\xi}(t)$ of the IPV derived from a boundary condition and observed connected data, we predict the driving

state reference of the controlled vehicles over a prediction horizon based on the CACC driving policy (see the middle plot in Fig. 6). In this paper, we formulate the CACC driving policy as a constrained FHOC (i.e. Finite-Horizon Optimal Control) problem in Eqs. (4)–(10). We also compare our FHOC-based CACC driving policy with a microscopic traffic simulation–based CACC driving policy, the MICroscopic model for Simulation of Intelligent Cruise control (MIXIC) model (Van Arem et al., 2006), which is based on the closed-form CACC controller in VanderWerf et al. (2001).

$$\min_{u} \sum_{t=k}^{k+PH} \left\{ \begin{array}{l} \left\{ \left[\hat{l}_0^{\xi}(t) - l_1(t) - \tau^h \times v_1(t) \right]^2 + \left[\hat{v}_0^{\xi}(t) - v_1(t) \right]^2 + [u_1(t)]^2 \right\} \\ + \sum_{n=2}^{N} \left\{ \left[l_{n-1}(t) - l_n(t) - \tau^h \times v_n(t) \right]^2 + [v_{n-1}(t) - v_n(t)]^2 + [u_n(t)]^2 \right\} \end{array} \right\} \tag{4}$$

s.t.

$$l_n(t) = l_n^{obs}(k), v_n(t) = v_n^{obs}(k), \forall n = 1, \ldots, N, \ t = k \tag{5}$$

$$l_n(t+1) = l_n(t) + \Delta t \times v_n(t) + \frac{1}{2}\Delta t^2 \times u_n(t), \forall n = 1, \ldots, N, t = k, \ldots, k + PH \tag{6}$$

$$v_n(t+1) = v_n(t) + \Delta t \times u_n(t), \forall n = 1, \ldots, N, t = k, \ldots, k + PH \tag{7}$$

$$l_{n-1}(t) - l_n(t) \geq \tau^{min} \times v_n(t) + s_n^{min}, \forall n = 2, \ldots, N, t = k+1, \ldots, k + PH \tag{8}$$

$$\hat{l}_0^{\xi}(t) - l_1(t) \geq \tau^{min} \times v_1(t) + s_n^{min}, \forall t = k+1, \ldots, k + PH \tag{9}$$

$$u_n^{min} \leq u_n(t) \leq u_n^{max}, 0 \leq v_n(t) \leq v^{limit}(t), \forall n = 1, \ldots, N, t = k, \ldots, k + PH \tag{10}$$

where $\hat{l}_0^{\xi}(t)$ and $\hat{v}_0^{\xi}(t)$ are the predicted position and velocity of the IPV from historical observations for the predicted driving states of the BCPV of Section 3.1.1.

The objective function in Eq. (4) has two parts designed to regulate the CACC driving of the leading controlled vehicle and the following controlled vehicles, respectively. In each part, the three terms are minimized to maintain a constant-time-headway policy, driving stability, and driving comfort. The constraints in Eq. (5) set the initial conditions of vehicle longitudinal positions and velocities. Eq. (6) is the longitudinal position dynamic constraint. Eq. (7) is the velocity dynamic constraint. The controlled vehicle safety constraints in Eq. (8) and Eq. (9) guarantee minimum spacing by a given minimum safe time headway (for moving vehicles) and a given minimum safe spacing (for stopped vehicles considering vehicle length) for the following controlled vehicles and the leading controlled vehicle, respectively. These two constraints will avoid collisions, even when vehicle velocities are close to zero. Eq. (10) represents the acceleration or deceleration capability constraint and the speed-limit constraint.

By solving Eqs. (4)–(10) at time step k with the predicted driving states $\hat{l}_0^{\xi}(t)$ and $\hat{v}_0^{\xi}(t)$ of the IPV, we will obtain the predicted driving states of the controlled vehicles: $\hat{l}_n^{\xi}(t)$ and $\hat{v}_n^{\xi}(t)$. We repeat the steps of Section 3.1.2 and Section 3.1.3 for the rest of the boundary conditions from Section 3.1.1 to generate a set of predicted driving states of the controlled vehicles during the prediction horizon $[k, k + PH]$. The set of predicted driving states $\hat{l}_n^{\xi}(t)$ and $\hat{v}_n^{\xi}(t)$ will be the reference state in the tracking term of the DRSO-DRCC–based MPC model in Section 3.2.

In addition to the FHOC model in Eqs. (4)–(10), we can implement a microscopic traffic simulation model, MIXIC (Van Arem et al., 1997, 2006), in Eq. (11) to estimate the CACC driving states of the controlled vehicles:

$$\begin{aligned} u_n(t) &= \min\left[u_n^{M,a}(t), u_n^{M,b}(t)\right] u_n^{M,a}(t) = k^M \times \left[v_n^{M,des} - v_n(t)\right] \\ u_n^{M,b}(t) &= k_a^M \times u_{n-1}(t) + k_v^M \times [v_{n-1}(t) - v(t)] + k_d^M \times \left[g_n(t) - g_n^{N,des}\right] \end{aligned} \tag{11}$$

where $v_n^{M,des}$ is the given desired velocity (e.g. the speed limit), $v(t)$ is the current velocity, $u_{n-1}(t)$ is the acceleration of its preceding vehicle, $v_{n-1}(t)$ is the velocity of the preceding vehicle, $g_n(t)$ is the current distance gap to the preceding vehicle, and $g_n^{N,des}$ is the desired distance gap to the preceding vehicle. Note that k^M, k_a^M, k_v^M, and k_d^M are constant factors to be calibrated. In our paper, we apply the MIXIC model to predict the homogeneous driving behaviors of the controlled vehicles using a set of given constant factors.

3.5. A DRSO-DRCC–based MPC model for CACC problem under uncertain traffic conditions

In this section, we formulate the CACC control problem under uncertain traffic conditions as a DRSO-DRCC model in Eqs. (12)–(18). At each time step k, we solve the DRSO-DRCC model in the data-driven optimization-based MPC modeling framework. At time step k, we predict the driving states of the IPV and controlled vehicles over the prediction horizon $[k, k + PH]$ by the steps outlined in Section 3.1. The predicted driving states will be used as the input for the DRSO-DRCC model.

We then solve a minimax program in the DRSO-DRCC model to obtain the optimal acceleration or deceleration commands for the controlled vehicles over the prediction horizon $[k, k + PH]$.

$$\min_{u}\left[\begin{array}{l}\max\limits_{\boldsymbol{F}_p\in\mathbb{D}_p}\mathbb{E}_{\boldsymbol{F}_p}\left[\sum\limits_{t=k}^{k+PH}\left\{\left[\hat{l}_0^{\xi}(t)-l_1(t)-\tau^h\times v_1(t)\right]^2+\left[\hat{v}_0^{\xi}(t)-v_1(t)\right]^2+[u_1(t)]^2\right\}\right]\\ +\max\limits_{\boldsymbol{F}_r\in\mathbb{D}_r}\mathbb{E}_{\boldsymbol{F}_r}\left[\sum\limits_{t=k}^{k+PH}\sum\limits_{n=1}^{N}\left\{\left[l_n(t)-\hat{l}_n^{\xi}\right]^2+\left[v_n(t)-\hat{v}_n^{\xi}\right]^2\right\}\right]\\ +\sum\limits_{t=k}^{k+PH}\sum\limits_{n=2}^{N}\left\{\left[l_{n-1}(t)-l_n(t)-\tau^h\times v_n(t)\right]^2+[v_{n-1}(t)-v_n(t)]^2+[u_n(t)]^2\right\}\end{array}\right] \tag{12}$$

s.t.

$$l_n(t)=l_n^{obs}(k),\ v_n(t)=v_n^{obs}(k),\ \forall n=1,\ldots,N,\ t=k \tag{13}$$

$$l_n(t+1)=l_n(t)+\Delta t\times v_n(t)+\frac{1}{2}\Delta t^2\times u_n(t),\ \forall n=1,\ldots,N,\ t=k,\ldots,k+PH \tag{14}$$

$$v_n(t+1)=v_n(t)+\Delta t\times u_n(t),\ \forall n=1,\ldots,N,\ t=k,\ldots,k+PH \tag{15}$$

$$l_{n-1}(t)-l_n(t)\geq\tau^{min}\times v_n(t)+s_n^{min},\ \forall n=2,\ldots,N,\ t=k+1,\ldots,k+PH \tag{16}$$

$$\inf_{\boldsymbol{F}_p\in\mathbb{D}_p}\mathbb{P}_{\boldsymbol{F}_p}\left[\hat{l}_0^{\xi}(t)-l_1(t)\geq\tau^{min}\times v_1(t)+s_n^{min}\right]\geq\gamma_p,\ \hat{l}_0^{\xi}(t)\sim\boldsymbol{F}_p,\ \forall t=k+1,\ldots,k+PH \tag{17}$$

$$u_n^{min}\leq u_n(t)\leq u_n^{max},\ 0\leq v_n(t)\leq v^{limit}(t),\ \forall n=1,\ldots,N,\ t=k,\ldots,k+PH \tag{18}$$

where $u_n(t)$ is the decision variable $l_n(t)$ and $v_n(t)$ are the state variables. $l_n^{\xi}(t)$ and $v_n^{\xi}(t)$ are the random parameters, which can be represented as $\boldsymbol{x}^{\xi}(t)=\{[l_n^{\xi}(t),v_n^{\xi}(t)]^T|\forall n=0,\ldots,N\}$. In a DRSO model, we estimate the support of $l_n^{\xi}(t)$ and $v_n^{\xi}(t)$ from observations such that the random parameters take values in the set of observations $\Xi=\{[\ \hat{l}_n^{\xi_i}(t)\quad\hat{v}_n^{\xi_i}(t)\ ]^T|\forall n=0,\ldots,N,\forall i=1,\ldots,M\}$ with M samples. In the DRSO formulation, $\hat{l}_n^{\xi_i}(t)$ and $\hat{v}_n^{\xi_i}$ are the predicted driving states using historical observations (Delage and Ye, 2010).

The objective function Eq. (12) has two minimax terms and one minimization term. The first minimax term describes the CACC driving objective for the leading controlled vehicle. The second minimax term is designed to minimize the worst-case tracking deviation between the controlled driving states and the predicted reference driving states of all the controlled vehicles based on a CACC driving policy described in Section 3.1.3. The deterministic term is designed to regulate CACC driving for the following controlled vehicles. The first minimax term and the deterministic minimization term maintain the constant-time-headway policy, driving stability, and driving comfort. Note that we can combine the two minimax terms in Eq. (12) into one single term by incorporating data-driven uncertainty sets $\mathbb{D}_p$ and $\mathbb{D}_r$ in one single set $\mathbb{D}$ (Section 4.1). In this objective function, we consider the penalty weights for various terms (i.e. constant-time-headway policy, driving stability, the driving comfort) as one. We can, however, use different values for the penalty weights in the proposed model based on realistic CACC control requirements.

We apply a data-driven uncertainty set to define a set of probability distributions with support in Ξ for $\boldsymbol{x}_p^{\xi}(t)=[l_0^{\xi}(t),v_0^{\xi}(t)]^T$, given that it follows the probability distribution $\boldsymbol{F}_p$. In DRSO models, one must estimate the first and second moments from limited historical observations assumed to be drawn from the probability distribution $\boldsymbol{F}_p$. Based on the observations $\{[\ \hat{l}_0^{\xi_i}(t)\quad\hat{v}_0^{\xi_i}(t)\ ]^T|\forall i=1,\ldots,M\}$, $\mathbb{D}_p$ is defined as the data-driven uncertainty set of the random parameters $\boldsymbol{x}_p^{\xi}(t)$ for the IPV.

$$\mathbb{D}_p\left(S,\hat{\boldsymbol{\mu}}_{\boldsymbol{p}},\hat{\boldsymbol{\Sigma}}_{\boldsymbol{p}},\gamma_1,\gamma_2\right)=\left\{\begin{array}{c}P\left(\hat{\boldsymbol{x}}_p^{\xi}(t)\in\boldsymbol{S}\right)=1\\ \left(\mathbb{E}\left[\hat{\boldsymbol{x}}_p^{\xi}(t)\right]-\hat{\boldsymbol{\mu}}_{\boldsymbol{p}}\right)^T\hat{\boldsymbol{\Sigma}}_{\boldsymbol{p}}^{-1}\left(\mathbb{E}\left[\hat{\boldsymbol{x}}_p^{\xi}(t)\right]-\hat{\boldsymbol{\mu}}_{\boldsymbol{p}}\right)\leq\gamma_1\\ E\left[\left(\hat{\boldsymbol{x}}_p^{\xi}(t)-\hat{\boldsymbol{\mu}}_{\boldsymbol{p}}\right)\left(\hat{\boldsymbol{x}}_p^{\xi}(t)-\hat{\boldsymbol{\mu}}_{\boldsymbol{p}}\right)^T\right]\preccurlyeq\gamma_2\hat{\boldsymbol{\Sigma}}_{\boldsymbol{p}}\end{array}\right\} \tag{19}$$

In Eq. (19), we use the constraint parameter $\gamma_1\geq 0$ such that the mean of $\boldsymbol{x}_p^{\xi}$ lies in an ellipsoid of size γ_1 centered at the estimate $\hat{\boldsymbol{\mu}}_{\boldsymbol{p}}$. We use the constraint parameter $\gamma_2\geq 1$ such that the second-moment matrix of $\boldsymbol{x}_p^{\xi}$ lies in a positive semidefinite cone defined with a matrix inequality. It describes how likely $\boldsymbol{x}_p^{\xi}$ is to be close to the estimate $\hat{\boldsymbol{\mu}}_{\boldsymbol{p}}$ with respect to the correlations expressed in $\hat{\boldsymbol{\Sigma}}_{\boldsymbol{p}}$ (Delage and Ye, 2010).

Similarly, based on historical observations $\{[\ \hat{l}_n^{\xi^i}(t)\quad \hat{v}_n^{\xi^i}(t)\ ]^T | \forall n = 1,\ldots,N, \forall i = 1,\ldots,M\}$, we define $\boldsymbol{F}_r$ as the probability distribution and $\mathbb{D}_r$ as the data-driven uncertainty set of the random parameters $\boldsymbol{x}_r^{\xi}(t) = [l_1^{\xi}(t), v_1^{\xi}(t), \ldots, l_N^{\xi}(t), v_N^{\xi}(t)]^T$ of the controlled vehicles in Eq. (20).

$$\mathbb{D}_r\left(S, \hat{\boldsymbol{\mu}}_{\boldsymbol{r}}, \hat{\boldsymbol{\Sigma}}_{\boldsymbol{r}}, \gamma_1, \gamma_2\right) = \left\{ \begin{array}{c} P\left(\hat{\boldsymbol{x}}_r^{\xi}(t) \in \boldsymbol{S}\right) = 1 \\ \left(\mathbb{E}\left[\hat{\boldsymbol{x}}_r^{\xi}(t)\right] - \hat{\boldsymbol{\mu}}_{\boldsymbol{r}}\right)^T \hat{\boldsymbol{\Sigma}}_{\boldsymbol{r}}^{-1} \left(\mathbb{E}\left[\hat{\boldsymbol{x}}_r^{\xi}(t)\right] - \hat{\boldsymbol{\mu}}_{\boldsymbol{r}}\right) \leq \gamma_1 \\ E\left[\left(\hat{\boldsymbol{x}}_r^{\xi}(t) - \hat{\boldsymbol{\mu}}_{\boldsymbol{r}}\right)\left(\hat{\boldsymbol{x}}_r^{\xi}(t) - \hat{\boldsymbol{\mu}}_{\boldsymbol{r}}\right)^T\right] \preccurlyeq \gamma_2 \hat{\boldsymbol{\Sigma}}_{\boldsymbol{r}} \end{array} \right\} \tag{20}$$

The constraints in Eq. (13) represent the initial conditions of vehicle longitudinal positions and velocities. Eq. (14) is the longitudinal position dynamic constraint. Eq. (15) is the velocity dynamic constraint. The constraint in Eq. (16) guarantees a safe distance by considering a given minimum time headway and a given minimum safe spacing. Eq. (18) represents the acceleration or deceleration capability constraint and the speed-limit constraint.

We apply the DRCC constraint in Eq. (17) to deal with the uncertainty of the predicted driving states of the IPV in the leading controlled vehicle safety constraint. Using this constraint, we obtain the restrictions on state variables $l_1(t)$ and $v_1(t)$ such that the probability of the leading controlled vehicle's safety achieves a certain threshold. In this paper, we assume that the distribution of $\hat{l}_0^{\xi}(t)$ is not known in advance owing to uncertainties. The first two moments (i.e. the mean and the covariance) can, however, be estimated from historical observations.

3.6. Stability analysis of the DRSO-DRCC–based MPC model

This section presents a stability analysis method for the proposed DRSO-DRCC–based MPC model. Vehicle driving controllers based on car-following models generally have the low-pass filtering property (Li et al., 2012; Boashash, 2015). The disturbance in the frequency domain is likely to be dampened by the low-pass filter (Slotine and Li 1991; Qian and Schutter, 1992). However, MPC-based CACC controllers with multiple objective terms and constraints are not low-pass filters in nature (Camacho and Alba, 2013). Reflecting concerns for safety, tracking deviations (especially spacing deviation) between the controlled spacing and the desired spacing in MPC-based controllers should not be amplified downstream from vehicle to vehicle (Swaroop and Hedrick, 1996). String stability is elementary in the performance measurement of CACC controllers based on closed-form optimal control or MPC-based control models, which can be theoretically proved or empirically evaluated based on the Lyapunov function (Lyapunov, 1992; Mayne et al., 2000).

The Lyapunov function has been used to derive a control law of CAV driving that reduces spacing deviations in CAV driving control problems (Stotsky et al., 1995; No et al., 2001). Consequently, Lyapunov stability is used to describe the string stability of dynamic systems with initial-condition perturbations (Lu et al., 2002; Ploeg et al., 2014). Based on Lyapunov stability, some studies measure stability conditions of CAV driving using the spacing deviations between driving states and the desired driving states of controlled vehicles (Stotsky et al., 1995; Dunbar and Caveney, 2012; Oncu et al., 2012). The Lyapunov-based methods for analyzing the string stability of CACC controllers include time-domain methods (Stotsky et al., 1995; Dunbar and Caveney, 2012; Alipour-Fanid et al., 2017) and frequency-domain methods (Ward, 2009; Kianfar et al., 2012; Naus et al., 2010; Talebpour and Mahmassani, 2016).

With time-domain methods, string stability is measured by the response of a vehicle in a string to its leader's sudden break. If the perturbation decays as it propagates along the string upstream, it is then called string-stable (Ploeg et al., 2011). String stability can be empirically evaluated using partial differential equations of accelerations (Ward, 2009; Talebpour and Mahmassani, 2016) and proved based on the Lyapunov theory (Li and Shrivastava, 2002; Li et al., 2013) for car-following models or closed-form optimal control models. For receding horizon control or MPC-based optimal control models, string stability can be theoretically proved based on Lyapunov functions (Grüne, 2009; Grüne and Stieler, 2014) or empirically evaluated by measuring the propagation of spacing or acceleration deviations (Stotsky et al., 1995; Dunbar and Caveney, 2012). In this paper, we will show the acceleration, spacing, and velocity patterns of the controlled vehicles to evaluate the stability of the proposed data-driven optimization-based MPC model in the time domain.

String stability cannot be well elaborated in the time domain under traffic oscillations, however, owing to local random perturbations (Li et al., 2010). Herman et al. (1959) use a frequency-domain method to measure local string stability under traffic oscillations. In this paper, the CACC driving trajectories are long enough to include periodic patterns so we can measure the oscillation amplitude for string-stability analysis using the Discrete Fourier Transform (DFT). The constant-time-headway policy in the proposed DRSO-DRCC–based MPC model in Section 3.2 requires reducing the spacing deviation to achieve string stability. Therefore, we also apply the DFT to the spacing deviations of the control vehicles to evaluate string stability in the frequency domain (Rhoades et al., 2016).

Spacing deviations in this paper are determined by calculating the difference between observed spacing and desired spacing. The spacing deviation of the controlled vehicles in the time domain is expressed in Eq. (21).

$$\delta_n(t) = l_{n-1}(t) - l_n(t) - L_n - \tau^h \times v_n(t), \forall n = 1,\ldots,N \tag{21}$$

To evaluate the frequency-domain spacing deviations, we use the transfer function of spacing deviations to Fourier transforms using the DFT in the frequency domain in Eq. (22).

$$E_n(\omega) = \sum_t \delta_n(t) e^{-i\omega t}, \forall \omega \in [0, \pi], i = \sqrt{-1}, \forall n = 1, \ldots, N \tag{22}$$

As string stability concerns the amplification of signals (i.e. spacing deviations) along with the controlled CAVs, we focus on the magnitude of the string-stability transfer function to analyze string stability in the frequency domain (Vugts, 2010; Alipour-Fanid et al., 2017; Sun et al., 2018). We use the transfer function of string stability for the proposed model using the spacing deviations of two neighboring vehicles in Eq. (23).

$$|\Gamma_n(\omega)| = \left| \frac{E_n(\omega)}{E_{n-1}(\omega)} \right|, \forall \omega \in [0, \pi], \forall n = 1, \ldots, N \tag{23}$$

where $E_n(\omega)$ and $E_{n\_1}(\omega)$ comprise the Fourier transformation of the spacing deviation of the controlled vehicle n and its IPV $n-1$, respectively.

4. Model reformulation and solution method

This section presents model reformulations and a solution method for obtaining tractable solutions that can be applied in real-time under certain settings. The DRSO-DRCC model formulation of Section 3.2 cannot be directly solved by existing solvers. Moreover, the original minimax problem constrained by a DRCC constraint is computationally expensive (Shapiro and Nemirovski, 2005; Goh and Sim, 2010; Zymler et al., 2013) and is not suitable for real-time applications. In Section 4.1, for the sake of simplicity, we present the matrix form of the DRSO-DRCC model as a standard SDP form. Based on the standard SDP form, in Section 4.2, we reformulate the DRSO-DRCC model as a tractable relaxed SDP model. Specifically, in Section 4.2.1, we replace the DRCC constraint in the DRSO-DRCC model by an equivalent deterministic convex constraint based on historical sample data (Calafiore and El Ghaoui, 2006; Jiang and Guan, 2016). In Sections 4.2.2–4.2.4, we reformulate the DRSO model by applying the strong duality theory and the Semidefinite Relaxation technique (Delage and Ye, 2010; Bertsimas et al., 2011). A solution method is presented in Section 4.3 to solve the reformulated model (i.e. a relaxed SDP problem).

4.1. Matrix form of the DRSO-DRCC model

To succinctly and concisely express the proposed DRSO-DRCC model of Section 3.2, we formulate Eqs. (12)–(18) in matrix form. Consider two matrices $\boldsymbol{Q}_{\boldsymbol{p}}^{\boldsymbol{\xi}}$ and $\boldsymbol{Q}_{\boldsymbol{p}}$ for the constant-time-headway policy and driving stability in the objective with respect to the leading controlled vehicle:

$$\boldsymbol{Q}_{\boldsymbol{p}}^{\boldsymbol{\xi}} = \begin{bmatrix} \begin{bmatrix} 1 & 0 \\ 0 & 1 \end{bmatrix} & & 0 \\ & 0 & \\ & & \end{bmatrix}_{(2N+2)\times(2N+2)} \tag{24}$$

$$\boldsymbol{Q}_{\boldsymbol{p}} = \begin{bmatrix} \begin{bmatrix} 1 & \tau^h \\ 0 & 1 \end{bmatrix} & & 0 \\ & 0 & \\ & & \end{bmatrix}_{(2N+2)\times 2N} \tag{25}$$

We then define two matrices $\boldsymbol{Q}_{\boldsymbol{r}}^{\boldsymbol{\xi}}$ and $\boldsymbol{Q}_{\boldsymbol{r}}$ for reference tracking under uncertainties for the predicted driving states of the controlled vehicles in the objective function Eq. (12):

$$\boldsymbol{Q}_{\boldsymbol{r}}^{\boldsymbol{\xi}} = \begin{bmatrix} 0 & \boldsymbol{I}_{2N\times 2N} \end{bmatrix}_{2N\times(2N+2)} \tag{26}$$

$$\boldsymbol{Q}_{\boldsymbol{r}} = \begin{bmatrix} 1 & 0 & -1 & 0 & 0 & 0 & \ldots & 0 & 0 & 0 & 0 \\ 0 & 1 & 0 & -1 & 0 & 0 & \ldots & 0 & 0 & 0 & 0 \\ -1 & 0 & 2 & 0 & -1 & 0 & \ldots & 0 & 0 & 0 & 0 \\ 0 & -1 & 0 & 2 & 0 & -1 & \ldots & 0 & 0 & 0 & 0 \\ 0 & 0 & -1 & 0 & 2 & 0 & \cdots & 0 & 0 & 0 & 0 \\ 0 & 0 & 0 & -1 & 0 & 2 & \ldots & 0 & 0 & 0 & 0 \\ \vdots & \vdots & \vdots & \vdots & \vdots & \vdots & \ddots & \vdots & \vdots & \vdots & \vdots \\ 0 & 0 & 0 & 0 & 0 & 0 & 0 & 2 & 0 & -1 & 0 \\ 0 & 0 & 0 & 0 & 0 & 0 & 0 & 0 & 2 & 0 & -1 \\ 0 & 0 & 0 & 0 & 0 & 0 & 0 & -1 & 0 & 1 & 0 \\ 0 & 0 & 0 & 0 & 0 & 0 & 0 & 0 & -1 & 0 & 1 \end{bmatrix}_{2N\times 2N} \tag{27}$$

We define a matrix $\boldsymbol{Q}$ for the constant-time-headway policy and the driving stability of the controlled vehicles in the objective function Eq. (12):

(28)

For the driving comfort of all the controlled vehicles in the objective function Eq. (12), we define a matrix $\boldsymbol{R}$. In this paper we let the matrix $\boldsymbol{R}$ be equal to an identity matrix, as we want only to reduce acceleration or deceleration perturbations.

$$\boldsymbol{R} = \boldsymbol{I}_{N\times N} \tag{29}$$

Furthermore, we define two matrices $\boldsymbol{A}$ and $\boldsymbol{B}$ for the state dynamic constraints in Eqs. (14)–(15):

$$\boldsymbol{A} = \begin{bmatrix} 1 & \Delta t & 0 & 0 & \dots & 0 & 0 \\ 0 & 1 & 0 & 0 & \dots & 0 & 0 \\ 0 & 0 & 1 & \Delta t & \dots & 0 & 0 \\ 0 & 0 & 0 & 1 & \dots & 0 & 0 \\ \vdots & \vdots & \vdots & \vdots & \dots & \vdots & \vdots \\ 0 & 0 & 0 & 0 & \dots & 1 & \Delta t \\ 0 & 0 & 0 & 0 & \dots & 0 & 1 \end{bmatrix}_{2N\times 2N} \tag{30}$$

$$\boldsymbol{B} = \begin{bmatrix} \frac{\Delta t^2}{2} & 0 & \dots & 0 \\ \Delta t & 0 & \dots & 0 \\ 0 & \frac{\Delta t^2}{2} & \dots & 0 \\ 0 & \Delta t & \dots & 0 \\ \vdots & \vdots & \dots & \vdots \\ 0 & 0 & \dots & \frac{\Delta t^2}{2} \\ 0 & 0 & \dots & \Delta t \end{bmatrix}_{2N\times N} \tag{31}$$

We define two matrices $\boldsymbol{K_f}$ and $\boldsymbol{G_f}(t)$ for the following vehicle state constraints, i.e. the safety and speed limit constraints in Eqs. (16) and (18):

$$\boldsymbol{K_f} = \begin{bmatrix} \begin{bmatrix} -1 & 0 & 1 & \tau^{min} & 0 & 0 & \cdots & 0 & 0 & 0 & 0 \\ 0 & 0 & -1 & 0 & 1 & \tau^{min} & \dots & 0 & 0 & 0 & 0 \\ \vdots & \vdots & \vdots & \vdots & \vdots & \vdots & \dots & \vdots & \vdots & \vdots & \vdots \\ 0 & 0 & 0 & 0 & 0 & 0 & \dots & -1 & 0 & 1 & \tau^{min} \end{bmatrix}_{(2N-2)\times 2N} \\ \begin{bmatrix} 0 & 1 & 0 & 0 & 0 & 0 & \dots & 0 & 0 & 0 & 0 \\ 0 & 0 & 0 & 1 & 0 & 0 & \dots & 0 & 0 & 0 & 0 \\ \vdots & \vdots & \vdots & \vdots & \vdots & \vdots & \dots & \vdots & \vdots & \vdots & \vdots \\ 0 & 0 & 0 & 0 & 0 & 0 & \dots & 0 & 0 & 0 & 1 \end{bmatrix}_{N\times 2N} \end{bmatrix}_{(3N-2)\times 2N} \tag{32}$$

$$\boldsymbol{G_f}(t) = \begin{bmatrix} s_2^{min} \\ \vdots \\ s_n^{min}{}_{(2N-2)\times 1} \\ v^{limit}(t)_{N\times 1} \end{bmatrix}_{(3N-2)\times 1} \tag{33}$$

We define two matrices $\boldsymbol{K_l}$ and $\boldsymbol{G_l}$ for the DRCC constraint in Eq. (17):

$$\boldsymbol{K_l} = \begin{bmatrix} 1 & \tau^{min} & 0_{1\times(2N-2)} \end{bmatrix}_{1\times 2N} \tag{34}$$

$$\boldsymbol{G_l} = \begin{bmatrix} -1 & 0 \end{bmatrix}_{1\times 2} \tag{35}$$

With the matrices mentioned above, we reformulate the DRSO-DRCC model of Eqs. (12)–(18) as:

$$\min_{\boldsymbol{u}} \left\{ \begin{array}{c} \max\limits_{\boldsymbol{F}_p\in\mathbb{D}_p} \sum\limits_{t=k}^{k+PH} \mathbb{E}_{\boldsymbol{F}_p}\left[\boldsymbol{Q}_p^{\xi}\hat{\boldsymbol{x}}^{\xi}(t) - \boldsymbol{Q}_p\boldsymbol{x}(t)\right]^{\boldsymbol{T}}\left[\boldsymbol{Q}_p^{\xi}\hat{\boldsymbol{x}}^{\xi}(t) - \boldsymbol{Q}_p\boldsymbol{x}(t)\right] \\ +\max\limits_{\boldsymbol{F}_r\in\mathbb{D}_r} \sum\limits_{t=k}^{k+PH} \mathbb{E}_{\boldsymbol{F}_r}\left[\boldsymbol{Q}_r^{\xi}\hat{\boldsymbol{x}}^{\xi}(t) - \boldsymbol{x}(t)\right]^{\boldsymbol{T}}\boldsymbol{Q}_r\left[\boldsymbol{Q}_r^{\xi}\hat{\boldsymbol{x}}^{\xi}(t) - \boldsymbol{x}(t)\right] \\ +[\boldsymbol{x}(t)]^{\boldsymbol{T}}Qx(t) \\ +[\boldsymbol{u}(t)]^{\boldsymbol{T}}Ru(t) \end{array} \right\} \tag{36}$$

s.t.

$$\boldsymbol{x}(t) = \boldsymbol{x}^{obs}(k), t = k \tag{37}$$

$$\boldsymbol{x}(t+1) = \boldsymbol{A}\boldsymbol{x}(t) + \boldsymbol{B}\boldsymbol{u}(t), \forall t = k, \ldots, k+PH \tag{38}$$

$$\boldsymbol{K}_{\boldsymbol{f}}\boldsymbol{x}(t) \leq \boldsymbol{G}_{\boldsymbol{f}}(t), \forall t = k, \ldots, k+PH \tag{39}$$

$$\boldsymbol{u}^{min} \leq \boldsymbol{u}(t) \leq \boldsymbol{u}^{max}, \forall t = k, \ldots, k+PH \tag{40}$$

$$\begin{aligned} &\inf_{\boldsymbol{F}_p \in \mathbb{D}_p} \mathbb{P}_{\boldsymbol{F}_p}\left(\boldsymbol{K}_{\boldsymbol{l}}\boldsymbol{x}(t) + \boldsymbol{G}_{\boldsymbol{l}}\hat{\boldsymbol{x}}_p^{\xi}(t) \leq -s_n^{min}\right) \geq \gamma_p, \forall t = k, \ldots, k+PH \\ &\mathbb{D}_p\left(S, \hat{\boldsymbol{\mu}}_{\boldsymbol{p}}, \hat{\boldsymbol{\Sigma}}_{\boldsymbol{p}}, \gamma_{p,1}, \gamma_{p,2}\right) = \left\{ \begin{array}{c} P\left(\hat{\boldsymbol{x}}_p^{\xi}(t) \in \boldsymbol{S}\right) = 1 \\ \left(\mathbb{E}\left[\hat{\boldsymbol{x}}_p^{\xi}(t)\right] - \hat{\boldsymbol{\mu}}_{\boldsymbol{p}}\right)^T \hat{\boldsymbol{\Sigma}}_{\boldsymbol{p}}^{-1}\left(\mathbb{E}\left[\hat{\boldsymbol{x}}_p^{\xi}(t)\right] - \hat{\boldsymbol{\mu}}_{\boldsymbol{p}}\right) \leq \gamma_{p,1} \\ E\left[\left(\hat{\boldsymbol{x}}_p^{\xi}(t) - \hat{\boldsymbol{\mu}}_{\boldsymbol{p}}\right)\left(\hat{\boldsymbol{x}}_p^{\xi}(t) - \hat{\boldsymbol{\mu}}_{\boldsymbol{p}}\right)^T\right] \preccurlyeq \gamma_{p,2}\hat{\boldsymbol{\Sigma}}_{\boldsymbol{p}} \end{array} \right\} \end{aligned} \tag{41}$$

$$\mathbb{D}_r\left(S, \hat{\boldsymbol{\mu}}_{\boldsymbol{r}}, \hat{\boldsymbol{\Sigma}}_{\boldsymbol{r}}, \gamma_{r,1}, \gamma_{r,2}\right) = \left\{ \begin{array}{c} P\left(\hat{\boldsymbol{x}}_r^{\xi}(t) \in \boldsymbol{S}\right) = 1 \\ \left(\mathbb{E}\left[\hat{\boldsymbol{x}}_r^{\xi}(t)\right] - \hat{\boldsymbol{\mu}}_{\boldsymbol{r}}\right)^T \hat{\boldsymbol{\Sigma}}_{\boldsymbol{r}}^{-1}\left(\mathbb{E}\left[\hat{\boldsymbol{x}}_r^{\xi}(t)\right] - \hat{\boldsymbol{\mu}}_{\boldsymbol{r}}\right) \leq \gamma_{r,1} \\ E\left[\left(\hat{\boldsymbol{x}}_r^{\xi}(t) - \hat{\boldsymbol{\mu}}_{\boldsymbol{r}}\right)\left(\hat{\boldsymbol{x}}_r^{\xi}(t) - \hat{\boldsymbol{\mu}}_{\boldsymbol{r}}\right)^T\right] \preccurlyeq \gamma_{r,2}\hat{\boldsymbol{\Sigma}}_{\boldsymbol{r}} \end{array} \right\} \tag{42}$$

where $\boldsymbol{u}$ in the objective function represents acceleration or deceleration as the control variable. $\boldsymbol{F}_p$ and $\boldsymbol{F}_r$ are the probability distributions of the random parameters $\boldsymbol{x}_p^{\xi}$ and $\boldsymbol{x}_r^{\xi}$, respectively. Eq. (37) is the initial-condition constraint using the observation at time k. Eq. (38) is the state dynamics constraint. Eq. (39) is the state constraint in terms of inter-vehicle safety and speed limits. Eq. (40) is the acceleration or deceleration capability constraint. Eq. (41) is the DRCC constraint designed to deal with the uncertainty of the predicted driving states of the IPV in the leading controlled vehicle safety constraint. Eq. (42) contains the data-driven uncertainty set constraints for the random state variables $\boldsymbol{x}_p^{\xi}$ and $\boldsymbol{x}_r^{\xi}$, respectively.

For the data-driven uncertainty set $\mathbb{D}_p$, we use the constraint parameter $\gamma_{p,1} \geq 0$ such that the mean of $\boldsymbol{x}_p^{\xi}$ lies in an ellipsoid of size $\gamma_{p,1}$ centered at the estimate $\hat{\boldsymbol{\mu}}_{\boldsymbol{p}}$. We use the constraint parameter $\gamma_{p,2} \geq 1$ such that the second-moment matrix of $\boldsymbol{x}_p^{\xi}$ lies in a positive semidefinite cone defined with a matrix inequality. It describes how likely $\boldsymbol{x}_p^{\xi}$ is to be close to the estimate $\hat{\boldsymbol{\mu}}_{\boldsymbol{p}}$ with respect to the correlations expressed in $\hat{\boldsymbol{\Sigma}}_{\boldsymbol{p}}$ (Delage and Ye, 2010). Similarly, we apply $\gamma_{r,1} \geq 0$ and $\gamma_{r,2} \geq 1$ for the data-driven uncertainty set $\mathbb{D}_r$.

4.2. Model reformulation

This section reformulates the matrix-form DRSO-DRCC model of Section 4.1 into a relaxed SDP dual problem by applying the strong duality theory and the Semidefinite Relaxation technique. The original formulation with a DRCC constraint is difficult to solve because the empirical estimates are themselves random and cannot be used directly as the exact unknown mean and covariance (Calafiore and El Ghaoui, 2006). In addition, the original DRSO formulation of the problem is computationally expensive as a result of the minimax program (Shapiro and Nemirovski, 2005; Goh and Sim, 2010; Zymler et al., 2013). Applying the strong duality theory, the minimax program will be reformulated as a quadratically constrained minimization problem. The complexity of the quadratically constrained minimization problem is, however, unknown and therefore is still computationally expensive (Floudas and Visweswaran, 1995; Ye and Zhang, 2003; Luo et al., 2010).

To deal with the computational issue, the reformulations include four steps. First, in Section 4.2.1, we replace the DRCC constraint by a deterministic convex constraint. Second, we formulate the dual problem of the inner problem of the DRSO model of Section 4.2.2 by applying strong duality (Nilim and El Ghaoui, 2005). Third, in Section 4.2.3, we approximate the solution to the quadratically constrained dual problem in a numerically efficient way using the Semidefinite Relaxation technique (Luo et al., 2010). Fourth, in Section 4.2.4, we combine the original outer minimization problem with the relaxed SDP problem of the original inner maximization problem as a relaxed SDP counterpart to the original minimax program.

4.3. An equivalent convex constraint of the DRCC constraint

The DRCC constraint in Eq. (41) can be explicitly expressed as an explicit counterpart—a deterministic convex constraint (Calafiore and El Ghaoui, 2006). We believe that the data-driven uncertainty set $\mathbb{D}$ can be constructed using the mean and covariance information derived from observations.

Proposition 1. *For any given $\gamma_p \in (0, 1)$, the DRCC constraint $\inf_{F_p \in \mathbb{D}} \mathbb{P}_{F_p}(\boldsymbol{K_l x}(t) + \boldsymbol{G_l}\hat{\boldsymbol{x}}^{\xi}(t) \le -s_n^{min}) \ge \gamma_p$ is equivalent to the convex constraint:*

$$\sqrt{\left(\gamma_p/1-\gamma_p\right)\boldsymbol{G_l}\hat{\boldsymbol{\sigma}}_{00}(t)\boldsymbol{G_l}^{\boldsymbol{T}}} + \begin{bmatrix} \boldsymbol{K_l} & \bar{\boldsymbol{x}}_p^{\xi}(t)^T \end{bmatrix}\begin{bmatrix} x(t) \\ \boldsymbol{G_l}^T \end{bmatrix} \le -s_n^{min} \tag{43}$$

where $\bar{\boldsymbol{x}}_p^{\xi}(t)$ is the mean and $\hat{\boldsymbol{\sigma}}_{00}(t)$ is the covariance matrix of $\{\hat{\boldsymbol{x}}_p^{\xi_i}(t) | \forall i = 1, \ldots, M\}$.

Proof. To prove that the DRCC constraint is equivalent to its deterministic convex counterpart, we apply the equivalent reformulation from Calafiore and El Ghaoui (2006) based on the one-sided Chebyshev inequality (Marshall and Olkin, 1960; Bertsimas and Popescu, 2005; Calafiore and El Ghaoui, 2006).

First, we express the DRCC constraint in Eq. (41) by:

$$\inf_{F_p \in \mathbb{D}} \mathbb{P}_{F_p}\left(\boldsymbol{K_l x}(t) + \left[\hat{x}^{\xi}(t)\right]^T \boldsymbol{G_l}^{\boldsymbol{T}} \le -s_n^{min}\right) \ge \gamma_p \tag{44}$$

We define the random vector $d = [\ \boldsymbol{k_l} \quad [\hat{\boldsymbol{x}}^{\xi}(t)]^T \boldsymbol{G_l}^T\ ]$ and $\tilde{x} = [\ \boldsymbol{x}(t) \quad 1\ ]^T$ so that the left-hand side of the DRCC constraint Eq. (44) can be expressed as $\varphi(\boldsymbol{x}) = d\tilde{\boldsymbol{x}}$.

Then, the mean of the random vector d is:

$$\bar{d} = \mathbb{E}[d] = \begin{bmatrix} \boldsymbol{K_l} & \boldsymbol{G_l}\bar{\boldsymbol{x}}^{\xi}(t) \end{bmatrix} \tag{45}$$

The covariance of the random vector d is:

$$\boldsymbol{\Gamma} = \mathrm{cov}[d] = \begin{bmatrix} \Gamma_{11} & \Gamma_{12} \\ \Gamma_{21} & \hat{\boldsymbol{\sigma}}_{00}(t) \end{bmatrix} \succcurlyeq 0 \tag{46}$$

where the mean $\bar{\boldsymbol{x}}^{\xi}(t)$ and covariance $\hat{\boldsymbol{\sigma}}_{00}(t)$ are calculated from data. In our problem, Γ_{11}, Γ_{12}, and Γ_{21} are constant because $\boldsymbol{K_l}$ is constant.

Furthermore, we have:

$$\bar{\varphi}(\boldsymbol{x}) = \mathbb{E}[\varphi(\boldsymbol{x})] = \bar{d}\tilde{\boldsymbol{x}} \tag{47}$$

The covariance matrix of the random variable is:

$$var[\varphi(\boldsymbol{x})] = \tilde{\boldsymbol{x}}^T \boldsymbol{\Gamma}\tilde{\boldsymbol{x}} = \boldsymbol{G_l}\hat{\boldsymbol{\sigma}}_{00}(t)\boldsymbol{G_l}^{\boldsymbol{T}} \tag{48}$$

Theorem 3.1 in Calafiore and El Ghaoui (2006) concludes that a convex constraint $\sqrt{\frac{\gamma}{1-\gamma} var[\varphi(\boldsymbol{x})]} + \bar{\varphi}(\boldsymbol{x}) \le 0$ is equivalent to $\inf_{d \sim (\bar{d}, \Gamma)} \mathbb{P}(d^{\boldsymbol{T}}\tilde{\boldsymbol{x}} \le 0) \ge \gamma$ for any $\gamma \in (0, 1)$ by applying the one-sided Chebyshev inequality (see detailed proofs in Marshall and Olkin, 1960; Propositions 6.3 and 6.4 in Bertsimas and Popescu, 2005; and Theorem 3.1 in Calafiore and El Ghaoui, 2006). We need to show that the equivalent condition to the DRCC constraint applies to our DRCC constraint in Eq. (44).

The equivalent convex constraint of Eq. (44) can be expressed in Eq. (49) based on Theorem 3.1 in Calafiore and El Ghaoui (2006):

$$\sqrt{\left(\gamma_p/1-\gamma_p\right)\tilde{\boldsymbol{x}}^T\boldsymbol{\Gamma}\tilde{\boldsymbol{x}}} + \bar{d}\tilde{\boldsymbol{x}} \le -s_n^{min}, \gamma_p \in (0, 1) \tag{49}$$

The equivalent convex constraint can be rewritten as Eq. (50) based on Eq. (48):

$$\sqrt{\left(\gamma_p/1-\gamma_p\right)\boldsymbol{G_l}\hat{\boldsymbol{\sigma}}_{00}(t)\boldsymbol{G_l}^{\boldsymbol{T}}} + \boldsymbol{K_l x}(t) + \boldsymbol{D}\bar{\boldsymbol{x}}_{\boldsymbol{p}}^{\xi}(t) \le -s_n^{min}, \gamma_p \in (0, 1) \tag{50}$$

Eq. (50) is the equivalent deterministic convex constraint of Eq. (44). This completes the proof.

The DRSO-DRCC model can then be reformulated in Eqs. (51)–(57) as an equivalent DRSO model by applying **Proposition 1** for the DRCC constraint:

$$\min_{\boldsymbol{u}} \max_{\boldsymbol{F} \in \mathbb{D} = \{\mathbb{D}_p, \mathbb{D}_r\}} \sum_{t=k}^{k+PH} \mathbb{E}_F \left\{ \begin{array}{c} \left[\boldsymbol{Q}_{\boldsymbol{p}}^{\xi}\hat{\boldsymbol{x}}^{\xi}(t) - \boldsymbol{Q_p x}(t)\right]^{\boldsymbol{T}}\left[\boldsymbol{Q}_{\boldsymbol{p}}^{\xi}\hat{\boldsymbol{x}}^{\xi}(t) - \boldsymbol{Q_p x}(t)\right] \\ +\left[\boldsymbol{Q}_{\boldsymbol{r}}^{\xi}\hat{\boldsymbol{x}}^{\xi}(t) - \boldsymbol{x}(t)\right]^{\boldsymbol{T}}\boldsymbol{Q_r}\left[\boldsymbol{Q}_{\boldsymbol{r}}^{\xi}\hat{\boldsymbol{x}}^{\xi}(t) - \boldsymbol{x}(t)\right] \\ +[\boldsymbol{x}(t)]^{\boldsymbol{T}}Qx(t) \\ +[\boldsymbol{u}(t)]^{\boldsymbol{T}}Ru(t) \end{array} \right\} \tag{51}$$

s.t.

$$\boldsymbol{x}(t) = \boldsymbol{x}^{obs}(k), t = k \tag{52}$$

$$\boldsymbol{x}(t+1) = \boldsymbol{A}\boldsymbol{x}(t) + \boldsymbol{B}\boldsymbol{u}(t), \forall t = k, \ldots, k+PH \tag{53}$$

$$\boldsymbol{K_f}\boldsymbol{x}(t) \le \boldsymbol{G_f}(t), \forall t = k, \ldots, k+PH \tag{54}$$

$$\boldsymbol{u}^{min} \le \boldsymbol{u}(t) \le \boldsymbol{u}^{max}, \forall t = k, \ldots, k+PH \tag{55}$$

$$\sqrt{\left(\gamma_p/1-\gamma_p\right)\boldsymbol{G_l}\hat{\boldsymbol{\sigma}}_{00}(t)\boldsymbol{G_l}^{\boldsymbol{T}}} + \boldsymbol{K_l}\boldsymbol{x}(t) + \boldsymbol{D}\bar{\boldsymbol{x}}_{\boldsymbol{p}}^{\boldsymbol{\xi}}(t) \le -s_n^{min}, \gamma_p \in (0,1) \tag{56}$$

$$\mathbb{D}\left(\boldsymbol{S}, \hat{\boldsymbol{\mu}}, \hat{\boldsymbol{\Sigma}}, \gamma_1, \gamma_2\right) = \left\{ \begin{array}{c} P\left(\hat{\boldsymbol{x}}^{\boldsymbol{\xi}}(t) \in \boldsymbol{S}\right) = 1 \\ \left(\mathbb{E}\left[\hat{\boldsymbol{x}}^{\boldsymbol{\xi}}(t)\right] - \hat{\boldsymbol{\mu}}\right)^T \hat{\boldsymbol{\Sigma}}^{-1}\left(\mathbb{E}\left[\hat{\boldsymbol{x}}^{\boldsymbol{\xi}}(t)\right] - \hat{\boldsymbol{\mu}}\right) \le \gamma_1 \\ E\left[\left(\hat{\boldsymbol{x}}^{\boldsymbol{\xi}}(t) - \hat{\boldsymbol{\mu}}\right)\left(\hat{\boldsymbol{x}}^{\boldsymbol{\xi}}(t) - \hat{\boldsymbol{\mu}}\right)^T\right] \preccurlyeq \gamma_2 \hat{\boldsymbol{\Sigma}} \end{array} \right\}, \forall t = k, \ldots, k+PH \tag{57}$$

where Eq. (56) is the equivalent constraint of the original DRCC constraint, in which $\bar{\boldsymbol{x}}^{\boldsymbol{\xi}}(t)$ is the mean and $\hat{\boldsymbol{\sigma}}_{00}(t)$ is the covariance matrix of the variable $\hat{\boldsymbol{x}}_p^{\xi}(t)$ calculated from data. $\hat{\boldsymbol{\mu}}$ and $\hat{\boldsymbol{\Sigma}}$ are the mean vector and covariance of state variables $\hat{l}_i^{\xi}(t)$ and $\hat{v}_i^{\xi}$, $i = 0, \ldots, N$, from observations. The set $\boldsymbol{S}$ is any convex set that contains the support of $\boldsymbol{F}$. Note that we convert the two minimax terms in Eq. (36) to a single minimax term in Eq. (51) by letting $\boldsymbol{F} = \{\boldsymbol{F_p}, \boldsymbol{F_r}\}$ and $\mathbb{D} = \{\mathbb{D}_p, \mathbb{D}_r\}$. With the moment constraints in Eq. (57), the equivalent reformulated DRSO model is an SDP problem.

4.4. The dual problem of the inner maximization problem of the reformulated DRSO model

We can obtain tractable solutions in a computationally efficient way by solving the dual problem of the inner maximization problem in Eqs. (36)–(42) as long as we show that strong duality holds for the inner problem in **Proposition 2**.

To show strong duality, we need to explicitly reformulate the moment-based uncertainty set to the conic constraints in the inner problem. Specifically, the inner problem is reformulated as $\boldsymbol{F}$-integrable for all $\boldsymbol{F} \in \mathbb{D}$ in Eqs. (59)–(62), which is an infinity-dimensional convex problem. This reformulation allows us to utilize the strong duality theory in the infinity-dimensional convex problems for these moment constraints (Rockafellar, 2015).

For the sake of simplicity, we represent the objective function in Eq. (51) as Eq. (58):

$$J\left(\boldsymbol{u}, \boldsymbol{x}, \hat{\boldsymbol{x}}^{\boldsymbol{\xi}}, t\right) = \left\{ \begin{array}{c} \left[\boldsymbol{Q}_{\boldsymbol{p}}^{\boldsymbol{\xi}}\hat{\boldsymbol{x}}^{\boldsymbol{\xi}}(t) - \boldsymbol{Q}_{\boldsymbol{p}}\boldsymbol{x}(t)\right]^{\boldsymbol{T}} I\left[\boldsymbol{Q}_{\boldsymbol{p}}^{\boldsymbol{\xi}}\hat{\boldsymbol{x}}^{\boldsymbol{\xi}}(t) - \boldsymbol{Q}_{\boldsymbol{p}}\boldsymbol{x}(t)\right] \\ +\left[\boldsymbol{Q}_{\boldsymbol{r}}^{\boldsymbol{\xi}}\hat{\boldsymbol{x}}^{\boldsymbol{\xi}}(t) - \boldsymbol{x}(t)\right]^{\boldsymbol{T}} \boldsymbol{Q}_{\boldsymbol{r}}\left[\boldsymbol{Q}_{\boldsymbol{r}}^{\boldsymbol{\xi}}\hat{\boldsymbol{x}}^{\boldsymbol{\xi}}(t) - \boldsymbol{x}(t)\right] \\ +[\boldsymbol{x}(t)]^{\boldsymbol{T}} Qx(t) \\ +[\boldsymbol{u}(t)]^{\boldsymbol{T}} Ru(t) \end{array} \right\} \tag{58}$$

The inner maximization problem with conic constraints can be described as Eq. (59):

$$\max_{\boldsymbol{F}\in\mathbb{D}} \int_{\boldsymbol{S}} \sum_{t=k}^{k+PH} J\left(\boldsymbol{u}, \boldsymbol{x}, \hat{\boldsymbol{x}}^{\boldsymbol{\xi}}, t\right) d\boldsymbol{F}\left(\hat{\boldsymbol{x}}^{\boldsymbol{\xi}}(t)\right) \tag{59}$$

s.t.

$$\int_{\boldsymbol{S}} d\boldsymbol{F}\left(\hat{\boldsymbol{x}}^{\boldsymbol{\xi}}(t)\right) = 1, \forall t = k, \ldots, k+PH \tag{60}$$

$$\int_{\boldsymbol{S}} \begin{bmatrix} \hat{\boldsymbol{\Sigma}} & \left(\hat{\boldsymbol{x}}^{\boldsymbol{\xi}}(t) - \hat{\boldsymbol{\mu}}\right)^T \\ \hat{\boldsymbol{x}}^{\boldsymbol{\xi}}(t) - \hat{\boldsymbol{\mu}} & \gamma_1 \end{bmatrix} d\boldsymbol{F}\left(\hat{\boldsymbol{x}}^{\boldsymbol{\xi}}(t)\right) \succcurlyeq 0, \forall t = k, \ldots, k+PH \tag{61}$$

$$\int_{\boldsymbol{S}} \left[\left(\hat{\boldsymbol{x}}^{\boldsymbol{\xi}}(t) - \hat{\boldsymbol{\mu}}\right)\left(\hat{\boldsymbol{x}}^{\boldsymbol{\xi}}(t) - \hat{\boldsymbol{\mu}}\right)^T\right] d\boldsymbol{F}\left(\hat{\boldsymbol{x}}^{\boldsymbol{\xi}}(t)\right) \preccurlyeq \gamma_2 \hat{\boldsymbol{\Sigma}}, \forall t = k, \ldots, k+PH \tag{62}$$

In Eq. (61), the original first-moment constraint in Eq. (57) is replaced by a semidefinite cone constraint by Schur complement (Boyd and Vandenberghe, 2004). Note that $\boldsymbol{S}$ is any closed convex set known to contain the support of $\boldsymbol{F}$.

Proposition 2. *Suppose that $\gamma_1 \ge 0$, $\gamma_2 \ge 1$ and $J(\boldsymbol{u}, \boldsymbol{x}, \hat{\boldsymbol{x}}^{\boldsymbol{\xi}}, t)$ is $\boldsymbol{F}$-integrable where $\boldsymbol{F} \in \mathbb{D}$. Given any $\boldsymbol{u}(t)$, we denote $\Psi(\boldsymbol{u}(t), \gamma_1, \gamma_2)$ as the optimal solution to the inner maximization problem in Eqs. (59)–(62). The duality gap between the primal optimal solution $\Psi(\boldsymbol{u}(t), \gamma_1, \gamma_2)$ and the optimal solution of the dual problem is then zero.*

Proof. Strong duality does not hold in general while it usually holds for convex problems Calafiore and El Ghaoui, 2014). To show that strong duality holds for the inner problem, we first need to demonstrate that the objective function of the inner problem is convex. We also need to prove that the regularity conditions and Slater's constraint qualifications (i.e. the conditions that guarantee strong duality in convex problems) are satisfied (Shapiro, 2001; Liu et al., 2015; Wiesemann et al., 2014). We can then show that solving the dual problem is equal to solving the primal inner maximization problem in Eqs. (59)–((62).

First, we need to show that the quadratic terms in the objective function are convex quadratic. Without loss of generality, we denote any quadratic term in the objective function of the conic-constrained inner maximization problem as $f(\boldsymbol{x}) = \boldsymbol{x}^{\boldsymbol{T}}\boldsymbol{Z}\boldsymbol{x}$, where $\boldsymbol{Z}$ is a given positive semidefinite matrix. Note that in the objective function Eq. (51), the matrices $\boldsymbol{I}$, $\boldsymbol{Q_r}$, $\boldsymbol{Q}$, and $\boldsymbol{R}$ are positive semidefinite. By the definition of convex functions in Boyd and Vandenberghe (2004), for any $\boldsymbol{x}_1, \boldsymbol{x}_2 \in \mathbb{R}$, we need to show that $f(\lambda\boldsymbol{x}_1 + (1-\lambda)\boldsymbol{x}_2) \le \lambda f(\boldsymbol{x}_1) + (1-\lambda)f(\boldsymbol{x}_2)$. For the quadratic function $f(\boldsymbol{x})$, we have:

$$\begin{aligned}
&[\lambda\boldsymbol{x}_1 + (1-\lambda)\boldsymbol{x}_2]^T Z[\lambda\boldsymbol{x}_1 + (1-\lambda)\boldsymbol{x}_2] \le \lambda\boldsymbol{x}_1{}^{\boldsymbol{T}}\boldsymbol{Z}\boldsymbol{x}_1 + (1-\lambda)\boldsymbol{x}_2{}^{\boldsymbol{T}}\boldsymbol{Z}\boldsymbol{x}_2\lambda^2\boldsymbol{x}_1{}^{\boldsymbol{T}}\boldsymbol{Z}\boldsymbol{x}_1 + (1-\lambda)^2\boldsymbol{x}_2{}^{\boldsymbol{T}}\boldsymbol{Z}\boldsymbol{x}_2 \\
&\quad + \lambda(1-\lambda)\boldsymbol{x}_1{}^{\boldsymbol{T}}\boldsymbol{Z}\boldsymbol{x}_2 + \lambda(1-\lambda)\boldsymbol{x}_2{}^{\boldsymbol{T}}\boldsymbol{Z}\boldsymbol{x}_1 \le \lambda\boldsymbol{x}_1{}^{\boldsymbol{T}}\boldsymbol{Z}\boldsymbol{x}_1 + (1-\lambda)\boldsymbol{x}_2{}^{\boldsymbol{T}}\boldsymbol{Z}\boldsymbol{x}_2\lambda(1-\lambda)\left[\boldsymbol{x}_1{}^{\boldsymbol{T}}\boldsymbol{Z}\boldsymbol{x}_1 + \boldsymbol{x}_2{}^{\boldsymbol{T}}\boldsymbol{Z}\boldsymbol{x}_2\right] \\
&\quad \ge \lambda(1-\lambda)\left[\boldsymbol{x}_1{}^{\boldsymbol{T}}\boldsymbol{Z}\boldsymbol{x}_2 + \boldsymbol{x}_2{}^{\boldsymbol{T}}\boldsymbol{Z}\boldsymbol{x}_1\right]\boldsymbol{x}_1{}^{\boldsymbol{T}}\boldsymbol{Z}\boldsymbol{x}_2 + \boldsymbol{x}_2{}^{\boldsymbol{T}}\boldsymbol{Z}\boldsymbol{x}_1 \le \boldsymbol{x}_1{}^{\boldsymbol{T}}\boldsymbol{Z}\boldsymbol{x}_1 + \boldsymbol{x}_2{}^{\boldsymbol{T}}\boldsymbol{Z}\boldsymbol{x}_2(\boldsymbol{x}_1 - \boldsymbol{x}_2)^T\boldsymbol{Z}(\boldsymbol{x}_1 - \boldsymbol{x}_2) \ge 0
\end{aligned} \tag{63}$$

In Eq. (63), $(\boldsymbol{x}_1 - \boldsymbol{x}_2)^T\boldsymbol{Z}(\boldsymbol{x}_1 - \boldsymbol{x}_2) \ge 0$ is true for any positive semidefinite matrix $\boldsymbol{Z}$, which shows the convexity of $f(\boldsymbol{x}) = \boldsymbol{x}^{\boldsymbol{T}}\boldsymbol{Z}\boldsymbol{x}$. This applies to the quadratic terms with semidefinite matrices in the objective function Eq. (51). Thus, the objective function of the conic-constrained inner maximization problem is quadratic convex.

We then need to show that Slater's constraint qualification conditions hold. Based on the definition of convex problems in Boyd and Vandenberghe (2004), strong duality holds if the primal problem is convex and Slater's condition holds as long as the inner maximization problem (i.e. the primal problem) has a nonempty and bounded interior solution (i.e. the regularity condition for finite-dimensional mathematical programs holds). According to our definition of the data-driven uncertainty set $\mathbb{D}$ in Eqs. (19)–(20), the probability distribution $\boldsymbol{F}$ is bounded and the regularity condition is then applicable as long as the inner maximization problem has finite nonempty solutions (Liu et al., 2015; Wiesemann et al., 2014). Such regularity conditions regarding nonempty and bounded interior solutions for the proof of strong duality in convex programs are addressed in Proposition 3.4 of Shapiro (2001) and in Bertsimas and Popescu (2005). With the regularity condition, we can show that Slater's condition holds if there exists a strictly feasible solution that satisfies the linear equality constraint and the convex inequality constraint.

To prove that Slater's condition holds for the conic-constrained inner maximization problem, we need to show that the equality constraint in Eq. (60) is linear and the inequality constraints in Eqs. (61)–(62) are convex. Eq. (60) is linear because it is just the integral of the first constraint in Eq.(57). For the first-moment inequality constraint in Eq. (57)—the equivalent of Eq.(61)—we define $\boldsymbol{z} = \mathbb{E}[\hat{\boldsymbol{x}}^{\boldsymbol{\xi}}(t)] - \hat{\boldsymbol{\mu}}$ such that the inequality constraint can be expressed as $z^T\hat{\Sigma}^{-1}z - \gamma_1 \le 0$, which is quadratic convex based on the procedure in Eq. (63). Similarly, the second-moment inequality constraint in Eq. (57), the equivalent of Eq. (62), is quadratic convex.

The optimal duality gap is zero if there is a feasible solution that satisfies the linear equality constraint and the convex inequality constraint of the conic-constrained inner maximization problem. This completes the proof.

To formulate the dual problem of the conic-constrained inner maximization problem, we begin with the Lagrangian of the conic-constrained inner optimization problem as Eq. (64) by relaxing moment-based conic constraints.

$$\begin{aligned}
\mathcal{L}\left(\hat{\boldsymbol{x}}^{\boldsymbol{\xi}}, s_d, \boldsymbol{Q_d}, \boldsymbol{P_d}, \boldsymbol{p_d}\right) &= J\left(\boldsymbol{u}, \boldsymbol{x}, \hat{\boldsymbol{x}}^{\boldsymbol{\xi}}, t\right) + \gamma_2\hat{\boldsymbol{\Sigma}} - \left[\hat{\boldsymbol{x}}^{\boldsymbol{\xi}}(t) - \hat{\boldsymbol{\mu}}\right]\left[\hat{\boldsymbol{x}}^{\boldsymbol{\xi}}(t) - \hat{\boldsymbol{\mu}}\right]^{\boldsymbol{T}}, \boldsymbol{Q_d}(t) \\
&\quad + \begin{bmatrix} \hat{\boldsymbol{\Sigma}} & \hat{\boldsymbol{x}}^{\boldsymbol{\xi}}(t) - \hat{\boldsymbol{\mu}} \\ \left(\hat{\boldsymbol{x}}^{\boldsymbol{\xi}}(t) - \hat{\boldsymbol{\mu}}\right)^T & \gamma_1 \end{bmatrix}, \begin{bmatrix} \boldsymbol{P_d}(t) & \boldsymbol{p_d}(t) \\ (\boldsymbol{p_d}(t))^T & s_d(t) \end{bmatrix}
\end{aligned} \tag{64}$$

where Δ, Δ denotes the inner product. $\boldsymbol{Q_d}(t) \in \mathbb{R}^{m\times m}$ is the dual variable for the second-moment constraint in Eq. (57) and $\boldsymbol{P_d}(t) \in \mathbb{R}^{m\times m}$, $\boldsymbol{p_d}(t) \in \mathbb{R}^m$, $s_d(t) \in \mathbb{R}$ are the dual variables for the first-moment constraint in Eq. (57). Note that m is the length of the random vector $\hat{\boldsymbol{x}}^{\boldsymbol{\xi}}$.

To remove the inner products from Eq. (64), the Lagrangian of the inner optimization problem can be further expanded as Eq. (65).

$$\mathcal{L}\left(\hat{\boldsymbol{x}}^{\boldsymbol{\xi}}, s_d, \boldsymbol{Q_d}, \boldsymbol{P_d}, \boldsymbol{p_d}\right) = J\left(\boldsymbol{u}, \boldsymbol{x}, \hat{\boldsymbol{x}}^{\boldsymbol{\xi}}, t\right) + \gamma_2\hat{\boldsymbol{\Sigma}} \bullet \boldsymbol{Q_d}(t) - \boldsymbol{tr}\left(\left[\hat{\boldsymbol{x}}^{\boldsymbol{\xi}}(t) - \hat{\boldsymbol{\mu}}\right]^{\boldsymbol{T}}\boldsymbol{Q_d}(t)\left[\hat{\boldsymbol{x}}^{\boldsymbol{\xi}}(t) - \hat{\boldsymbol{\mu}}\right]\right) \tag{65}$$

$$\begin{aligned}
&+ \boldsymbol{tr}\left(\begin{bmatrix} \hat{\boldsymbol{\Sigma}} & \left(\hat{\boldsymbol{x}}^{\boldsymbol{\xi}}(t) - \hat{\boldsymbol{\mu}}\right)^T \\ \hat{\boldsymbol{x}}^{\boldsymbol{\xi}}(t) - \hat{\boldsymbol{\mu}} & \gamma_1 \end{bmatrix}\begin{bmatrix} \boldsymbol{P_d}(t) & \boldsymbol{p_d}(t) \\ (\boldsymbol{p_d}(t))^T & s_d(t) \end{bmatrix}\right) \\
&= \left\{J\left(\boldsymbol{u}, \boldsymbol{x}, \hat{\boldsymbol{x}}^{\boldsymbol{\xi}}, t\right) - \left[\hat{\boldsymbol{x}}^{\boldsymbol{\xi}}(t)\right]^T\boldsymbol{Q_d}(t)\hat{\boldsymbol{x}}^{\boldsymbol{\xi}}(t) - 2\left[\hat{\boldsymbol{x}}^{\boldsymbol{\xi}}(t)\right]^T\boldsymbol{Q_d}(t)\hat{\boldsymbol{\mu}} + 2\left[\hat{\boldsymbol{x}}^{\boldsymbol{\xi}}(t)\right]^T\boldsymbol{p_d}(t)\right\} \\
&- 2\hat{\boldsymbol{\mu}}^T\boldsymbol{p_d}(t) + \gamma_1 s_d(t) + \gamma_2\hat{\boldsymbol{\Sigma}} \bullet \boldsymbol{Q_d}(t) + \hat{\boldsymbol{\mu}}^{\boldsymbol{T}}\boldsymbol{Q_d}(t)\hat{\boldsymbol{\mu}} + \hat{\boldsymbol{\Sigma}} \bullet \boldsymbol{P_d}(t)
\end{aligned} \tag{65}$$

where $(\bullet)$ denotes the Frobenius inner product.

For illustration, we decompose the Lagrangian into two parts such that

$$\mathcal{L}\left(\hat{\boldsymbol{x}}^{\xi}, s_d, \boldsymbol{Q_d}, \boldsymbol{P_d}, \boldsymbol{p_d}\right) = \mathcal{L}_1\left(\hat{\boldsymbol{x}}^{\xi}, \boldsymbol{Q_d}, \boldsymbol{p_d}\right) + \mathcal{L}_2(s_d, \boldsymbol{Q_d}, \boldsymbol{P_d}, \boldsymbol{p_d})$$
$$\mathcal{L}_1\left(\hat{\boldsymbol{x}}^{\xi}, \boldsymbol{Q_d}, \boldsymbol{p_d}\right) = \left\{J\left(\boldsymbol{u}, \boldsymbol{x}, \hat{\boldsymbol{x}}^{\xi}, t\right) - \left[\hat{\boldsymbol{x}}^{\xi}(t)\right]^T \boldsymbol{Q_d}(t)\hat{\boldsymbol{x}}^{\xi}(t) - 2\left[\hat{\boldsymbol{x}}^{\xi}(t)\right]^T \boldsymbol{Q_d}(t)\hat{\boldsymbol{\mu}} + 2\left[\hat{\boldsymbol{x}}^{\xi}(t)\right]^T \boldsymbol{p_d}(t)\right\}$$
$$\mathcal{L}_2(s_d, \boldsymbol{Q_d}, \boldsymbol{P_d}, \boldsymbol{p_d}) = -2\hat{\boldsymbol{\mu}}^T \boldsymbol{p_d}(t) + \gamma_1 s_d(t) + \gamma_2 \hat{\boldsymbol{\Sigma}} \bullet \boldsymbol{Q_d}(t) + \hat{\boldsymbol{\mu}}^T \boldsymbol{Q_d}(t)\hat{\boldsymbol{\mu}} + \hat{\boldsymbol{\Sigma}} \bullet \boldsymbol{P_d}(t). \tag{66}$$

Based on the definition of the Lagrangian dual problem in Bazaraa et al. (2013), the dual problem can be formulated as minimizing the supreme (i.e. the least upper bound) of the Lagrangian function Eq. (65). This dual problem can be further expressed by incorporating the function $\mathcal{L}_2(s_d, \boldsymbol{Q_d}, \boldsymbol{P_d}, \boldsymbol{p_d})$ that consists of dual variables and minimizing the supremum of the function $\mathcal{L}_1(\hat{\boldsymbol{x}}^{\xi}, \boldsymbol{Q_d}, \boldsymbol{p_d})$ in Eq. (67).

$$\min_{\boldsymbol{Q_d}, \boldsymbol{P_d}, \boldsymbol{p_d}} \mathcal{L}_2(s_d, \boldsymbol{Q_d}, \boldsymbol{P_d}, \boldsymbol{p_d}) + \left[\sup_{\hat{\boldsymbol{x}}^{\xi}} \mathcal{L}_1\left(\hat{\boldsymbol{x}}^{\xi}, \boldsymbol{Q_d}, \boldsymbol{p_d}\right)\right] \tag{67}$$

s.t.

$$\begin{bmatrix} \boldsymbol{P_d}(t) & \boldsymbol{p_d}(t) \\ (\boldsymbol{p_d}(t))^T & s_d(t) \end{bmatrix} \succcurlyeq 0, Q_d(t) \succcurlyeq 0, \forall t = k, \ldots, k + PH \tag{68}$$

where the objective function in Eq. (67) minimizes the Lagrangian function, in which $\sup_{\hat{\boldsymbol{x}}^{\xi}} \mathcal{L}_1(\hat{\boldsymbol{x}}^{\xi}, \boldsymbol{Q_d}, \boldsymbol{p_d})$ considers the worst-case distribution of the stochastic parameter $\hat{\boldsymbol{x}}^{\xi}$. Eq. (68) contains the dual variable constraints.

By adding a dual variable r_d for $\sup_{\hat{\boldsymbol{x}}^{\xi}} \mathcal{L}_1(\hat{\boldsymbol{x}}^{\xi}, \boldsymbol{Q_d}, \boldsymbol{p_d})$, we can rewrite the dual problem as Eq. (69) (see Delage and Ye, 2010).

$$\min_{\boldsymbol{Q_d}, \boldsymbol{P_d}, \boldsymbol{p_d}, r_d, s_d} \sum_{t=k}^{k+PH} \mathcal{L}_2(s_d, \boldsymbol{Q_d}, \boldsymbol{P_d}, \boldsymbol{p_d}) + r_d(t) \tag{69}$$

s.t.

$$r_d(t) \geq J\left(\boldsymbol{u}, \boldsymbol{x}, \hat{\boldsymbol{x}}^{\xi}, t\right) - \left[\hat{\boldsymbol{x}}^{\xi}(t)\right]^T \boldsymbol{Q_d}(t)\hat{\boldsymbol{x}}^{\xi}(t) - 2\left[\hat{\boldsymbol{x}}^{\xi}(t)\right]^T \boldsymbol{Q_d}(t)\hat{\boldsymbol{\mu}} + 2\left[\hat{\boldsymbol{x}}^{\xi}(t)\right]^T \boldsymbol{p_d}(t), \forall t = k, \ldots, k + PH \tag{70}$$

$$\begin{bmatrix} \boldsymbol{P_d}(t) & \boldsymbol{p_d}(t) \\ (\boldsymbol{p_d}(t))^T & s_d(t) \end{bmatrix} \succcurlyeq 0, \boldsymbol{Q_d} \succcurlyeq 0, r_d(t) \geq 0, \forall t = k, \ldots, k + PH \tag{71}$$

The dual problem in Eqs. (69)–(71) is a quadratically constrained program. Based on **Proposition 2**, we can obtain tractable solutions by solving the dual problem in Eqs. (69)–(71), which is equivalent to solving the primal conic-constrained inner maximization problem in the DRSO model. The complexity of the dual problem is, however, unknown and is not suitable for real-time application of the proposed CACC control model because of the quadratic constraint in Eq. (70) (Floudas and Visweswaran, 1995; Ye and Zhang, 2003; Luo et al., 2010).

4.5. The relaxed SDP of the dual problem

To obtain a computationally efficient approximation of the quadratically constrained optimization problems in Eqs. (69)–(71), this section applies the Semidefinite Relaxation technique in Luo et al. (2010) to deal with the quadratic constraint in Eq. (70). Using the Semidefinite Relaxation technique, we introduce two new variables: $\boldsymbol{X}(t) = \boldsymbol{x}(t)[\boldsymbol{x}(t)]^T$ and $\boldsymbol{U}(t) = \boldsymbol{u}(t)[\boldsymbol{u}(t)]^T$. The quadratic constraint in Eq. (70) can then be reformulated as Eq. (72):

$$\begin{aligned} & r_d + \left[\hat{\boldsymbol{x}}^{\xi}(t)\right]^T \left(\boldsymbol{Q_d}(t) - \left(\boldsymbol{Q_p^{\xi}}\right)^T \boldsymbol{Q_p^{\xi}} - \left(\boldsymbol{Q_r^{\xi}}\right)^T \boldsymbol{Q_r^{\xi}}\right)\hat{\boldsymbol{x}}^{\xi}(t) \\ & + \left[\hat{\boldsymbol{x}}^{\xi}(t)\right]^T \left(r_d + \left[\hat{\boldsymbol{x}}^{\xi}(t)\right]^T \left(\boldsymbol{Q_d}(t) - \left(\boldsymbol{Q_p^{\xi}}\right)^T \boldsymbol{Q_p^{\xi}} - \left(\boldsymbol{Q_r^{\xi}}\right)^T \boldsymbol{Q_r^{\xi}}\right)\hat{\boldsymbol{x}}^{\xi}(t) + \left[\hat{\boldsymbol{x}}^{\xi}(t)\right]^T\right) \\ & - \boldsymbol{tr}\left(\left(\boldsymbol{Q_p}^T \boldsymbol{Q_p} + \boldsymbol{Q} + \boldsymbol{Q_r}\right)\boldsymbol{X}(t)\right) - \boldsymbol{tr}(\boldsymbol{R}\boldsymbol{U}(t)) \geq 0, rank(\boldsymbol{X}(t)) \\ & = 1, rank(\boldsymbol{U}(t))1, \boldsymbol{X}(t) \succcurlyeq 0, \boldsymbol{U}(t) \succcurlyeq 0, \forall t = k, \ldots, k + PH \end{aligned} \tag{72}$$

In Eq. (72), we show that $[\boldsymbol{u}(t)]^T \boldsymbol{R}\boldsymbol{u}(t) = \boldsymbol{tr}([\boldsymbol{u}(t)]^T \boldsymbol{R}\boldsymbol{u}(t)) = \boldsymbol{tr}(\boldsymbol{R}\boldsymbol{U}(t))$. Note that the constraint $rank(\boldsymbol{X}(t)) = 1$, $\boldsymbol{X}(t) \succcurlyeq 0$ is equivalent to restricting $\boldsymbol{X}(t) = \boldsymbol{x}(t)[\boldsymbol{x}(t)]^T$, which makes the problem still difficult to solve Luo et al., 2010). To reduce computational expense while obtaining a tractable approximation of the optimal solution to the quadratically constrained dual problem in Eqs. (69)–((71), we can drop the rank constraints on $\boldsymbol{X}(t)$ and $\boldsymbol{U}(t)$ to obtain a numerically efficient approximation (Zhang, 2000; Kim and Kojima, 2003; Luo et al., 2010).

Without the rank constraints, the quadratic form of the constraint in Eq. (72) can then be written as Eq. (73):

$$\begin{bmatrix} \left(\hat{\boldsymbol{x}}^{\xi}(t)\right)^{T} & 1 \end{bmatrix} \times \begin{bmatrix} \boldsymbol{Q_d}(t) - \left(\boldsymbol{Q_p^{\xi}}\right)^{\boldsymbol{T}} \boldsymbol{Q_p^{\xi}} - \left(\boldsymbol{Q_r^{\xi}}\right)^{\boldsymbol{T}} \boldsymbol{Q_r^{\xi}} & -\boldsymbol{p_d}(t) - \boldsymbol{Q_d}(t)\hat{\boldsymbol{\mu}} + \left(\left(\boldsymbol{Q_p^{\xi}}\right)^{\boldsymbol{T}} \boldsymbol{Q_p^{\xi}} + \left(\boldsymbol{Q_r^{\xi}}\right)^{\boldsymbol{T}} \boldsymbol{Q_r^{\xi}}\right)\boldsymbol{x}(t) \\ -\boldsymbol{p_d}(t)^{\boldsymbol{T}} - \hat{\boldsymbol{\mu}}^{T}\boldsymbol{Q_d}(t)^{\boldsymbol{T}} + \boldsymbol{x}(t)^{\boldsymbol{T}}\left(\left(\boldsymbol{Q_p^{\xi}}\right)^{\boldsymbol{T}} \boldsymbol{Q_p^{\xi}} + \left(\boldsymbol{Q_r^{\xi}}\right)^{\boldsymbol{T}} \boldsymbol{Q_r^{\xi}}\right)^{T} & r_d(t) - \boldsymbol{tr}\left(\left(\boldsymbol{Q_p}^{\boldsymbol{T}}\boldsymbol{Q_p} + \boldsymbol{Q} + \boldsymbol{Q_r}\right)\boldsymbol{X}(t)\right) - \boldsymbol{tr}(\boldsymbol{RU}(t)) \end{bmatrix} \times \begin{bmatrix} \hat{\boldsymbol{x}}^{\xi}(t) \\ 1 \end{bmatrix} \succcurlyeq 0,\ \boldsymbol{X}(t) \succcurlyeq 0, \boldsymbol{U}(t) \succcurlyeq 0, \forall t = k, \ldots, k+PH \tag{73}$$

The stochastic term $\begin{bmatrix} \left(\hat{\boldsymbol{x}}^{\xi}(t)\right)^{T} & 1 \end{bmatrix}$ in Eq. (73) makes the quadratic constraint difficult to solve. By the S-Lemma (Yakubovic, 1971; Pólik and Terlaky, 2007; Lemma 2.2 in Zymler et al., 2013), we remove the stochastic term and replace the constraint in Eq. (73) with Eq. (74).

$$\begin{bmatrix} \boldsymbol{Q_d}(t) - \left(\boldsymbol{Q_p^{\xi}}\right)^{\boldsymbol{T}} \boldsymbol{Q_p^{\xi}} - \left(\boldsymbol{Q_r^{\xi}}\right)^{\boldsymbol{T}} \boldsymbol{Q_r^{\xi}} & -\boldsymbol{p_d}(t) - \boldsymbol{Q_d}(t)\hat{\mu} + \left(\left(\boldsymbol{Q_p^{\xi}}\right)^{\boldsymbol{T}} \boldsymbol{Q_p^{\xi}} + \left(\boldsymbol{Q_r^{\xi}}\right)^{\boldsymbol{T}} \boldsymbol{Q_r^{\xi}}\right)\boldsymbol{x}(t) \\ -\boldsymbol{p_d}(t)^{\boldsymbol{T}} - \hat{\boldsymbol{\mu}}^{T}\boldsymbol{Q_d}(t)^{\boldsymbol{T}} + \boldsymbol{x}(t)^{\boldsymbol{T}}\left(\left(\boldsymbol{Q_p^{\xi}}\right)^{\boldsymbol{T}} \boldsymbol{Q_p^{\xi}} + \left(\boldsymbol{Q_r^{\xi}}\right)^{\boldsymbol{T}} \boldsymbol{Q_r^{\xi}}\right)^{T} & r_d(t) - \boldsymbol{tr}\left(\left(\boldsymbol{Q_p}^{\boldsymbol{T}}\boldsymbol{Q_p} + \boldsymbol{Q} + \boldsymbol{Q_r}\right)\boldsymbol{X}(t)\right) - \boldsymbol{tr}(\boldsymbol{RU}(t)) \end{bmatrix} \succcurlyeq 0, \boldsymbol{X}(t) \succcurlyeq 0, \boldsymbol{U}(t) \succcurlyeq 0, \forall t = k, \ldots, k+PH \tag{74}$$

Finally, the dual problem in Eqs. (67)–(68) is reformulated as a relaxed dual problem in Eqs. (75)–(77).

$$\min_{\boldsymbol{Q_d}, \boldsymbol{P_d}, \boldsymbol{p_d}, r_d, s_d} \sum_{t=k}^{k+PH} -2\hat{\boldsymbol{\mu}}^{\boldsymbol{T}}\boldsymbol{p_d}(t) + \gamma_1 s_d(t) + \gamma_2 \hat{\boldsymbol{\Sigma}} \bullet \boldsymbol{Q_d}(t) + \hat{\boldsymbol{\mu}}^{\boldsymbol{T}}\boldsymbol{Q_d}(\boldsymbol{t})\hat{\boldsymbol{\mu}} + \hat{\boldsymbol{\Sigma}} \bullet \boldsymbol{P_d}(t) + r_d(t) \tag{75}$$

s.t.

$$\begin{bmatrix} \boldsymbol{Q_d}(t) - \left(\boldsymbol{Q_p^{\xi}}\right)^{\boldsymbol{T}} \boldsymbol{Q_p^{\xi}} - \left(\boldsymbol{Q_r^{\xi}}\right)^{\boldsymbol{T}} \boldsymbol{Q_r^{\xi}} & \frac{1}{2}\boldsymbol{q_d}(t) + \left(\left(\boldsymbol{Q_p^{\xi}}\right)^{\boldsymbol{T}} \boldsymbol{Q_p^{\xi}} + \left(\boldsymbol{Q_r^{\xi}}\right)^{\boldsymbol{T}} \boldsymbol{Q_r^{\xi}}\right)\boldsymbol{x}(t) \\ \frac{1}{2}(\boldsymbol{q_d}(t))^{T} + \boldsymbol{x}(t)^{T}\left(\left(\boldsymbol{Q_p^{\xi}}\right)^{\boldsymbol{T}} \boldsymbol{Q_p^{\xi}} + \left(\boldsymbol{Q_r^{\xi}}\right)^{\boldsymbol{T}} \boldsymbol{Q_r^{\xi}}\right)^{T} & r_d - \boldsymbol{tr}\left(\left(\boldsymbol{Q_p}^{\boldsymbol{T}}\boldsymbol{Q_p} + \boldsymbol{Q} + \boldsymbol{Q_r}\right)\boldsymbol{X}(t)\right) - \boldsymbol{tr}(\boldsymbol{RU}(t)) \end{bmatrix} \succcurlyeq 0, \boldsymbol{q_d}(t) = -\boldsymbol{p_d}(t) - \boldsymbol{Q_d}(t)\hat{\boldsymbol{\mu}}, \boldsymbol{X}(t) \succcurlyeq 0, \boldsymbol{U}(t) \succcurlyeq 0, \forall t = k, \ldots, k+PH \tag{76}$$

$$\begin{bmatrix} \boldsymbol{P_d}(t) & \boldsymbol{p_d}(t) \\ (\boldsymbol{p_d}(t))^{T} & s_d(t) \end{bmatrix} \succcurlyeq 0, \boldsymbol{Q_d}(t) \succcurlyeq 0, r_d(t) \geq 0, \forall t = k, \ldots, k+PH \tag{77}$$

where the relaxed dual problem in Eqs. (75)-(77) is an SDP program. Solving this relaxed dual problem will obtain an approximation of the optimal solution to the primal inner maximization problem of the DRSO model in Eqs. (51)–(57). Note that the Semidefinite Relaxation works well empirically in many applications that can generate reliable solutions efficiently (Ma et al., 2002, 2004; Sidiropoulos et al., 2006; Biswas et al., 2006; Li and Jiang, 2007; Luo et al., 2010). The relaxed dual problem will be integrated with the outer minimization problem of the DRSO model in Section 4.2.4.

4.5.1. The reformulated DRSO-DRCC model—a relaxed SDP

This section reformulates the proposed DRSO-DRCC model of Section 4.1 as a relaxed SDP problem based on the discussions in Sections 4.2.1, 4.2.2, and 4.2.3. We formulate an equivalent convex constraint for the DRCC constraint of Section 4.2.1 using mean and variance information on the predictive uncertain driving states of the IPV. For the conic-constrained inner maximization problem of the DRSO model, we formulate its dual problem as a quadratically constrained program by applying the strong duality theory of Section 4.2.2. We then reformulate a relaxed SDP in Section 4.2.3 to obtain the approximation of the optimal solution to the quadratically constrained dual problem using the Semidefinite Relaxation technique.

We combine the relaxed dual problem in Eqs. (75)–(77) with the outer minimization problem in Eqs. (51)–(57) as a minimization problem in Eqs. (78)–(84):

$$\min_{\boldsymbol{u},\boldsymbol{Q_d},\boldsymbol{P_d},\boldsymbol{p_d},r_d,s_d} \sum_{t=k}^{k+PH} \gamma_2 \hat{\boldsymbol{\Sigma}} \bullet \boldsymbol{Q_d}(t) - \hat{\boldsymbol{\mu}}\hat{\boldsymbol{\mu}}^T \bullet \boldsymbol{Q_d}(t) + r_d(t) + \hat{\boldsymbol{\Sigma}} \bullet \boldsymbol{P_d}(t) - 2\hat{\boldsymbol{\mu}}^T \boldsymbol{p_d}(t) + \gamma_1 s_d(t) \tag{78}$$

s.t.

$$\begin{bmatrix} \boldsymbol{Q_d}(t) - \left(\boldsymbol{Q_p^\xi}\right)^T \boldsymbol{Q_p^\xi} - \left(\boldsymbol{Q_r^\xi}\right)^T \boldsymbol{Q_r^\xi} & \frac{1}{2}\boldsymbol{q_d}(t) + \left(\left(\boldsymbol{Q_p^\xi}\right)^T \boldsymbol{Q_p^\xi} + \left(\boldsymbol{Q_r^\xi}\right)^T \boldsymbol{Q_r^\xi}\right)\boldsymbol{x}(t) \\ \frac{1}{2}(\boldsymbol{q_d}(t))^T + \boldsymbol{x}(t)^T\left(\left(\boldsymbol{Q_p^\xi}\right)^T \boldsymbol{Q_p^\xi} + \left(\boldsymbol{Q_r^\xi}\right)^T \boldsymbol{Q_r^\xi}\right)^T & r_d - \boldsymbol{tr}\left(\left(\boldsymbol{Q_p}^T\boldsymbol{Q_p} + \boldsymbol{Q} + \boldsymbol{Q_r}\right)\boldsymbol{X}(t)\right) - \boldsymbol{tr}(\boldsymbol{R}\boldsymbol{U}(t)) \end{bmatrix}$$
$$\succcurlyeq 0, \boldsymbol{q_d}(t) = -\boldsymbol{p_d}(t) - \boldsymbol{Q_d}(t)\hat{\boldsymbol{\mu}}, \boldsymbol{X}(t) \succcurlyeq 0, \boldsymbol{U}(t) \succcurlyeq 0, \forall t = k, \ldots, k+PH \tag{79}$$

$$\begin{bmatrix} \boldsymbol{P_d}(t) & \boldsymbol{p_d}(t) \\ (\boldsymbol{p_d}(t))^T & s_d(t) \end{bmatrix} \succcurlyeq 0, \boldsymbol{Q_d}(t) \succcurlyeq 0, r_d(t) \geq 0, \forall t = k, \ldots, k+PH \tag{80}$$

$$\boldsymbol{x}(t+1) = \boldsymbol{A}\boldsymbol{x}(t) + \boldsymbol{B}\boldsymbol{u}(t), \forall t = k, \ldots, k+PH \tag{81}$$

$$\boldsymbol{x}(t) = \boldsymbol{x}^{obs}(k), t = k, \boldsymbol{K_f}\boldsymbol{x}(t) \leq \boldsymbol{G_f}(t), \forall t = k, \ldots, k+PH \tag{82}$$

$$\boldsymbol{u}^{min} \leq \boldsymbol{u}(t) \leq \boldsymbol{u}^{max}, \forall t = k, \ldots, k+PH \tag{83}$$

$$\sqrt{\left(\gamma_p/1-\gamma_p\right)\boldsymbol{G_l}\hat{\boldsymbol{\sigma}}_{00}(t)\boldsymbol{G_l}^T} + \boldsymbol{K_l}\boldsymbol{x}(t) + \boldsymbol{D}\bar{\boldsymbol{x}}_{\boldsymbol{p}}^{\boldsymbol{\xi}}(t) \leq -s_n^{min}, \gamma_p \in (0,1) \tag{84}$$

This minimization problem is actually a relaxed SDP problem. In the objective function, r_d is the dual variable for $\sup_{\hat{\boldsymbol{x}}^\xi} \mathcal{L}_1(\hat{\boldsymbol{x}}^\xi, \boldsymbol{Q_d}, \boldsymbol{p_d})$ in Eq. (67). All the other terms in the objective function are from the Lagrangian function $\mathcal{L}_2(s_d, \boldsymbol{Q_d}, \boldsymbol{P_d}, \boldsymbol{p_d})$ in Eq. (67). The constraint in Eq. (79) is the relaxed constraint of the quadratic constraint in Eq. (70) after applying the dual variable r_d. Eq. (80) is the constraint obtained by applying dual variables $\boldsymbol{Q_d}(t)$—the dual variable for the second-moment constraint in Eq. (62) and $\boldsymbol{P_d}(t)$,$\boldsymbol{p_d}(t)$,$s_d(t)$—the dual variables for the first-moment constraint in Eq.(61). Eqs. (81)–(83) are the original constraints of the outer minimization problem. Eq. (84) is the equivalent constraint of the original DRCC constraint.

Solving the relaxed SDP problem in Eqs. (78)–(84) will obtain a tractable approximation of the optimal solution to the DRSO-DRCC model in Eqs. (36)–(42). Given the historical data $\{\hat{\boldsymbol{x}}^{\boldsymbol{\xi_i}}(k) | \forall i = 1, \ldots, M\}$ on the predicted driving states estimated from various boundary conditions in Section 3.1, we can select γ_1 and γ_2 by Eq. (85) according to Corollary 3 and Definition 2 in Delage and Ye (2010) to solve the problem.

$$\hat{\gamma}_1 = \frac{\beta}{1-\alpha-\beta}, \hat{\gamma}_2 = \frac{1+\beta}{1-\alpha-\beta}, \alpha = O\left(1/\sqrt{M}\right), \beta = O\left(1/M\right) \tag{85}$$

4.6. Solution method

To implement a real-time control system using the reformulated SDP model, we present an efficient implementation to reduce the computational expense of solving the proposed model for real-time applications.

Solution Method: An efficient implementation based on hot-start and parallel computing methods for solving the reformulated SDP model

Boundary conditions of driving states

1: At time step k, collect vehicle velocity $\{\hat{v}_b^{\xi_i}(k)|\forall i=1,\ldots,M\}$ of the BCPV during $[k-T^{obs},k]$.

2: Calculate a set of vehicle longitudinal positions $\{\hat{l}_b^{\xi_i}(t)|\forall t=k,\ldots,k+PH,\forall i=1,\ldots,M\}$ for the BCPV by constant velocities over $[k, \ldots, k+PH]$.

Online learning-based driving dynamics prediction by parallel computing with the update interval ΔT^p

3: For each vehicle n under each boundary condition, if $k \geq T^p$ and $mod(k, \Delta T^p)=0$, go to Step 4; otherwise, use the online calibrated parameters from the last step:, set $\tau_n^{Ne}(k)=\tau_n^{Ne}(k-1)$ and $d_n^{Ne}(k)=d_n^{Ne}(k-1)$ and go to Step 5. (Parallel Computing)

4: Solve the learning-based prediction model in Eqs. (1)–(2) to get the online calibrated car-following parameters, e.g. $\tau_n^{Ne}(k)$ and $d_n^{Ne}(k)$, for the preceding vehicles with a given boundary condition. (Parallel Computing)

5: Given the set of driving states of the BCPV and the calibrated parameters, solve the learning-based prediction model, e.g. Newell's model of Eq. (3), to predict the driving dynamics $\{[\ \hat{l}_0^{\xi_i}(t)\quad \hat{v}_0^{\xi_i}(t)\ ]^T|\forall t=k,\ldots,k+PH,\forall i=1,\ldots,M\}$ of the IPV. (Parallel Computing)

6: Given the predicted driving states of the IPV, solve the FHOC model in Eqs. (4)–(10) or the MIXIC model in Eq. (11) to predict the dynamic driving states $\{[\ \hat{l}_n^{\xi_i}(t)\quad \hat{v}_n^{\xi_i}(t)\ ]^T|\forall t=k,\ldots,k+PH,n=1,\ldots,N,i=1,\ldots,M\}$ of the controlled vehicles. (Parallel Computing)

Real-time DRSO-DRCC–based optimal control by solving the reformulated SDP model using the previous optimal solutions as hot-start

7: Collect observations $l_n^{obs}(k)$ and $v_n^{obs}(k)$ of the controlled vehicles at time step k for the initial-condition constraint of the reformulated SDP model.

8: Input the predicted driving states (from Step 4 and Step 5) into the reformulated SDP model in Eqs. (78)–(84).

9: Select likelihood threshold $\hat{\gamma}_1=\frac{\beta}{1-\alpha-\beta}$, $\hat{\gamma}_2=\frac{1+\beta}{1-\alpha-\beta}$, $\alpha=O(1/\sqrt{M})$, $\beta=O(1/M)$, where M is the number of boundary conditions.

10: Input the previous primal and dual optimal solution at time step $k-1$ as the initial starting point for the SDP model at time step k. (Hot-start)

11: Solve the reformulated SDP Eqs. (78)–(84) with the initial starting point from the last time step $k-1$ and the selected γ_1 and γ_2 using an SDP solver.

12: Save the optimal solution at current time step k as the initial point for the next time step $k+1$.

Step 1 and Step 2 predict the uncertain driving states of the BCPV (see Section 3.1.1). We iteratively check whether the online calibrated car-following parameters are stable at Step 3. Step 4 solves the learning-based prediction model to obtain the calibrated car-following parameters for the preceding vehicles. Step 5 predicts the uncertain driving states of the preceding vehicles using the online calibrated parameters from Step 3. Step 6 solves the proposed FHOC model to predict the uncertain driving states of the controlled vehicles that are constrained by the predicted driving states of the preceding vehicles from Step 5. Steps 3–6 are independent parts that can be processed concurrently. Step 7 collects historical observations of the controlled vehicles as the initial conditions for the MPC model. Step 8 uses the predicted driving states of the preceding vehicles in the safety constraint of the proposed model. Step 9 calculates the parameters for the data-driven uncertainty set of the proposed DRSO-DRCC model. Step 10 solves the reformulated SDP to obtain the optimal acceleration or deceleration commands for the controlled CAVs. We use a hot-start-based method to solve the reformulated SDP model in Steps 11–12. The hot-start techniques can be applied to reduce the computational expense involved in solving SDP problems (Sturm, 2002; Biswas and Ye, 2006; Skajaa et al., 2013; Sun et al., 2020) and especially in an MPC framework (Zeilinger et al., 2014). The reformulated SDP can be solved using an SDP solver such as MOSEK (https://www.mosek.com/) with interior-point methods (Sturm, 1999; Benson et al., 2000; Benson and Ye, 2005; Biswas and Ye, 2006).

5. Numerical analysis

In this section, we will use the NGSIM vehicle trajectory data to evaluate and validate the proposed DRSO-DRCC–based MPC model. We first describe the dataset and the experimental design in Section 5.1. We then measure the performance of the proposed model from our experimental results using the empirical NGSIM data presented in Section 5.2. In Section 5.3, we show the computational analysis of the proposed procedure for solving the model.

5.1. Overview of the datasets and experimental design

In Section 5.1.1, we describe the datasets from the NGSIM program used for the implementation of the proposed DRSO-DRCC–based MPC model. We then design four experiments to analyze the performance of the proposed model using the empirical NGSIM data presented in Section 5.1.2.

5.2. Input data preparation

To illustrate the proposed methodology, we use empirical data from two NGSIM datasets, recorded in 2005 at ten frames per second from southbound US-101 in Los Angeles, CA, and northbound I-80 in Emeryville, CA. Each of the two datasets contains 45-minute vehicle trajectory data that are segmented into three 15-minute periods. The data can be downloaded from the U.S. Department of Transportation's public data portal (https://data.transportation.gov/).

Table 1
The extracted vehicle trajectory datasets.

Dataset Index	NGSIM dataset	Collected Date Time	Direction	Lane ID	Velocity Average (mph)	Velocity Variance (mph)	Number of Shocks
1	The US 101 dataset	08:20 - 08:35 AM on June 15, 2005	Southbound	3	15.8	15.1	1
2	The US 101 dataset	08:05 - 08:20 AM on June 15, 2005	Southbound	2	13.4	11.4	2
3	The I-80 dataset	05:00 - 05:15 PM on April 13, 2005	Northbound	3	9.1	9	3

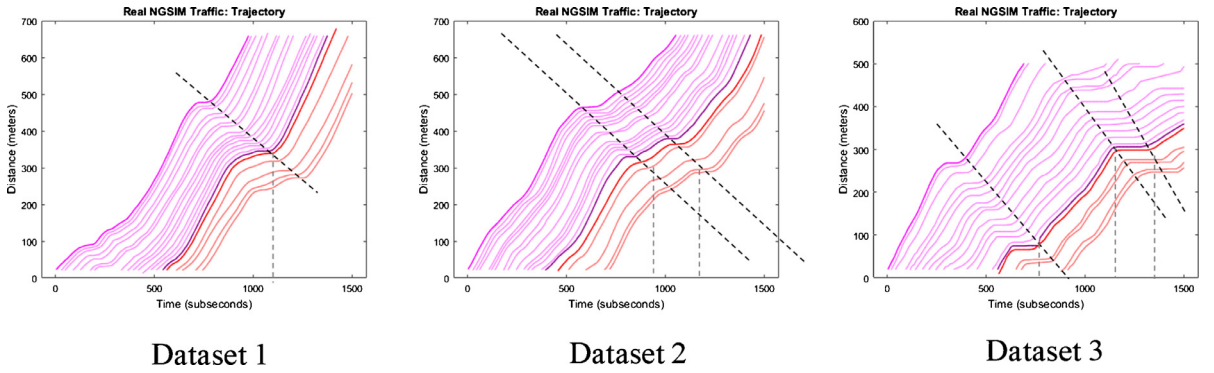

Fig. 7. Space-time diagram of vehicle trajectories of three datasets from NGSIM .

By way of illustration, we extract only the portions of vehicle trajectories in a single lane (i.e. without lane-changing) from the two NGSIM trajectory datasets. To demonstrate the proposed method at varying levels of traffic oscillations, we select three subsets from the NGSIM datasets with varying traffic oscillation patterns in a single lane. Detailed information about the extracted subsets of vehicle trajectories is summarized in Table 1. To measure model performance across datasets, each dataset in Table 1 is selected from the NGSIM datasets to contain twenty vehicles driving for more than 150 s.

Traffic oscillations cause the average velocities to be much lower than the speed limits. The raw trajectories are plotted in Fig. 7, where the three extracted datasets contain one, two, and three shocks, respectively. The vehicles in the dataset with three shocks exhibit slower average velocity than the other two datasets reported in Table 1.

5.3. Experimental design

This section describes the experimental design we applied to demonstrate the proposed model using the three datasets (Section 5.1.1). For consistency of performance measurement across extracted datasets, we consider the first fifteen vehicles as the preceding vehicles, while the last five vehicles are the controlled vehicles in our experiments. We predict the driving states of the fifteen preceding vehicles based on Newell's car-following law or the IDM car-following law. For the controlled vehicles, we predict driving states by solving the constrained FHOC (i.e. the Finite-Horizon Optimal Control) model or the MIXIC model (i.e. the MICroscopic model for Simulation of Intelligent Cruise control) of Section 3.1.3.

To measure model performance, especially string stability, we design four experiments:

Experiment 1. We compare the results of the proposed model with the extracted NGSIM datasets in the time and frequency domains.

Experiment 2. We compare string stability results obtained using the MIXIC model with the results using the FHOC model to predict the driving states of the controlled vehicles.

Experiment 3. We select differing prediction horizon lengths with a discounting factor to evaluate the string stability of the proposed model.

Experiment 4. We select differing time headways in the constant-time-headway policy to evaluate the string stability of the proposed model.

5.4. Experimental analysis

In this section, we evaluate the performance of the proposed DRSO-DRCC–based MPC model using the NGSIM data. We will evaluate the model performance of the proposed DRSO-DRCC–based MPC model in terms of string stability, errors in the preceding vehicle predictions, and the online learning patterns of the preceding vehicle driving behaviors.

5.5. Experiment 1: comparison with NGSIM trajectory data

To demonstrate the proposed model, in Experiment 1 we compare the results obtained with the proposed DRSO-DRCC–based MPC model with the raw NGSIM trajectory data with a focus on the IPV and the controlled vehicles. We apply the IDM model in the learning-based prediction (Section 3.1.2) of the IPV. In addition, we apply the FHOC model of Section 3.1.3 to predict the CACC driving states of the controlled vehicles. We set the time headway at 1.6 s, and the prediction horizon at 16 steps. In González-Villaseñor et al. (2007), a time headway of 0.2 s is used to model the close headway spacing for automated driving. For the longitudinal automated driving system in our problem, we use 0.2 s as the minimum safe time headway to guarantee the following safety of the controlled vehicles.

Note that the proposed model can also produce smooth trajectories with most of the car-following-based controllers if the exact constraints (e.g. the prediction of the IPV speed) are given. However, we consider realistic driving scenarios under uncertain traffic conditions without given distributions of the uncertain parameters or predicted traffic information. We plot the time-domain acceleration profiles, spacing profiles, and velocity profiles of the IPV (i.e. vehicle 0) and the controlled vehicles (i.e. vehicles 1–5) in Fig. 8. The results shown in Fig. 8 indicate that the acceleration perturbations are considerably reduced as it approaches the string tail. Even if the leading controlled vehicle has a wider spacing fluctuation, the spacing patterns of the following controlled vehicles are smooth. The velocity patterns of the controlled vehicles fluctuate less frequently than the NGSIM trajectory data in terms of the results of dataset 1.

In Fig. 8(c), the acceleration profiles of NGSIM dataset 2 show that the vehicles accelerate and decelerate very frequently in a small range, which is different from the other two datasets. The velocity profile of the DRSO-DRCC model using dataset 2 shifts more obviously than the raw NGSIM data. However, the acceleration and velocity profiles of the controlled CAVs vary less frequently than the NGSIM data. Instead of frequently accelerating or decelerating, the controlled vehicles by the DRSO-DRCC method accelerate and decelerate with a wider range but much less frequently than in the NGSIM data. This is due to the driving comfort term in the objective functions of the CACC policy (for predictive driving reference of the controlled vehicles) and the DRSO-DRCC model. The spacing profiles in the DRSO-DRCC method is much smoother than in the NGSIM data when there is a perturbation from the front traffic. The objective of the proposed DRSO-DRCC–based MPC model minimizes the perturbations of not only accelerations but also spacing and velocities. In dataset 2, the velocities may be regulated by the proposed model to mitigate the frequent variations in accelerations.

In the frequency domain, the amplitude values shown in Fig. 8 are calculated by the transfer function of Section 3.3. In Fig. 8(b), (d), and (f), all the mean amplitude patterns of the DRSO-DRCC results show decreasing patterns using the three datasets. The string amplitudes of spacing deviations (i.e. the individual amplitudes of all the controlled vehicles) diminish when approaching the string tail in all the DRSO-DRCC results. The amplitude patterns (including the mean and string) are increasing for all three NGSIM datasets, however, which shows string instability in the raw NGSIM trajectories. This demonstrates that the proposed CACC control model substantially improves string stability and mitigates the perturbations caused by traffic oscillations in our experiments.

5.6. Experiment 2: string stability based on distinct controlled-vehicle prediction methods

We evaluate the string stability of the proposed model using multiple controlled-vehicle prediction methods. We select dataset 2 to simulate CACC driving using the proposed DRSO-DRCC–based MPC model. We apply the IDM model to predict the driving states of the IPV. We compare the model results using the FHOC and MIXIC models to predict the driving states of the controlled vehicles as the tracking reference in the proposed MPC model. We set the time headway as 1.6 s and the prediction horizon as 16 steps. We set the minimum safe time headway as 0.2 s for the following safety of the controlled vehicles. Fig. 9: The profiles of MIXIC- and FHOC-based results in the time domain

We plot the acceleration, spacing, and velocity profiles of the IPV and controlled vehicles in the time domain (Fig. 9). The MIXIC-based results show that the acceleration perturbation does not decay along upstream controlled vehicles. Compared with the MIXIC-based results, the results obtained with the proposed FHOC model illustrates a lower acceleration perturbation in the acceleration profiles of the controlled vehicles. Moreover, the spacing and velocity fluctuations in the FHOC-based results are lower than in the MIXIC-based results.

In the frequency-domain plot in Fig. 10, the FHOC-based result shows a more obvious decline pattern than the MIXIC-based result in both the maximum and mean amplitudes of spacing deviations. The amplitude values of the FHOC-based results are almost below one, while the MIXIC-based results have much larger amplitude values. In the maximum amplitude plot, the decreasing trend in the FHOC-based results is more evident. The string amplitude (i.e. the rightmost graphs in Fig. 10) shows a decreasing pattern along the controlled vehicles in the FHOC-based results.

5.7. Experiment 3: string stability by varying prediction horizon lengths with a discounting factor

We measure the string stability of the proposed model under varying prediction horizon lengths using dataset 3. The selection of prediction horizon lengths in MPC models involves a trade-off between solution feasibility and model accuracy (Camponogara et al., 2002). An inappropriately selected prediction horizon can degrade performance because errors in the prediction will be large if the prediction horizon is too long. Moreover, constrained MPC models may not have strictly

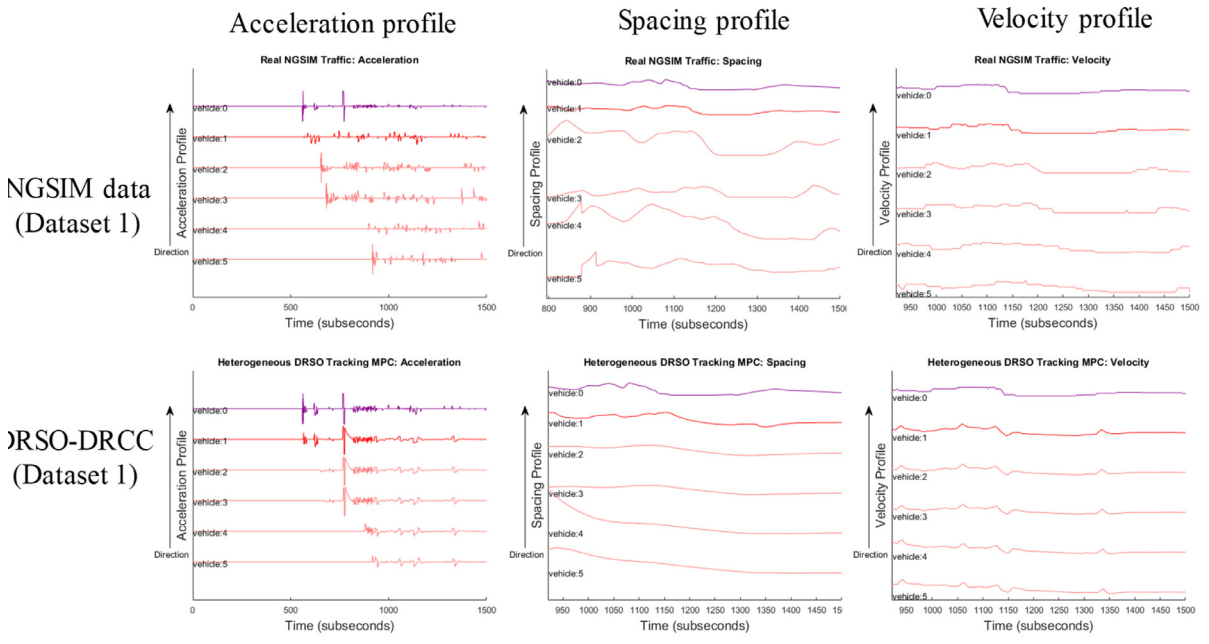

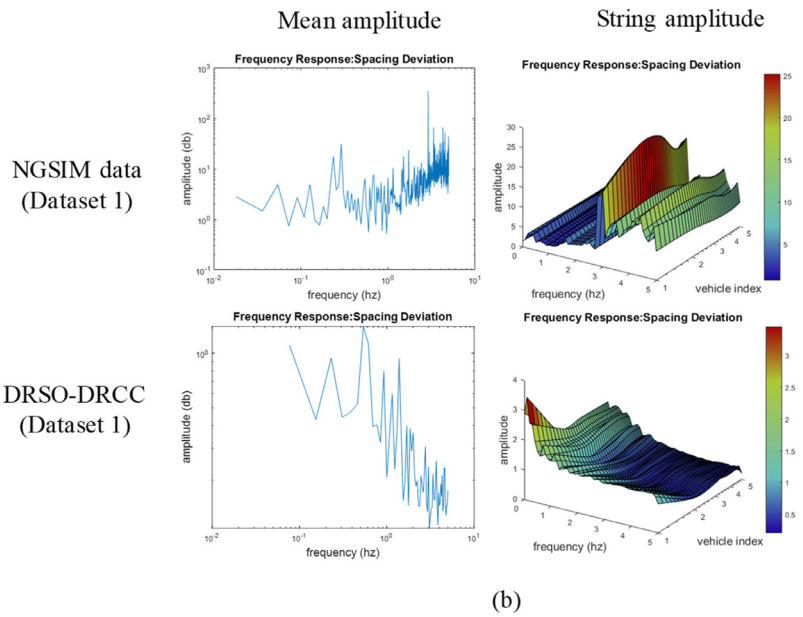

Fig. 8. Three NGSIM datasets and the proposed model in the time and frequency domains.

feasible solutions if the prediction horizon length is very large. To obtain a feasible solution with a variety of prediction horizon lengths, we apply exponential discounting (Pollak, 1968; Henderson and Bateman, 1995; Cajueiro, 2006) as a weighting method to the proposed DRSO-DRCC–based MPC model. The discounting factor at time t in the paper is expressed in Eq. (86):

$$q_t = e^{-t}, t = 1, \ldots, PH \tag{86}$$

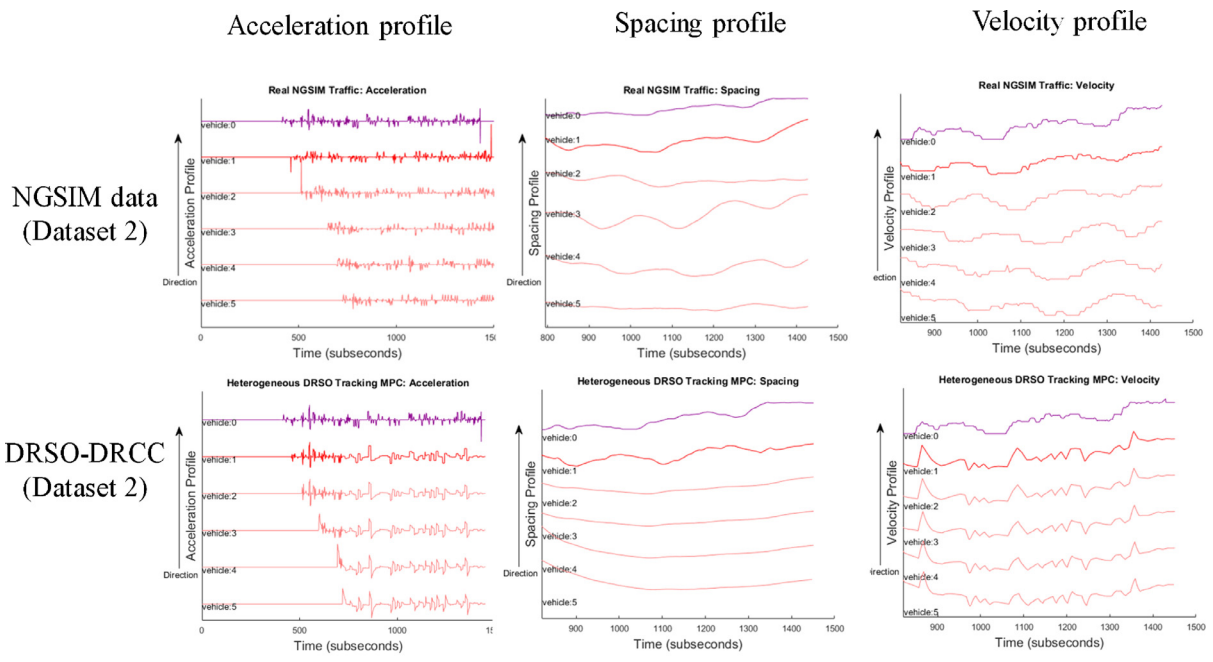

(c)

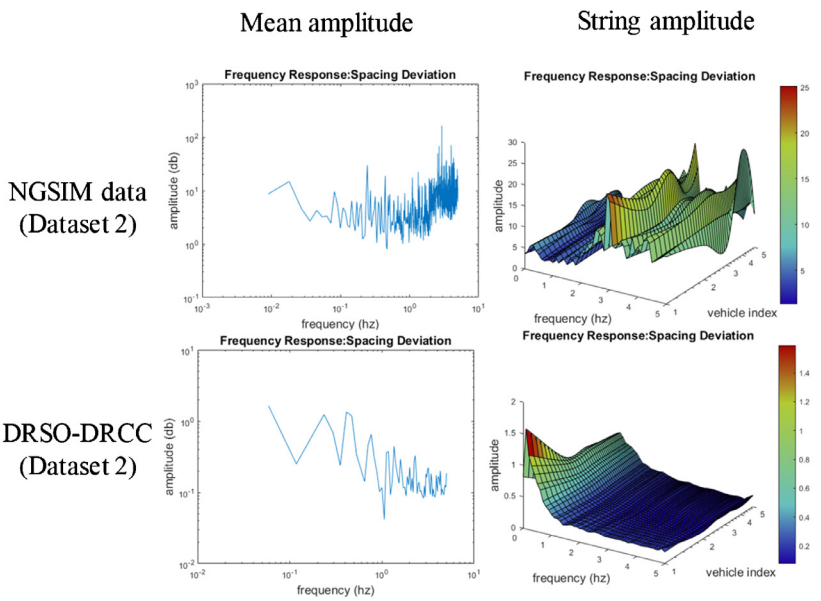

(d)

Fig. 8. Continued

The exponential discounting factors can be applied to the objective function of the relaxed SDP model as Eq. (87):

$$\min_{\boldsymbol{u},\boldsymbol{Q_d},\boldsymbol{P_d},\boldsymbol{p_d},r_d,s_d} \sum_{t=k}^{k+PH} q_{t-k+1} \times \left[\gamma_2 \hat{\boldsymbol{\Sigma}} \bullet \boldsymbol{Q_d}(t) - \hat{\boldsymbol{\mu}}\hat{\boldsymbol{\mu}}^T \bullet \boldsymbol{Q_d}(t) + r_d(t) + \hat{\boldsymbol{\Sigma}} \bullet \boldsymbol{P_d}(t) - 2\hat{\boldsymbol{\mu}}^T \boldsymbol{p_d}(t) + \gamma_1 s_d(t)\right] \tag{87}$$

To demonstrate string-stability performance with varying prediction horizon lengths, we select prediction horizon lengths of 5, 16, 24, 50, and 100 steps and apply the discounting factor to the DRSO-DRCC–based MPC model. The minimum time

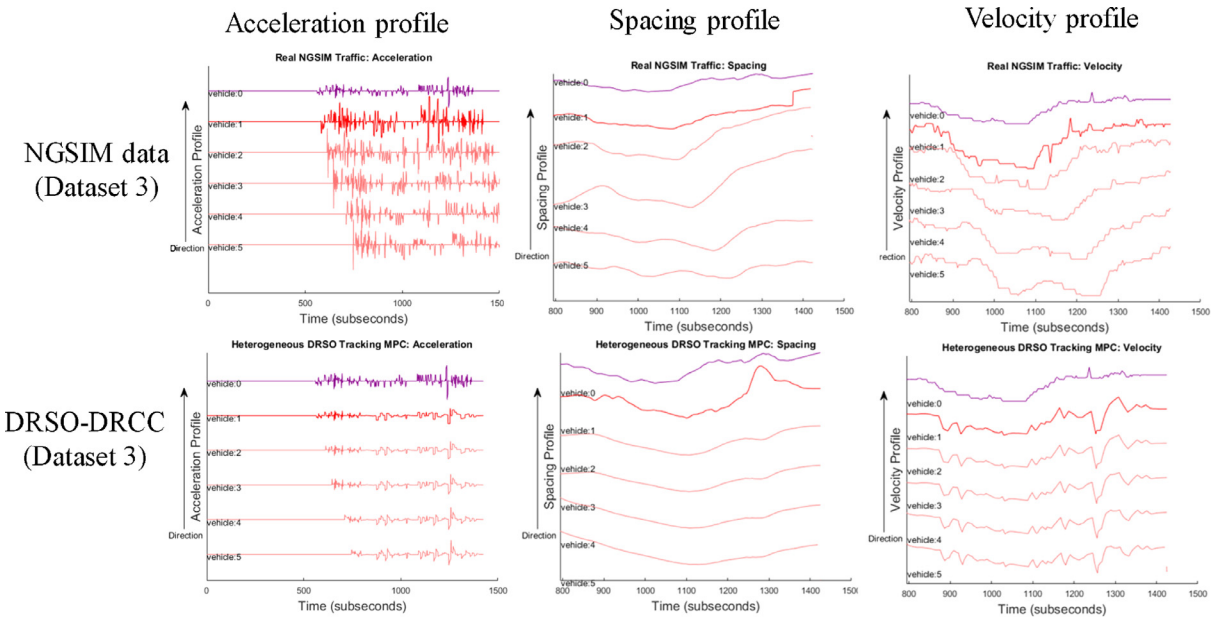

(e)

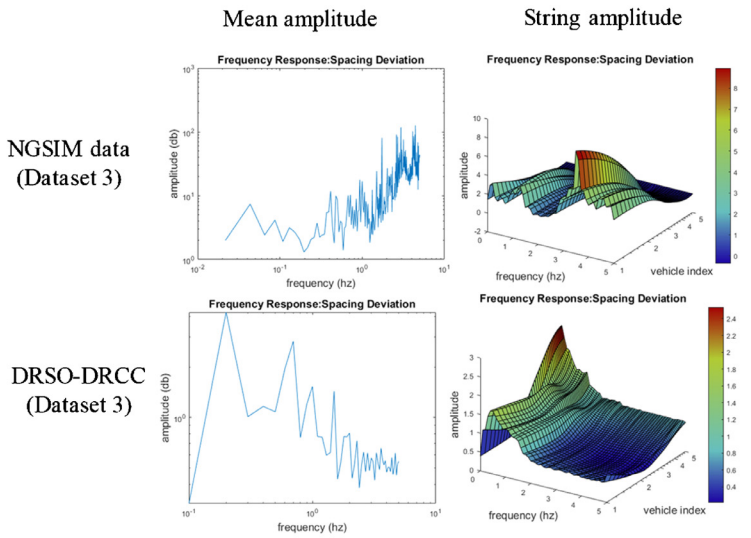

(f)

Fig. 8. Continued

headway selected is 0.2 s. We apply the IDM model to predict the driving states of the IPV and the constrained FHOC model to predict the driving states of the controlled vehicles. In Fig. 11, we can see that the acceleration perturbation obviously decays when we set the prediction horizon at no less than the time headway (i.e. 1.6 s). In the frequency domain, the mean and string amplitudes (i.e. the individual amplitudes of the controlled vehicles) of spacing deviations also show declining patterns as we set the prediction horizon at a higher value. If the prediction horizon is too small (e.g. the 5-step prediction horizon with the 1.6-second time headway), though, the system does not show string-stable conditions. Our results reported in Fig. 11 are consistent with the findings reported in Camponogara et al. (2002) that indicate that a properly chosen long prediction horizon could improve the performance of the system. Noted that in some of the period, the amplitude is above zero db due to the instability of the front uncertain traffic conditions. The amplitude in the frequency domain still shows a decreasing pattern, which indicates the proposed method can mitigate the disturbance of the CACC strings over time.

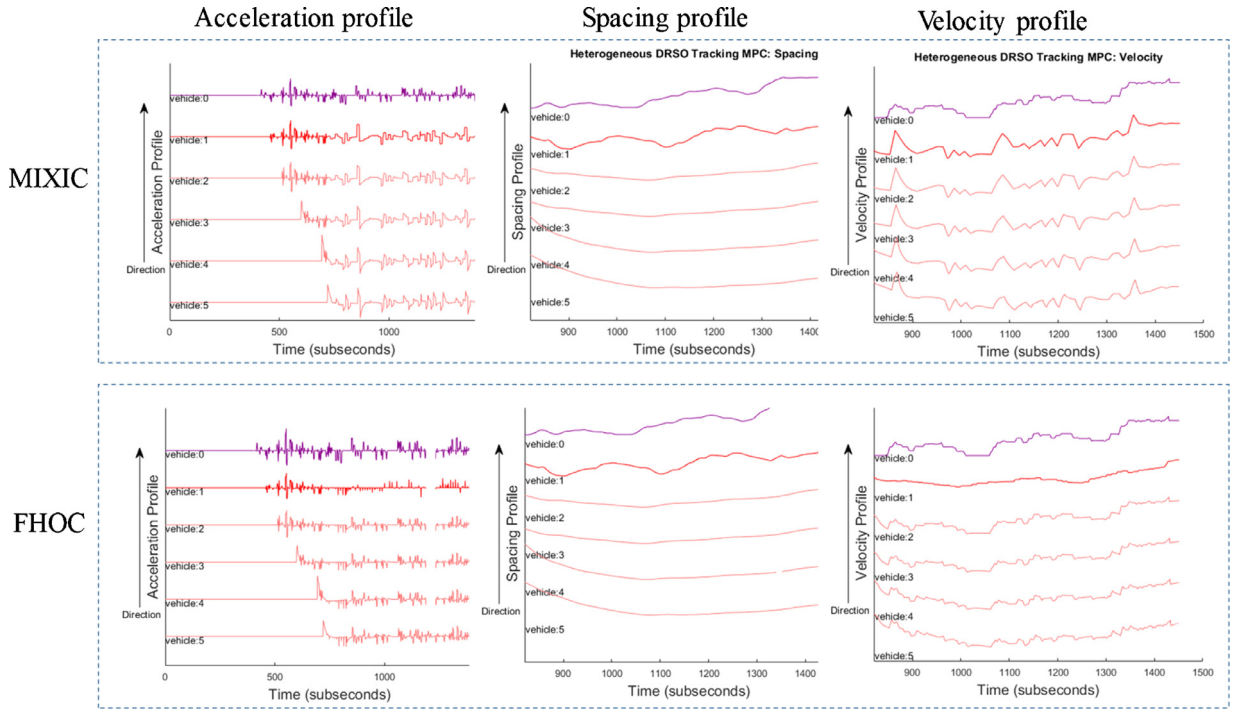

Fig. 9. . The profiles of MIXIC- and FHOC-based results in the time domain

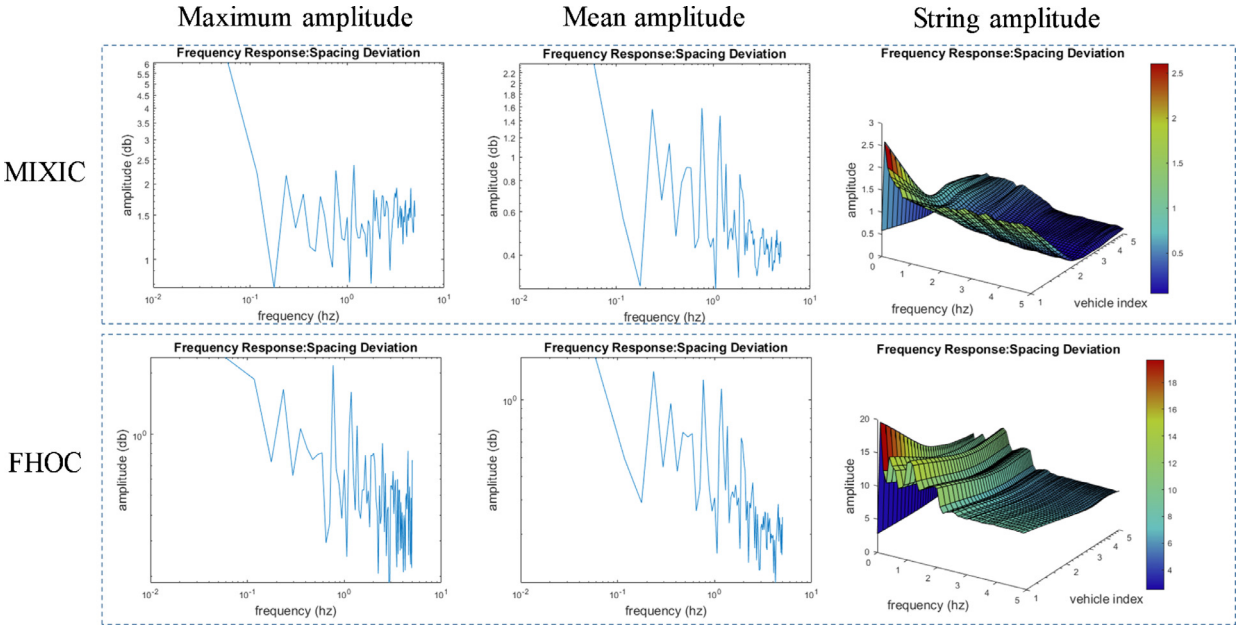

Fig. 10. The spacing deviation amplitude of MIXIC- and FHOC-based results in the frequency domain.

5.8. Experiment 4: string stability by varying time headways

We evaluate the string stability of the proposed model with varying time headways in the constant-time-headway policy using dataset 1 from Table 1. For highway driving, the time headway ranges from 0.4 to 4.0 s from actual measurements depending on driving velocities (Taieb-Maimon and Shinar, 2001; Lewis-Evans et al., 2010; Dang et al., 2013). To evaluate the longitudinal cooperative automated driving of CAVs, we select time headways of 0.4, 0.8, 1.2, 1.6, 2.0, and 2.4 s for the string-stability analysis in this experiment. The prediction horizon length is selected as the same as the time headways. In

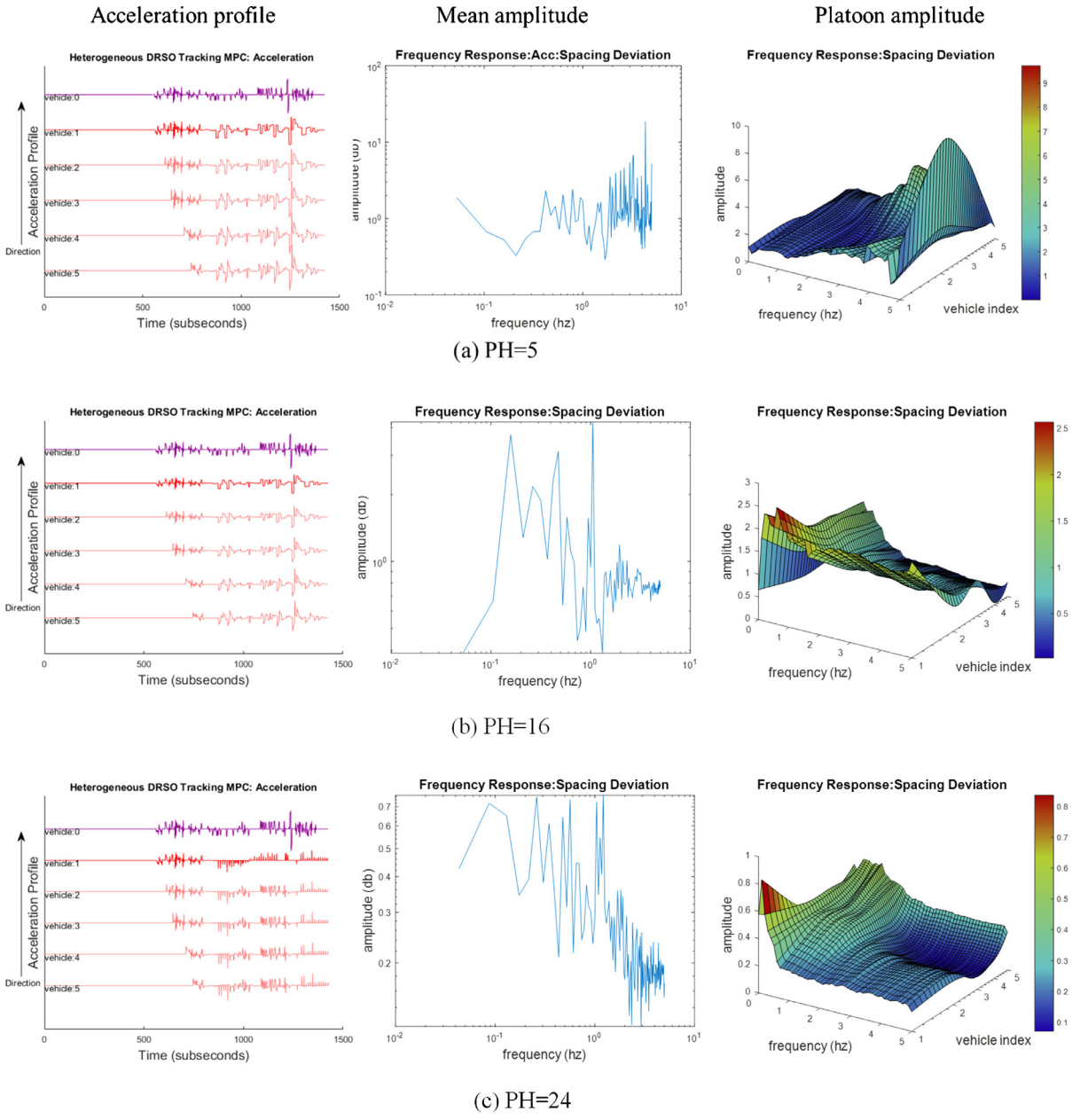

Fig. 11. The acceleration profiles in the time domain and spacing deviations in the frequency domain with varying prediction horizon lengths. (For interpretation of the references to colour in this figure legend, the reader is referred to the web version of this article.)

this experiment, we apply the IDM model to predict the driving states of the IPV and constrained FHOC models to predict the driving states of the controlled vehicles.

In Fig. 12, we plot the spacing deviation amplitude in the frequency domain for the results of the proposed DRSO-DRCC model under varying time headways of the constant-time-headway policy. When the time headway is selected as 0.4 or 0.8 s, the maximum spacing deviation amplitude shows no obvious decreasing patterns. However, when the time headway is selected as 1.2 s or above, our experiment shows that the maximum amplitude in the frequency domain decreases. Fig. 12 shows that as time headway increases the controlled CAV string becomes more stable (i.e. the maximum amplitude of the CAV string in the frequency domain tends to decrease more obviously). Similar patterns in the relationship between time headways and string stability can be found in Naus et al. (2010) and Lei et al. (2011), in which they use a closed-form control method based on a constant-time-headway policy and the smallest time headway that guarantees that string stability is 0.8 s in their experiments. The acceleration- or deceleration-capability constraint in the proposed DRSO-DRCC model may explain string instability under short time headways (e.g. 0.4 s). Bounded by the maximum acceleration and decel-

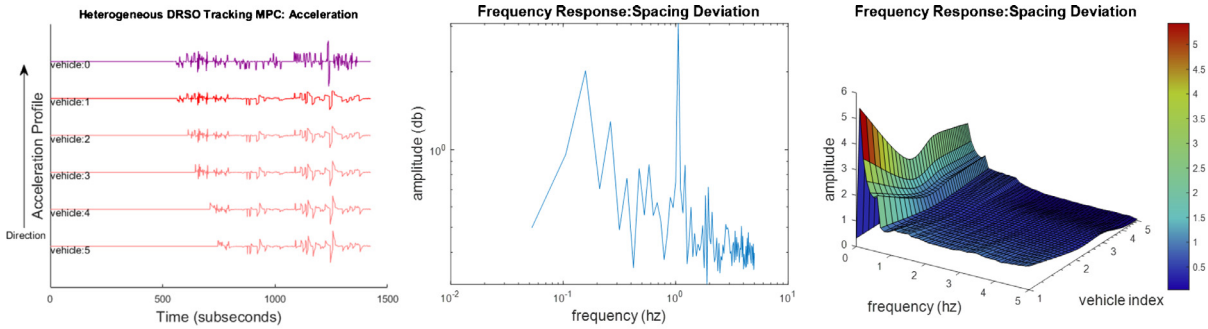

(d) PH=50

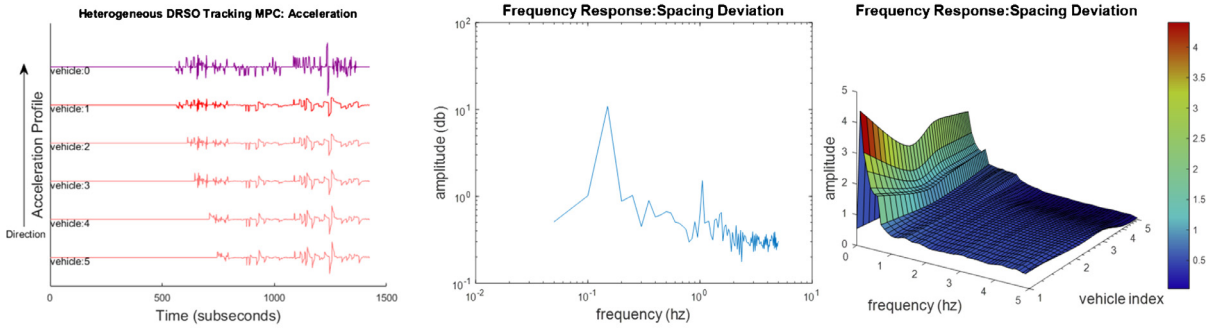

(e) PH=100

Fig. 11. Continued

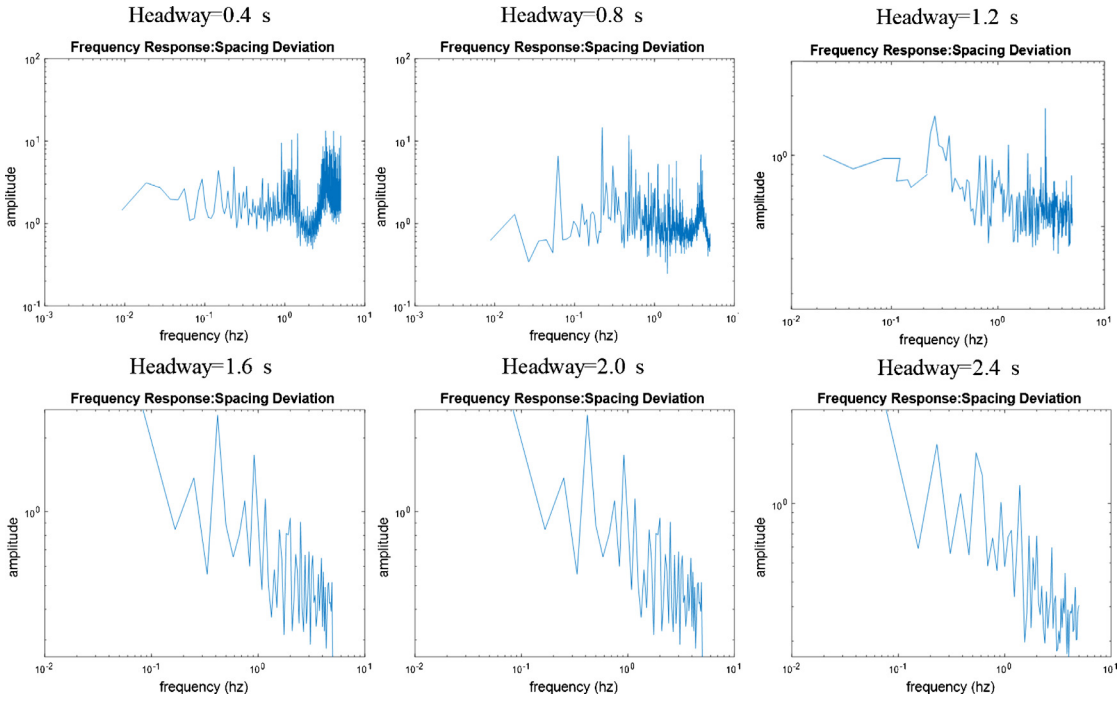

Fig. 12. The maximum spacing deviation amplitudes with varying time headways .

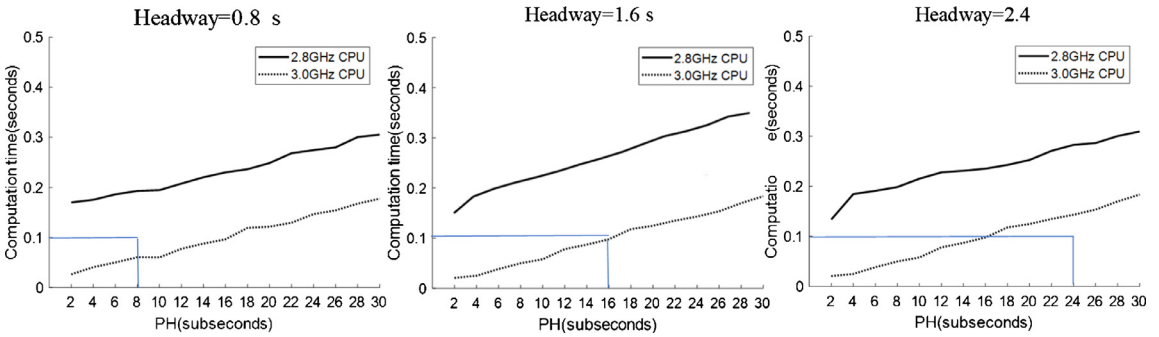

Fig. 13. Computation time of the Solution Method using 2.8 GHz CPU and 3.0 GHz CPU .

eration, the controlled vehicles will not be able to recover to normal driving states in a short time headway under traffic oscillations.

5.9. Computational analysis

In this section, we study the computation time of the proposed model. The proposed solution method is implemented in *C++* and run on a computer with Intel Xeon E5-2680 v2 2.8 GHz CPU (22 cores) and 192 GB RAM and a computer with Intel Xeon E5-1607 v2 3.0 GHz CPU (2 cores) and 64 GB RAM. We run Solution Method in the two computers under varying headways and prediction horizon lengths using empirical NGSIM data from dataset 1 (Table 1). We use the IDM model to predict the driving states of the IPV and the constrained FHOC model to predict the driving states of the controlled vehicles.

The time headways are selected as 0.8, 1.6, and 2.4 s. The prediction horizon is selected from 0.2 to 3 s with a 0.1-second increment. The results reported in Fig. 13 show that the computation time of the Solution Method is affected by the clock rate of CPUs on computers. This demonstrates that the computation time on a computer with a low clock rate (e.g. 2.8 GHz) is not low enough for real-time implementation of the proposed model. If we run on a computer with a 3.0 GHz CPU, however, the computation time will be reduced to 0.1 s or less under some time headway and prediction horizon settings. For example, the computation time with both the 0.8-second and 1.6-second time headways are less than 0.1 s under 8-step and 16-step prediction horizon lengths, respectively. Note that computers can be equipped with high-speed CPUs such as an Intel Core i7- 8086k CPU (4.0 GHz clock rate and 5.0 GHz max turbo clock rate) or an Intel Xeon E3-1280 v6 CPU (3.9 GHz clock rate and 4.2 GHz max turbo clock rate) to further reduce the computation time.

6. Conclusion

In this paper, we propose a data-driven optimization-based MPC modeling framework for smoother, more robust, and safer longitudinal cooperative automated driving control of a string of CAVs under uncertain traffic conditions. The present the proposed framework in four parts. First, we estimate the uncertain driving states of the first (farthest) preceding vehicle within the V2V communication range of the leading controlled CAV. We assume that the first preceding vehicle drives at constant velocities and serves as the boundary condition for the driving-dynamics prediction of its following vehicles. Second, we use a learning-based online prediction method to individually calibrate the car-following parameters. Using the online calibrated parameters, we predict the uncertain driving states of the preceding vehicles based on the concept of forecasting the forecasts of others. Third, based on the predicted driving states of the preceding vehicles, we predict a set of driving state references of the controlled vehicles under a CACC driving policy. Fourth, with the predicted driving states of the IPV and the predicted driving state references of the controlled vehicles, we can obtain the optimal acceleration or deceleration commands for the controlled vehicles by solving the proposed DRSO-DRCC model at each control step.

To solve the proposed DRSO-DRCC model, we reformulate a relaxed SDP problem by applying the strong duality theory and the Semidefinite Relaxation technique. We then present a solution method to solve the relaxed version of the dual problem as an SDP. To demonstrate the proposed model, we extract three empirical vehicle trajectory datasets from NGSIM data. We control the last five following vehicles in the three datasets with the proposed model while the other fifteen vehicles in front of the controlled vehicles are used to generate input data for the proposed DRSO-DRCC model. We evaluate the string stability of the proposed model in both the time and frequency domains through numerical experiments. We design four experiments to evaluate model performance based on varying settings (i.e. driving-dynamics prediction methods, prediction horizon lengths, and time headways). The first experiment compares the results of the proposed DRSO-DRCC model with the NGSIM data generated by the controlled vehicles. The second experiment evaluates the string stability of the proposed model using various controlled-vehicle prediction methods. The third experiment analyzes the string stability of the proposed model using varying prediction horizon lengths. The fourth experiment compares the string stability of the proposed model with varying time headways. Based on the experimental results, we conclude that the proposed model makes CACC driving more stable using the IDM model to predict the driving states of the preceding vehicles and the proposed FHOC

(i.e., Finite-Horizon Optimal Control) model to predict the driving states of the controlled vehicles when the time headway increases under longer prediction horizon lengths.

In addition, we measure the computation time of the proposed solution method. It shows that the computation time of the Solution Method can be further reduced by a CPU with higher clock rates. In the future, the proposed method can be extended in two ways: (1) by incorporating a communication delay inside the control loop using a delay-compensation method; or (2) by applying customized implementations to further reduce the computation time of the proposed model for long prediction horizon lengths.

Acknowledgments

This research was supported by a grant from the National Science Foundation award CMMI-1846795: CAREER: Tackling Congestion in Smart Cities via Data-Driven Optimization-Based Control of Connected and Automated Vehicles. The authors are grateful to the anonymous referees and associate editors for helpful comments that have considerably improved the manuscript. The authors would also like to thank Qinjie Lyu for her assistance in preparing the figures and tables in the Numerical Analysis section. Naturally, the authors are solely responsible for the content of the paper.

References

Bazaraa, M.S., Sherali, H.D., Shetty, C.M., 2013. Nonlinear programming: Theory and Algorithms. John Wiley & Sons.
Bemporad, A., Borrelli, F., Morari, M., 2003. Min-max control of constrained uncertain discrete-time linear systems. IEEE Trans. Automat. Contr. 48 (9), 1600–1606.
Van Arem, B., De Vos, A.P., Vanderschuren, M.J.W.A., 1997. The microscopic traffic simulation model MIXIC 1.3. TNO Report INRO-VVG 1997-02b.
U.S. Department of Transportation Federal Highway Administration. (2016). Next Generation Simulation (NGSIM) Vehicle Trajectories and Supporting Data. [Dataset]. Provided by ITS DataHub through Data.transportation.gov. Accessed 2018-08-01 from http://doi.org/10.21949/1504477
Alipour-Fanid, A., Dabaghchian, M., Zeng, K., 2017. Platoon stability and safety analysis of cooperative adaptive cruise control under wireless rician fading channels and jamming attacks. In Proc. IEEE 18th Int. Symp. High Assurance Syst. Eng., 2017, pp. 157–162.
Benson, S.J., Ye, Y., 2005. DSDP5: software for semidefinite programming. ACM Trans. Math. Software, Sept. 2005.
Benson, S.J., Ye, Y., Zhang, X., 2000. Solving large-scale sparse semidefinite programs for combinatorial optimization. SIAM J. Optim. 10 (2), 443–461.
Bertsimas, D., Thiele, A., 2006. Robust and data-driven optimization: modern decision-making under uncertainty. INFORMS Tutor. Opera. Res. 3, 95–122.
Bertsimas, D., Popescu, I., 2005. Optimal inequalities in probability theory: a convex optimization approach. SIAM J. Optim. 15 (3), 780–804.
Bertsimas, D., Gupta, V., Kallus, N., 2018. Data-driven robust optimization. Math. Program. 167 (2), 235–292.
Bertsimas, D., Brown, D.B., Caramanis, C., 2011. Theory and applications of robust optimization. SIAM Rev. 53 (3), 464–501.
Bertsekas, D.P., 2005. Dynamic Programming and Optimal Control, Vol. 1. Athena scientific, Belmont, MA.
Bichi, M., Ripaccioli, G., Di Cairano, S., Bernardini, D., Bemporad, A., Kolmanovsky, I.V., 2010. Stochastic model predictive control with driver behavior learning for improved powertrain control. In: Decision and Control (CDC), IEEE 49th Conference, pp. 6077–6082.
Biswas, P., Lian, T.C., Wang, T.C., Ye, Y., 2006. Semidefinite programming based algorithms for sensor network localization. ACM Trans. Sens. Netw. 2 (2), 188–220.
Biswas, P., Ye, Y., 2006. A distributed method for solving semidefinite programs arising from ad hoc wireless sensor network localization. Multiscale optimization methods and applications., pp. 69–84.
Bu, F., Tan, H.S., Huang, J., 2010. Design and field testing of a cooperative adaptive cruise control system. In: IEEE In American Control Conference (ACC), pp. 4616–4621.
Boyd, S., Vandenberghe, L., 2004. Convex Optimization. Cambridge University Press.
Blanchet, J., Kang, Y., Murthy, K., 2019. Robust Wasserstein profile inference and applications to machine learning Journal of Applied Probability 56, 830–857.
Boashash, B., 2015. Time-Frequency Signal Analysis and Processing: a Comprehensive Reference. Academic Press.
Camponogara, E., Jia, D., Krogh, B.H., Talukdar, S., 2002. Distributed model predictive control. IEEE Control Syst. 22 (1), 44–52.
Camacho, E.F., Alba, C.B., 2013. Model predictive control. Springer Science & Business Media.
Cajueiro, D.O., 2006. A note on the relevance of the q-exponential function in the context of intertemporal choices. Physica A 364, 385–388.
Calafiore, G.C., El Ghaoui, L., 2006. On distributionally robust chance-constrained linear programs. J. Optim. Theory Appl. 130 (1), 1–22.
Calafiore, G.C., 2007. Ambiguous risk measures and optimal robust portfolios. SIAM J. Optim. 18 (3), 853–877.
Calafiore, G.C., El Ghaoui, L., 2014. Optimization Models. Cambridge University Press.
Chen, D., Ahn, S., Chitturi, M., Noyce, D., 2017. Truck platooning on uphill grades under cooperative adaptive cruise control (CACC). Transport. Res. Part C: Emerg. Technol 1–17.
Dang, R., Zhang, F., Takae, Y., Chu, W., Li, K., 2013. Braking characteristics of Chinese driver in highway and urban road. IFAC Proceed. 46 (21), 322–327.
Delage, E., Ye, Y., 2010. Distributionally robust optimization under moment uncertainty with application to data-driven problems. Oper. Res. 58 (3), 595–612.
Dunbar, W.B., Caveney, D.S., 2012. Distributed receding horizon control of vehicle platoons: stability and string stability. IEEE Trans. Automat. Contr. 57 (3), 620–633.
Floudas, C.A., Visweswaran, V., 1995. Quadratic optimization. In: Handbook of Global Optimization. Springer, Boston, MA, pp. 217–269.
Glasserman, P., Yang, L., 2018. Bounding Wrong–Way Risk in CVA calculation. Math. Finance 28 (1), 268–305.
Goh, J., Sim, M., 2010. Distributionally robust optimization and its tractable approximations. Oper. Res. 58 (4–NaN–1), 902–917.
Gong, Q., Li, Y., Peng, Z., 2009. Power management of plug-in hybrid electric vehicles using neural network based trip modeling. In: IEEE In American Control Conference, ACC'09, pp. 4601–4606.
Gong, S., Shen, J., Du, L., 2016. Constrained optimization and distributed computation based car following control of a connected and autonomous vehicle platoon. Transport. Res. Part B 94, 314–334.
González-Villaseñor, A., Renfrew, A.C., Brunn, P.J., 2007. A controller design methodology for close headway spacing strategies for automated vehicles. Int. J. Control 80 (2), 179–189.
Goulart, P.J., Kerrigan, E.C., Maciejowski, J.M., 2006. Optimization over state feedback policies for robust control with constraints. Automatica 42 (4), 523–533.
Hägerstrand, T., 1970. What about people in regional science? Papers Reg. Sci. 24 (1), 7–24.
Hall, N.G., Long, D.Z., Qi, J., Sim, M., 2015. Managing underperformance risk in project portfolio selection. Oper. Res. 63 (3), 660–675.
Henderson, N., Bateman, I., 1995. Empirical and public choice evidence for hyperbolic social discount rates and the implications for intergenerational discounting. Environ. Resour. Econ. 5 (4), 413–423.
Herman, R., Montroll, E.W., Potts, R.B., Rothery, R.W., 1959. Traffic dynamics: analysis of stability in car following. Oper. Res. 7 (1), 86–106.
Herzog, F., Keel, S., Dondi, G., Schumann, L.M., Geering, H.P., 2006, June. Model predictive control for portfolio selection. In: American Control Conference, p. 8.

Hu, J., Shao, Y., Sun, Z., Wang, M., Bared, J., Huang, P., 2016. Integrated optimal eco-driving on rolling terrain for hybrid electric vehicle with vehicle-infrastructure communication. Transport. Res. Part C 68, 228–244.
Jiang, R., Guan, Y., 2016. Data-driven chance constrained stochastic program. Math. Program. 158 (1–2), 291–327.
Kianfar, R., Augusto, B., Ebadighajari, A., Hakeem, U., Nilsson, J., Raza, A., Tabar, R.S., Irukulapati, N.V., Englund, C., Falcone, P., Papanastasiou, S., 2012. Design and experimental validation of a cooperative driving system in the grand cooperative driving challenge. IEEE Trans. Intell. Transport. Syst. 13 (3), 994–1007.
Kim, S., Kojima, M., 2003. Exact solutions of some nonconvex quadratic optimization problems via SDP and SOCP relaxations. Comput. Optim. Appl. 26 (2), 143–154.
Kreuzen, C., 2012. Master Thesis. Delft University of Technology.
Lam, H., Zhou, E., 2015. Quantifying uncertainty in sample average approximation. In: IEEE In Proceedings of the 2015 Winter Simulation Conference, pp. 3846–3857.
Lang, D., Stanger, T., Schmied, R., del Re, L., 2014. Predictive cooperative adaptive cruise control: fuel consumption benefits and implementability. In: Optimization and Optimal Control in Automotive Systems, pp. 163–178.
Li, P.Y., Shrivastava, A., 2002. Traffic flow stability induced by constant time headway policy for adaptive cruise control vehicles. Transport. Res. Part C 10 (4), 275–301.
Liu, H., Han, K., Gayah, V.V., Friesz, T.L., Yao, T., 2015. Data-driven linear decision rule approach for distributionally robust optimization of on-line signal control. Transport. Res. Part C 59, 260–277.
Lei, C., Van Eenennaam, E.M., Wolterink, W.K., Karagiannis, G., Heijenk, G., Ploeg, J., 2011. Impact of packet loss on CACC string stability performance. In: ITS Telecommunications (ITST), 11th International Conference, pp. 381–386.
Lewis-Evans, B., De Waard, D., Brookhuis, K.A., 2010. That's close enough – A threshold effect of time headway on the experience of risk, task difficulty, effort, and comfort. Accident Analy. Prevent. 42 (6), 1926–1933.
Li, X., Jiang, H., 2007. Solving large-margin hidden Markov model estimation via semidefinite programming. IEEE Trans. Audio Speech Lang. Process 15 (8), 2383–2392.
Li, X., Peng, F., Ouyang, Y., 2010. Measurement and estimation of traffic oscillation properties. Transport. Res. Part B. 44 (1), 1–14.
Li, X., Wang, X., Ouyang, Y., 2012. Prediction and field validation of traffic oscillation propagation under nonlinear car-following laws. Transport. Res. Part B 46 (3), 409–423.
Li, Y., Zhu, H., Cen, M., Li, Y., Li, R., Sun, D., 2013. On the stability analysis of microscopic traffic car-following model: a case study. Nonlinear Dyn 74 (1–2), 335–343.
Lu, X.Y., Hedrick, J.K., Drew, M., 2002, May. ACC/CACC-control design, stability and robust performance. In: American Control Conference. Proceedings, 6, pp. 4327–4332.
Lu, Y., Arkun, Y., 2000. Quasi-min-max MPC algorithms for LPV systems. Automatica 36 (4), 527–540.
Luo, Z.Q., Ma, W.K., So, A.M.C., Ye, Y., Zhang, S., 2010. Semidefinite relaxation of quadratic optimization problems. IEEE Signal Process Mag. 27 (3), 20–34.
Lyapunov, A.M., 1992. The general problem of the stability of motion. Int. J. Control 55 (3), 531–534.
Ma, W.K., Davidson, T.N., Wong, K.M., Luo, Z.Q., Ching, P.C., 2002. Quasi-ML multiuser detection using SDR with application to sync. CDMA. IEEE Trans. Signal Process 50 (4), 912–922.
Ma, W.K., Ching, P.C., Vo, B.N., 2004. Crosstalk resilient interference cancellation in microphone arrays using capon beamforming. IEEE Trans. Speech Audio Process. 12 (5), 468–477.
Ma, J., Li, X., Zhou, F., Hu, J., Park, B.B., 2017. Parsimonious shooting heuristic for trajectory design of connected automated traffic part II: computational issues and optimization. Transport. Res. Part B: Methodol. 95, 421–441.
Marshall, A., Olkin, I., 1960. Multivariate Chebyshev Inequalities. Ann. Math. Stat. 31 (4), 1001–1014.
Mayne, D.Q., Rawlings, J.B., Rao, C.V., Scokaert, P.O., 2000. Constrained model predictive control: stability and optimality. Automatica 36 (6), 789–814.
Miller, H.J., 2005. A measurement theory for time geography. Geogr. Anal. 37 (1), 17–45.
Milanés, V., Shladover, S.E., Spring, J., Nowakowski, C., Kawazoe, H., Nakamura, M., 2014. Cooperative adaptive cruise control in real traffic situations. IEEE Trans. Intell. Transport. Syst. 15 (1), 296–305.
Naus, G.J., Vugts, R.P., Ploeg, J., van de Molengraft, M.J., Steinbuch, M., 2010. String-stable CACC design and experimental validation: a frequency-domain approach. IEEE Trans. Veh. Technol. 59 (9), 4268–4279.
Newell, G.F., 2002. A simplified car-following theory: a lower order model. Transport. Res. Part B 36 (3), 195–205.
Nilim, A., El Ghaoui, L., 2005. Robust control of Markov decision processes with uncertain transition matrices. Oper. Res. 53 (5), 780–798.
No, T.S., Chong, K.T., Roh, D.H., 2001. A Lyapunov function approach to longitudinal control of vehicles in a platoon. IEEE Trans. Veh. Technol. 50 (1), 116–124.
Oncu, S., Van de Wouw, N., Heemels, W.M.H., Nijmeijer, H., 2012. String stability of interconnected vehicles under communication constraints. In: Decision and Control (CDC), IEEE 51st Annual Conference, pp. 2459–2464.
Patrinos, P., Trimboli, S., Bemporad, A., 2011. Stochastic MPC for real-time market-based optimal power dispatch. In: Decision and Control and European Control Conference (CDC-ECC), IEEE 50th Conference, pp. 7111–7116.
Ploeg, J., Scheepers, B.T., Van Nunen, E., Van de Wouw, N., Nijmeijer, H., 2011. Design and experimental evaluation of cooperative adaptive cruise control. In: Intelligent Transportation Systems (ITSC), IEEE 14th International Conference, pp. 260–265.
Ploeg, J., Van De Wouw, N., Nijmeijer, H., 2014. Lp string stability of cascaded systems: application to vehicle platooning. IEEE Trans. Control Syst. Technol. 22 (2), 786–793.
Pólik, I., Terlaky, T., 2007. A survey of the S-lemma. SIAM Rev. 49 (3), 371–418.
Pollak, R.A., 1968. Consistent planning. Rev. Econ. Stud. 35 (2), 201–208.
Primbs, J.A., 2009. Dynamic hedging of basket options under proportional transaction costs using receding horizon control. Int. J. Control 82 (10), 1841–1855.
Propoi, A.I., 1963. Use of linear programming methods for synthesizing sampled-data automatic systems. Automn. Remote Control 24 (7), 837–844.
Qian, H.P., De Schutter, J., 1992. The role of damping and low pass filtering in the stability of discrete time implemented robot force control. In: Robotics and Automation. Proceedings. IEEE 1992 International Conference, pp. 1368–1373.
Rawlings, J.B., Mayne, D.Q., 2009. Model predictive control: theory and design. Nob Hill Publishing, pp. 3430–3433.
Rhoades, C., Wang, X., Ouyang, Y., 2016. Calibration of nonlinear car-following laws for traffic oscillation prediction. Transport. Res. Part C 69, 328–342.
Rockafellar, R.T., 2015. Convex Analysis. Princeton University Press.
Sancar, F.E., Fidan, B., Huissoon, J.P., Waslander, S.L., 2014. MPC based collaborative adaptive cruise control with rear end collision avoidance. In: IEEE In Intelligent Vehicles Symposium Proceedings, pp. 516–521.
Scarf, H., 1958. A min-max solution of an inventory problem. In: Arrow, K.J., Karlin, S., Scarf, H. (Eds.), Studies in the Mathematical Theory of Inventory and Production. Stanford University Press, Stanford, CA, pp. 201–209.
Schwarm, A.T., Nikolaou, M., 1999. Chance-constrained model predictive control. AIChE J. 45 (8), 1743–1752.
Scokaert, P.O., Mayne, D.Q., 1998. Min-max feedback model predictive control for constrained linear systems. IEEE Trans. Automat. Contr. 43 (8), 1136–1142.
Shapiro, A., 2001. On duality theory of conic linear problems. In: Semi-infinite Programming. Springer, Boston, MA, pp. 135–165.
Shapiro, A., Nemirovski, A., 2005. On complexity of stochastic programming problems. Continuous Optimization. 111–146.
Sheikholeslam, S., Desoer, C.A., 1990. Longitudinal control of a platoon of vehicles. In: IEEE In American Control Conference, pp. 291–296.
Skajaa, A., Andersen, E.D., Ye, Y., 2013. Warmstarting the homogeneous and self-dual interior point method for linear and conic quadratic problems. Math. Program. Comput. 5 (1), 1–25.
Sidiropoulos, N.D., Davidson, T.N., Luo, Z.Q., 2006. Transmit beamforming for physical-layer multicasting. IEEE Trans. Signal Process. 54 (6–1), 2239–2251.
Slotine, J.J.E., Li, W., 1991. Applied Nonlinear Control, 199. Prentice hall, Englewood Cliffs, NJ.

Stotsky, A., Chien, C.C., Ioannou, P., 1995. Robust platoon-stable controller design for autonomous intelligent vehicles. Math. Comput. Model. 22 (4–7), 287–303.
Sturm, J.F., 1999. Using SeDuMi 1.02, a MATLAB toolbox for optimization over symmetric cones. Optim. Method Softw. 11 (1–4), 625–653.
Sturm, J.F., 2002. Implementation of interior point methods for mixed semidefinite and second order cone optimization problems. Optim. Method Softw. 17 (6), 1105–1154.
Suh, J., Yi, K., Jung, J., Lee, K., Chong, H., Ko, B., 2016. Design and evaluation of a model predictive vehicle control algorithm for automated driving using a vehicle traffic simulator. Control Eng. Pract. 51, 92–107.
Sun, J., Zheng, Z., Sun, J., 2018. Stability analysis methods and their applicability to car-following models in conventional and connected environments. Transport. Res. Part B 109, 212–237.
Swaroop, D., Hedrick, J.K., 1996. String stability of interconnected systems. IEEE Trans. Automat. Contr. 41 (3), 349–357.
Taieb-Maimon, M., Shinar, D., 2001. Minimum and comfortable driving headways: reality versus perception. Hum. Fact. 43 (1), 159–172.
Talebpour, A., Mahmassani, H.S., 2016. Influence of connected and autonomous vehicles on traffic flow stability and throughput. Transport. Res. Part C: Emerg. Technol. 71, 143–163.
Townsend, R.M., 1983. Forecasting the forecasts of others. J. Polit. Econ. 91 (4), 546–588.
Treiber, M., Hennecke, A., Helbing, D., 2000. Congested traffic states in empirical observations and microscopic simulations. Phys. Rev. E 62 (2), 1805.
Sun, D., Toh, K.C., Yuan, Y., Zhao, X.Y., 2020. SDPNAL+: A Matlab software for semidefinite programming with bound constraints (version 1.0), Optimization Methods and Software, 35:1, 87-115
Van Arem, B., Van Driel, C.J., Visser, R., 2006. The impact of cooperative adaptive cruise control on traffic-flow characteristics. IEEE Trans. Intell. Transport. Syst. 7 (4), 429–436.
Van Hessem, D.H., Bosgra, O.H., 2002. A conic reformulation of model predictive control including bounded and stochastic disturbances under state and input constraints. In: Decision and Control, 2002, Proceedings of the 41st IEEE Conference, 4, pp. 4643–4648.
VanderWerf, J., Shladover, S., Kourjanskaia, N., Miller, M., Krishnan, H., 2001. Modeling effects of driver control assistance systems on traffic. Transport. Res. Rec. (1748) 167–174.
Varaiya, P., 1993. Smart cars on smart roads: problems of control. IEEE Trans. Automat. Contr. 38 (2), 195–207.
Vugts, R., 2010. Doctoral Dissertation.. Technische Universiteit Eindhoven.
Wang, C., Ong, C.J., Sim, M., 2009. Convergence properties of constrained linear system under MPC control law using affine disturbance feedback. Automatica 45 (7), 1715–1720.
Wang, J.Q., Li, S.E., Zheng, Y., Lu, X.Y., 2015. Longitudinal collision mitigation via coordinated braking of multiple vehicles using model predictive control. Integr. Comput. Aided Eng. 22 (2), 171–185.
Wang, M., Daamen, W., Hoogendoorn, S.P., van Arem, B., 2014. Rolling horizon control framework for driver assistance systems. Part II: Cooperative sensing and cooperative control. Transport. Res. Part C: Emerg. Technol. 40, 290–311.
Wang, Z., Glynn, P.W., Ye, Y., 2016. Likelihood robust optimization for data-driven problems. Comput. Manag. Sci. 13 (2), 241–261.
Ward, J.A., 2009. Doctoral dissertation. University of Bristol.
Wiesemann, W., Kuhn, D., Sim, M., 2014. Distributionally robust convex optimization. Oper. Res. 62 (6), 1358–1376.
Yakubovic, V.A., 1971. In: S-procedure in Nonlinear Control Theory, 1. Vestnik Leningrad University, pp. 62–77.
Ye, Y., Zhang, S., 2003. New results on quadratic minimization. SIAM J. Optim. 14 (1), 245–267.
Zeilinger, M.N., Raimondo, D.M., Domahidi, A., Morari, M., Jones, C.N., 2014. On real-time robust model predictive control. Automatica 50 (3), 683–694.
Zhang, S., 2000. Quadratic maximization and semidefinite relaxation. Math. Program. 87 (3), 453–465.
Zhao, S., Zhang, K., 2017. Observing individual dynamic choices of activity chains from location-based crowdsourced data. Transport. Res. Part C 85, 1–22.
Zhou, H., Saigal, R., Dion, F., Yang, L., 2012. Vehicle platoon control in high-latency wireless communications environment: model predictive control method. Transport. Res. Rec. (2324) 81–90.
Zhou, F., Li, X., Ma, J., 2017a. Parsimonious shooting heuristic for trajectory design of connected automated traffic part I: theoretical analysis with generalized time geography. Transport. Res. Part B 95, 394–420.
Zhou, Y., Ahn, S., Chitturi, M., Noyce, D.A., 2017b. Rolling horizon stochastic optimal control strategy for ACC and CACC under uncertainty. Transport. Res. Part C 83, 61–76.
Zulkefli, M.A.M., Zheng, J., Sun, Z., Liu, H.X., 2014. . Hybrid powertrain optimization with trajectory prediction based on inter-vehicle-communication and vehicle-infrastructure-integration. Transport. Res. Part C: Emerg. Technol. 45, 41–63.
Zymler, S., 2010. Distributionally Robust Optimization With Applications to Risk Management. Imperial College. London, UK https://spiral.imperial.ac.uk/bitstream/10044/1/6048/1/Zymler-S-2010-PhD-Thesis.pdf.
Zymler, S., Kuhn, D., Rustem, B., 2013. Distributionally robust joint chance constraints with second-order moment information. Math. Program. 137 (1–2), 167–198.